DETERMINATION OF MAGNETIC STRUCTURES

A NEUTRON DIFFRACTION INVESTIGATION OF CoO, Cr_5S_6, AND TRIGONAL Cr_2S_3

B. VAN LAAR

DETERMINATION OF MAGNETIC STRUCTURES

A NEUTRON DIFFRACTION INVESTIGATION OF CoO, Cr_5S_6, AND TRIGONAL Cr_2S_3

B. VAN LAAR

DETERMINATION OF MAGNETIC STRUCTURES

A NEUTRON DIFFRACTION INVESTIGATION OF CoO, Cr_5S_6, AND TRIGONAL Cr_2S_3

PROEFSCHRIFT

TER VERKRIJGING VAN DE GRAAD VAN DOCTOR IN
DE WISKUNDE EN NATUURWETENSCHAPPEN AAN
DE RIJKSUNIVERSITEIT TE LEIDEN, OP GEZAG VAN
DE RECTOR MAGNIFICUS DR P. MUNTENDAM,
HOOGLERAAR IN DE FACULTEIT DER GENEESKUNDE,
TEN OVERSTAAN VAN EEN COMMISSIE UIT DE SENAAT
TE VERDEDIGEN OP WOENSDAG 3 APRIL 1968
TE KLOKKE 14.15 UUR

DOOR

BOB VAN LAAR

GEBOREN TE AMSTERDAM IN 1933

PROMOTOREN: PROF.DR J.A.GOEDKOOP

PROF.DR F.JELLINEK

Aan mijn ouders

Aan Martine en Krijntje

Het werk, beschreven in dit proefschrift, maakt deel uit van het onderzoekprogramma van het Reactor Centrum Nederland, Petten, in samenwerking met het Institutt for Atomenergi, Kjeller, Noorwegen. De tekst wordt ook gepubliceerd als RCN rapport RCN-92.

Nu dit proefschrift is verschenen wil ik allen bedanken die, hetzij direkt, hetzij indirect, hebben bijgedragen tot het tot stand komen ervan.

Op Dr B.O.Loopstra heb ik nooit tevergeefs een beroep gedaan. Ik ben hem zeer dankbaar voor de grote belangstelling die hij voor het werk heeft getoond en voor de opbouwende kritiek die hij in vele gesprekken heeft gegeven.

Je tiens à exprimer ma grande reconnaissance envers Monsieur E.F.Bertaut du Centre d'Etudes Nucléaires de Grenoble qui m'a donné la possibilité de faire les expériences, décrites dans la partie 3.3, dans son laboratoire. J'en garde le meilleur souvenir à la collaboration amicale avec Messieurs R.Lemaire et J.Schweizer.

Dr H.M.Rietveld ben ik zeer erkentelijk voor de hulp die hij mij gegeven heeft bij het schrijven van rekenmachineprogramma's en voor het korrigeren van de engelse tekst van het proefschrift.

Dat de heren J.F.Strang, P.H.J.Disseldorp en M.de Beurs altijd op enthousiaste wijze geassisteerd hebben bij het experimentele werk, is voor mij van grote waarde geweest evenals het verzorgen van de elektronische apparatuur door de heren Th.H.Terwisscha van Scheltinga en A.Th.J.M.Overtoom.

Mevrouw E.A.M.Endel-Kramer en Mejuffrouw G.Möls dank ik voor de akkurate en blijmoedige wijze waarop zij het typewerk hebben verricht.

Bovenal dank ik jullie, mijn ouders, voor de grote opofferingen waarmee jullie, onder moeilijke omstandigheden, mijn studie hebben mogelijk gemaakt en jou, lieve Martine, voor alle steun en hulp die je mij gegeven hebt.

C O N T E N T S

INTRODUCTION

In compounds with atoms carrying magnetic moments, a long-range ordering of these moments will occur at sufficiently low temperatures.

This thesis describes the determination of some of these magnetic structures by neutron diffraction.

The methods currently used in the study of magnetic substances can be divided in macroscopic and microscopic methods. To the first group belong the conventional techniques as bulk magnetic measurements, specific heat measurements, and the measurement of electron transport phenomena.

Anomalies in the specific heat and in the electrical resistance or in other transport properties can indicate the occurrence of a magnetic transition and often they allow a very precise determination of the transition point.

In bulk magnetic measurements the magnetization is measured versus the temperature and also versus the magnitude and, if the sample is monocrystalline, the direction of the applied field. In this way much information is obtained about the type of magnetic ordering, the net magnetic moment of the sample, and its anisotropy. Sometimes the interpretation of these measurements is complicated due to a change in the spin pattern induced by the applied field when this is large enough.

Advantages of these methods are that they can be carried out rather quickly and that the apparatus is not too expensive. It is possible to scan systematically a large temperature range and to investigate a series of samples with different composition. These methods can also be used to obtain data with high accuracy from which much and valuable information can be deduced. However, one serious drawback is inherent to all macroscopic methods: the fact that all information obtained by these methods is an overall information.

Especially in more complex magnetic substances the number of parameters is often too large to allow an unambiguous interpretation of the observed behaviour of the sample under investigation in terms of the individual spin vectors.

When an investigation is aimed at obtaining information about magnetic systems on a microscopic scale, the available methods are resonance techniques, Mössbauer measurements, and neutron diffraction. Of these, neutron diffraction provides the most direct means to study magnetic structures on an atomic scale giving a possibility to clarify in more fundamental terms the observed magnetic data. A good example of this is the change in the spin structure causing the transition from a ferrimagnetic state to a state without net moment in Cr_5S_6, described later in this thesis.

As all known magnetic ordering schemes are periodic, every spin structure can be described in terms of a three dimensional Fourier series. With neutron diffraction the amplitude and the propagation vector of each Fourier component can be measured separately. This makes it possible, at least in principle, to obtain a detailed picture of the whole spin structure in which the direction and magnitude of the moment of each magnetic atom in the lattice is known.

Depending on the nature of the sample, neutron diffraction techniques can be divided into two groups: single-crystal work and powder work. The accuracy of the obtained spin structure depends strongly on the number and the accuracy of the measured Fourier components. This strongly favours the use of single crystals, especially in those cases where one is interested in the fine details of the spatial distribution of the unpaired electrons. In combination with the use of polarized neutrons, single-crystal work can yield impressive results. The applicability of this method is unfortunately restricted by the fact that crystals of sufficient size are usually difficult to obtain.

The most obvious advantage of powder work is that all materials, which exhibit interesting properties, can be obtained in powder form. In addition the extinction problem is avoided, one is not bothered by an unknown distribution of the magnetic domains in the sample, and it is quite simple, if necessary, to place the data on an absolute scale.

The main disadvantages of powder work are the low intensity scattered by the sample and the problem of indexing the observed reflections i.e. tracing back the direction of the propagation vector of a certain Fourier component of which only the length is observable. Another problem is the finite angular resolution of a neutron powder spectrometer, but partly due to the higher neutron fluxes available today and partly to newer insights in the optics of the system, this resolution has been improved drastically compared with that of spectrometers of some years ago. This means that nowadays problems of such a complexity can be solved by powder work as could only be dealt with by single-crystal methods.

It is certainly not true to say that neutron diffraction is able to solve all problems in magnetism independent of other techniques. Especially the numerical precision of powder work cannot compete with that obtained by magnetization measurements. Also, neutron diffraction is too time consuming and too expensive to scan systematically the whole temperature region; the region of interest should always be selected on the basis of the results of other measurements. Together with these other methods neutron diffraction can give very useful and illuminating results. For examples the reader is referred to the literature and to the compilation given by Bacon [1].

As the major part of the work described in this thesis has been carried out by means of the powder technique, some considerations on the resolution and the luminosity of a powder neutron diffractometer will be given in chapter I.

The calculation of the neutron intensity scattered by ordered spin systems will be dealt with in chapter II. In chapter III work carried out on powder and single-crystal samples of CoO will be described. The magnetic structures of Cr_5S_6 and trigonal Cr_2S_3, as determined by neutron diffraction on powders, will be given in chapters IV and V.

The essential parts of the work described in chapter III have already been published in references [2,3,4], those of chapter IV in reference [5], and those of chapter V in reference [6].

References:

1) G.E.Bacon, Neutron Diffraction, Clarendon Press, Oxford (1962).
2) B.van Laar, Phys.Rev. 138, A584 (1965).
3) B.van Laar, J.Phys.Soc.Japan 20, 1282 (1965).
4) B.van Laar, J.Schweizer and R.Lemaire, Phys.Rev. 141, 538 (1966).
5) B.van Laar, Phys.Rev. 156, 654 (1967).
6) B.van Laar, Phys.Letters 25A, 27 (1967).

Chapter I

SOME CONSIDERATIONS ON THE RESOLUTION AND LUMINOSITY OF A NEUTRON POWDER DIFFRACTOMETER

1.1 Introduction

The neutron fluxes available for neutron diffraction powder work have increased considerably during the last decade. Nevertheless, even at reactors especially designed for neutron beam experiments, these fluxes are still many orders of magnitude smaller than the usual photon fluxes in X-ray diffraction.

Furthermore, most of the simpler problems not requiring a very high angular resolving power have been studied already in the past and it can be expected that in the future the need for high resolution diffraction apparatus will become more and more pressing. As in all optical systems, an improvement of the resolving power of a powder diffractometer is always accompanied by a loss in intensity. Therefore it is of interest to consider in some more detail the problem of obtaining, in a neutron diffraction set up, both the required resolving power and the optimum intensity.

The resolution and the luminosity of a neutron powder diffractometer are determined by the following quantities, the meaning of which is illustrated by fig.1.1:

1) the angular divergence α_1 of the collimator between the neutron source and the monochromator,
2) the reflectivity of the monochromator,
3) the divergence β of the monochromator,
4) the angular divergence α_2 of the collimator between the monochromator and the powder sample,
5) the angular divergence α_3 of the collimator between the sample and the counting system.

The divergence α_i of the i-th collimator is defined as the full width of a slit divided by its length; the divergence β of the monochromator is the full width at half height of its rocking curve as obtained with a perfect second crystal and zero divergences in the other parts of the measuring system.

1.2 Resolving power

Caglioti et al.[1] calculated the full width at half height $A_{\frac{1}{2}}$ of an elastic neutron diffraction peak as a function of the above defined divergencies

$$A_{\frac{1}{2}}^2 = \alpha_3^2+\{\alpha_1^2\alpha_2^2(2a-1)^2+\alpha_2^2\beta^2(2a-2)^2+4\alpha_1^2\beta^2a^2\}/(\alpha_1^2+\alpha_2^2+4\beta^2). \quad (1.1)$$

Here $a = \tan\theta_B/\tan\theta_M$, θ_B and θ_M being the Bragg angles of the sample and the monochromator.

In the derivation of this formula it has been assumed that a neutron travelling in a direction which makes an angle ϕ_i with the mean direction of the i-th collimator has a probability to pass this collimator

$$W_i(\phi_i) = \exp(-4\phi_i^2 \ln 2/\alpha_i^2). \quad (1.2)$$

This means that the ideal triangular transmission curve of a collimator has been approximated by a Gaussian with the same full width at half height as the triangular function.

Further, the assumption has been made that the probability of scattering of a neutron incident on the monochromator with an angular deviation ϕ from the mean direction is given by

$$W(\phi) \sim \exp(-4\phi^2 \ln 2/\beta^2). \quad (1.3)$$

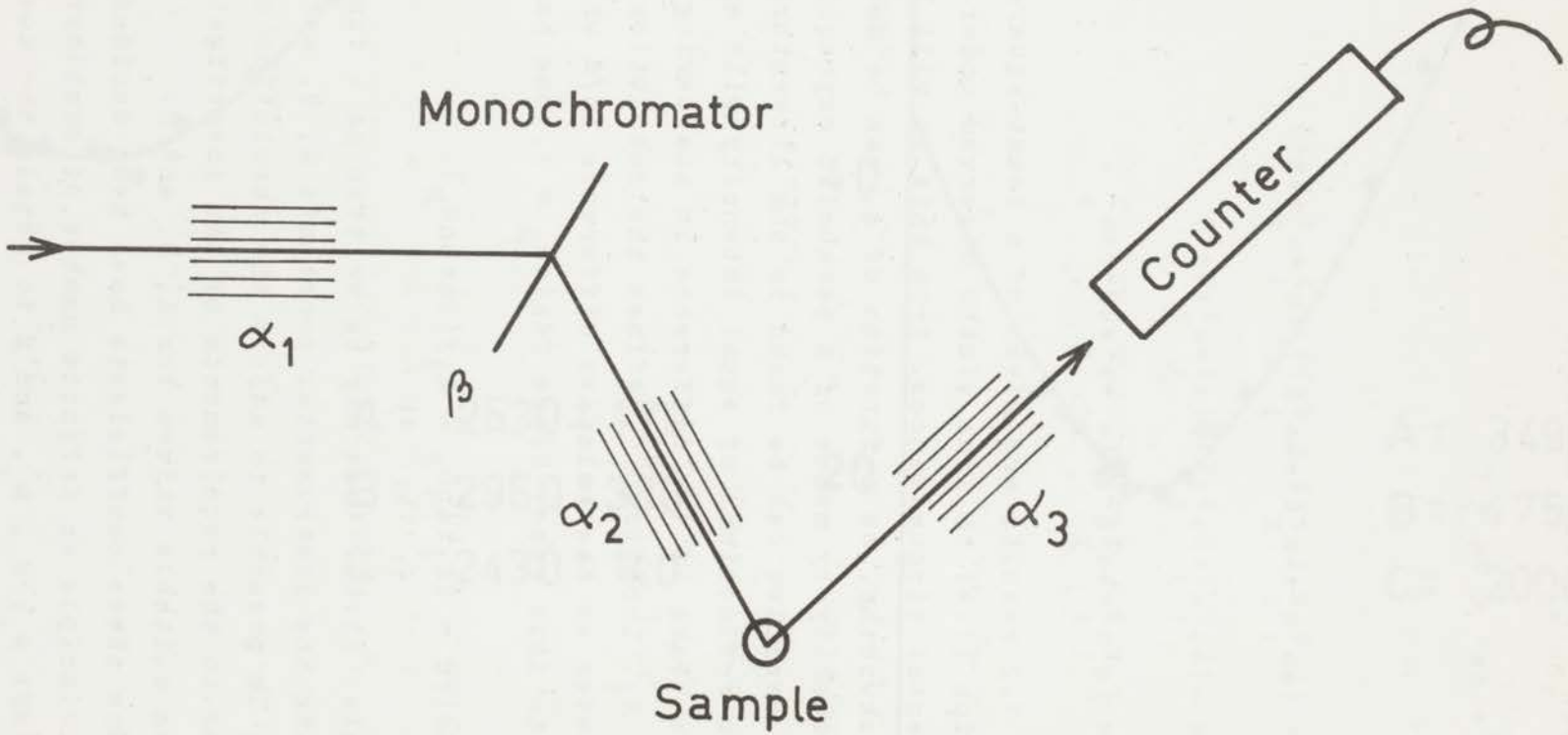

Fig. 1.1
Schematic representation of a neutron powder diffractometer.

Expression (1.1) can be written

$$A_{\frac{1}{2}}^2 = Aa^2 + Ba + C \qquad (1.4)$$

where

$$A = (4\alpha_1^2\alpha_2^2+4\alpha_2^2\beta^2+4\alpha_1^2\beta^2)/(\alpha_1^2+\alpha_2^2+4\beta^2) \ , \qquad (1.5)$$

$$B = -(4\alpha_1^2\alpha_2^2+8\alpha_2^2\beta^2)/(\alpha_1^2+\alpha_2^2+4\beta^2) \ , \qquad (1.6)$$

$$C = (\alpha_1^2\alpha_2^2+4\alpha_2^2\beta^2)/(\alpha_1^2+\alpha_2^2+4\beta^2)+\alpha_3^2 \ . \qquad (1.7)$$

In fig. 1.2 results are given of a least-squares fit of expression (1.4) to line widths observed under different experimental circumstances. From this it will be clear that peakwidths, as a function of a, can be described satisfactorily by means of a parabolic expression (1.4). Further examples can be found in the literature [3,4].

Two reflections of equal intensity will appear as separate peaks if the difference in scattering angle $2\Delta\theta_B$ exceeds $A_{\frac{1}{2}}$. Loopstra [4] defines the resolution of a diffractometer as the relative difference $\Delta d/d$ which corresponds to this case. Since $2d\sin\theta_B = \lambda$, one has

$$|\Delta d|/d = \tfrac{1}{2}A_{\frac{1}{2}}\tan\theta_B = A_{\frac{1}{2}}/(2a\tan\theta_M). \qquad (1.8)$$

Using also (1.4), this may be written as a function of a, involving the instrumental constants A, B, and C.
Thus it is possible to adjust the resolution of the spectrometer to the requirements of the investigation by choosing suitable values for A, B, and C.

Once these coefficients have been decided on, there is in principle an infinite number of combinations of the parameters α_1, α_2, α_3, and β to obtain the coefficients.

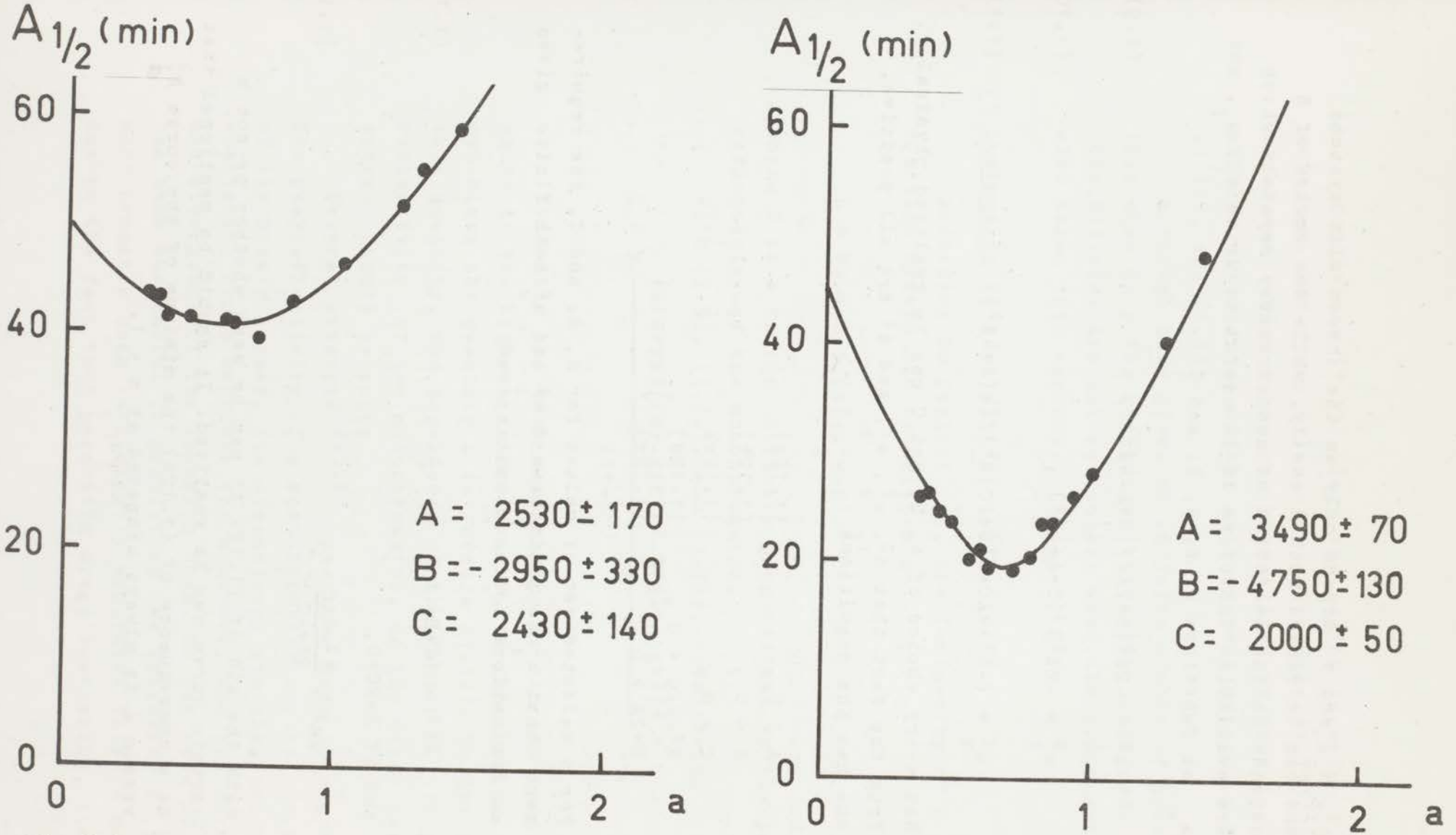

Fig. 1.2

Line-widths in neutron diffraction diagrams of Cr_5S_6 plotted vs $a=\tan\theta_B/\tan\theta_M$. The dots represent the observed full width at half height of peaks in the middle diagram shown in fig.4.4 (left) and the upper diagram (right). The drawn line is the result of a least-squares fit of the parameters A,B, and C. The values of A,B, and C in the figure are given in units of $(min)^2$.

α_1, α_2, and α_3 depend only on the chosen slit systems and can be varied rather easily, while the choice of β depends on the selection of monochromator crystals which are available. Therefore it is useful to write α_1, α_2, and α_3 as functions of β, A, B, and C

$$\alpha_1^2 = -2\beta^2(B+2A)/(B+A-4\beta^2) , \tag{1.9}$$

$$\alpha_2^2 = -2\beta^2 B/(B+A+4\beta^2) , \tag{1.10}$$

$$\alpha_3^2 = \{-B^2+4AC+8(B+2C)\beta^2\}/\{4(A+4\beta^2)\} . \tag{1.11}$$

Not every choice of A, B, and C can be realized physically. From the fact that α_1^2, α_2^2, α_3^2, and β^2 are all positive, one has the conditions

$$A > 0 , \tag{1.12a}$$
$$B < 0 , \tag{1.12b}$$
$$C > 0 , \tag{1.12c}$$
$$B^2-4AC < 0 , \tag{1.12d}$$
$$B+2A > 0 . \tag{1.12e}$$

For a selected set of values for A, B, and C, the requirement that α_3^2 is positive and α_1^2 and α_2^2 both finite gives as limitations to the mosaic spread

$$4\beta^2 > |A+B| \tag{1.13a}$$

and if $B+2C<0$,

$$4\beta^2 < \frac{B^2-4AC}{2B+4C} . \tag{1.13b}$$

With the aid of (1.12) it can be seen whether or not a certain curve can be realized. It should be mentioned that as a consequence of (1.12e) the minimum of the curve $A_{\frac{1}{2}}^2$ versus a is always situated at $a < 1$.

Conditions (1.13) limit the region in which β can be selected. For every value of β satisfying (1.13), the desired resolution curve can be realized by choosing the angular divergences of the slit systems according to (1.9), (1.10), and (1.11).

Although this gives an infinite number of possibilities when only the resolution curve is considered, these possibilities are not equivalent when the luminosity is also taken into account.

1.3 Luminosity

According to Caglioti [1], the luminosity of a diffraction system can be written as

$$L = P\alpha_1\alpha_2\alpha_3\beta/(\alpha_1^2+\alpha_2^2+4\beta^2)^{\frac{1}{2}} \qquad (1.14)$$

where P is a factor directly proportional to the peak-reflectivity of the monochromator.

With (1.9), (1.10), and (1.11), this yields

$$L = P\,\frac{\{B(B+2A)[(B^2-4AC)\beta^2-8(B+2C)\beta^4]\}^{\frac{1}{2}}}{(A+4\beta^2)} \qquad (1.15)$$

Evidently the best combination is the one that results in the highest intensity, or, in other words, that optimizes the quantity L in formula (1.14). To optimize this quantity, the dependence of the factor P, the peak-reflectivity of the monochromator, on the other parameters should be known.

Several attempts [2,5,6] have been made to express the peakreflectivity of a monochromator crystal in terms of its mosaic spread, its dimensions, its absorption, and scattering cross sections for neutrons, and the direction and divergence of the incoming beam. So far none of these has been successful in predicting the intensity of the monochromatic beam sufficiently accurate. This is mainly due to the fact that parasitic Bragg scattering, i.e.

Bragg scattering in all directions other than the desired one, depends on so many parameters that it is not possible to account for it even approximately.

1.4 Optimization

In the following, the reflectivity of a monochromator with divergence β for neutrons travelling in a direction which makes an angle ϕ with the mean direction will be assumed to be

$$I(\beta,\phi) = I_o \exp(-4\phi^2 \ln 2/\beta^2) \qquad (1.16)$$

where I_o is a constant independent of the parameters mentioned above. This means that the peak reflectivity is taken as a constant I_o of the material and that the total reflectivity is assumed to be directly proportional to the crystal divergence. This assumption and its consequences will be discussed later in this chapter.

Now, the optimum arrangement is given by that combination of α_1, α_2, α_3, and β that fulfils (1.5), (1.6), and (1.7) and optimizes

$$L' = \frac{\alpha_1\alpha_2\alpha_3\beta}{(\alpha_1^2+\alpha_2^2+4\beta^2)^{\frac{1}{2}}} . \qquad (1.17)$$

The value of the crystal divergence in the optimum arrangement is obtained from

$$\frac{d \ln L'}{d(\beta^2)} = \frac{d \ln(L/P)}{d(\beta^2)} = 0.$$

Substituting (1.15) in the above formula yields

$$\frac{(B^2-4AC)-16(B+2C)\beta_{opt}^2}{(B^2-4AC)\beta_{opt}^2-8(B+2C)\beta_{opt}^2} - \frac{8}{A+4\beta_{opt}^2} = 0$$

hence

$$4\beta^2_{opt} = (B^2-4AC)/(4C+4B+B^2/A) \ . \qquad (1.18)$$

It may be noted that this result satisfies the condition (1.13b).
The optimum exists only when

$$4C+4B+B^2/A < 0 \qquad (1.19a)$$

and, from (1.13a),

$$(B^2-4AC)/(4C+4B+B^2/A) > |A+B| . \qquad (1.19b)$$

Then, the corresponding collimator divergencies can be obtained by substituting (1.18) in (1.9), (1.10), and (1.11), yielding

$$\alpha^2_{1_{opt}} = - (B^2-4AC)/(8C+4B+2B^2/A) \ , \qquad (1.20)$$

$$\alpha^2_{2_{opt}} = - (B^2-4AC)/(8C+12B+8A+2B^2/A), \qquad (1.21)$$

$$\alpha^2_{3_{opt}} = - (B^2-4AC)/8A \ . \qquad (1.22)$$

When (1.19) has not been fulfilled, the arrangement, which gives maximum intensity, is given by

a) if $4C+4B+B^2/A > 0$, then $4\beta^2_{max} = \infty$,

b) if $4C+4B+B^2/A < 0$ and

$(B^2-4AC)/(4C+4B+B^2/A) < |A+B|$, then $4\beta^2_{max} = |A+B|$.

Summarizing, the following scheme for the selection of the combination of α_1, α_2, α_3, and β that gives the highest possible intensity and results in the wanted resolution curve is obtained:

1) $4C+4B+B^2/A > 0$: $4\beta^2_{max} = \infty$

$$\alpha^2_{1\,max} = (B+2A)/2$$

$$\alpha^2_{2\,max} = -B/2$$

$$\alpha^2_{3\,max} = (B+2C)/2 \ ,$$

2) $4C+4B+B^2/A < 0$

a) $(B^2-4AC)/(4C+4B+B^2/A) > |A+B|$: the optimum arrangement is given by (1.18), (1.20), (1.21), and (1.22).

b) $(B^2-4AC)/(4C+4B+B^2/A) < |A+B|$: $4\beta^2_{max} = |A+B|$, $\alpha^2_{1\,max}$, $\alpha^2_{2\,max}$, and $\alpha^2_{3\,max}$ can be calculated by substitution of the value for $4\beta^2_{max}$ in (1.9), (1.10), and (1.11).

1.5 Discussion

It should be realized that the basis of this scheme and of all the foregoing calculations on the optimum arrangement is the assumption that the peak reflectivity of a monochromator crystal is a constant of the material and independent of the divergence of the crystal. In other words, the calculated optimum arrangement optimizes L' of expression (1.17) instead of L of expression (1.8). Experiments have shown that the peak reflectivity is rather constant for a large number of crystals cut from different ingots. For example, the theoretical upper limit for the peak reflectivity of a monochromator used in transmission

is 50%, while it appeared always possible to obtain with copper crystals values of about 30% by merely adjusting the thickness of the crystal. For monochromator crystals used in reflection the theoretical upper limit is 100% with respect to the incident intensity, while up to 60% has been found.

It will be clear that the assumption of P being constant for large variations of β is not justified. This means that the above criteria for the optimalization of a set-up should not be used indiscriminately. This constitutes also a practical limit because in general one has not at his disposal a large series of crystals covering a broad range of divergencies. The criteria can be used to decide whether it is worthwhile trying to obtain monochromator crystals with higher or lower divergencies in order to increase the luminosity of an existing set-up while keeping the resolving power at the same level. For example, the neutron powder diffractometer at the H.F.R. in Petten is often used with the following parameters: $\alpha_1 = \alpha_3 = 10'$, $\alpha_2 = 60'$, $\beta = 14'$ (fig.1.3).

Calculation shows that the optimum set-up with the same resolution curve should have as parameters: $\alpha_1 = 11.0'$, $\alpha_2 = 39.0'$, $\alpha_3 = 9.1'$, $\beta = 17.8'$. The intensity gain is then 2.3%. It will be clear that it does not pay to realize this arrangement.

For neutron diagrams requiring less resolution, the parameters used up to now are:
$\alpha_1 = \alpha_3 = 30'$, $\alpha_2 = 60'$, $\beta = 14'$ (fig.1.3). The optimum arrangement for the same resolution should be:
$\alpha_1 = 35.8'$, $\alpha_2 = 43.2'$, $\alpha_3 = 23.0'$, $\beta = 41.4'$. The luminosity of these two arrangements is 8.3 and 11.8, respectively, times that of the high resolution arrangement. Hence, the intensity would be improved by 42% by optimizing.

In this case it could be useful to obtain monochromator crystals with a larger divergence. This has not been done because the same diffractometer is used to obtain high and low resolution diagrams. Under these circumstances it is very convenient to change from one resolution to another by interchanging the slit systems only. Thus, to avoid the rather laborious interchanging and subsequent alignment of the diffractometer system, one crystal with the optimum divergence for high resolution is used for all purposes.

One additional remark on the concept of the crystal divergence β should be made. Customarily this quantity is expressed in terms of the mosaic spread η of the crystal by $\beta = 2\eta(2 \ln 2)^{\frac{1}{2}}$. This expression is correct only when secondary extinction can be neglected, a condition that is never fulfilled for suitable monochromator crystals. When secondary extinction cannot be neglected, the peak reflectivity is lower than it should be in the extinction-free case which results in a broadening of the rocking-curve and thus $\beta > 2\eta(2 \ln 2)^{\frac{1}{2}}$. In practice a considerable correction has often to be applied to the measured full width at half height in order to calculate η. For example, for a crystal in the symmetric reflection position this correction amounts to 32% when the peak intensity is 50% of the incident intensity.

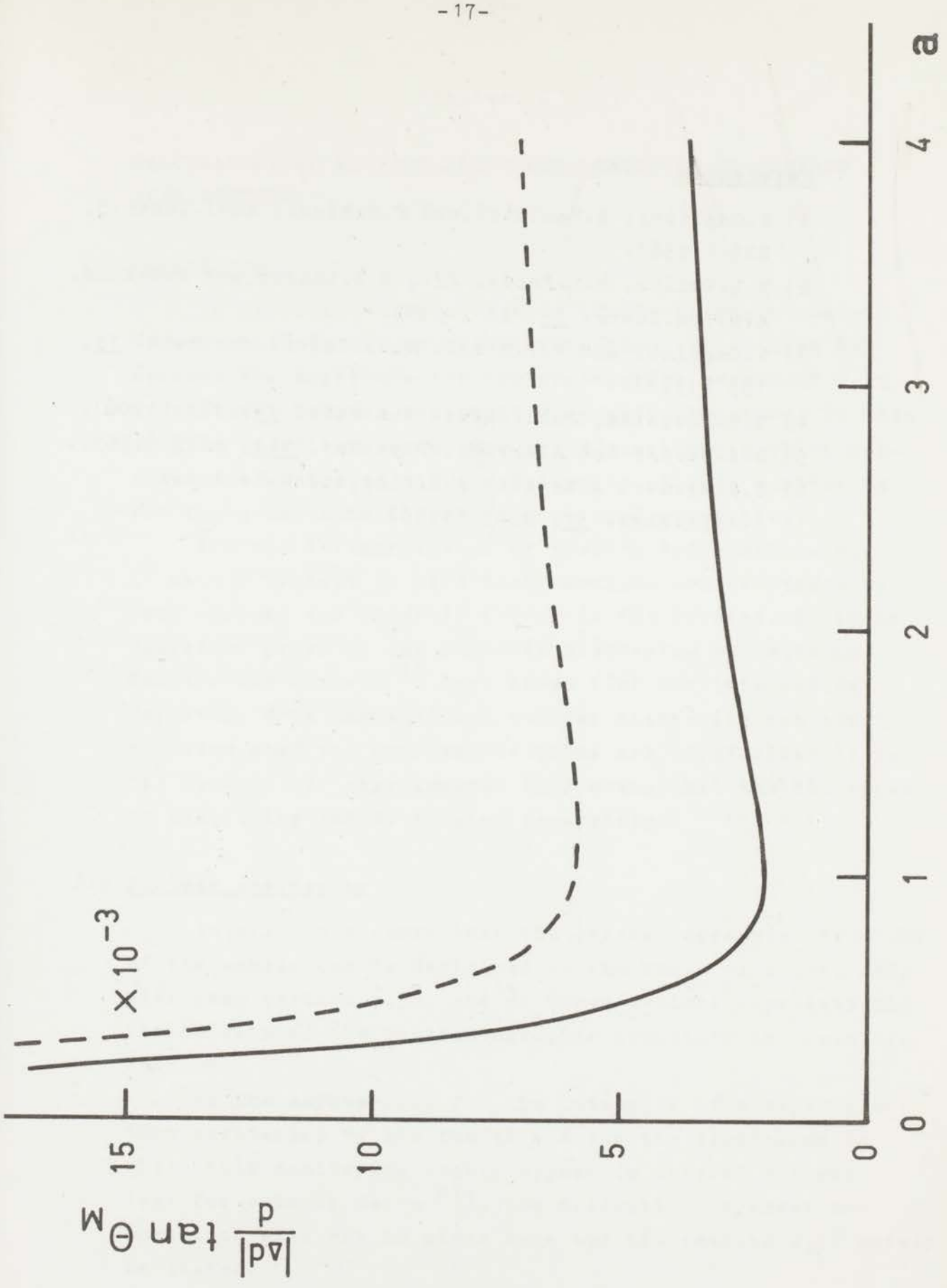

Fig.1.3
Resolution of a neutron powder diffractometer, expressed as $\{|\Delta d|/d\}\tan\theta_M$, as a function of $a=(\tan\theta_B)/(\tan\theta_M)$ for two different sets of parameters. The drawn line represents the resolution for $\alpha_1=\alpha_3=30'$, $\alpha_2=60'$, and $\beta=14'$, the broken line that for $\alpha_1=\alpha_3=10'$, $\alpha_2=60'$, and $\beta=14'$.

References

1) G.Caglioti, A.Paoletti,and F.P.Ricci, Nucl.Instr.3, 223 (1958).
2) V.L.Sailor, H.L.Foote, Jr., H.H.Landon,and R.E.Wood, Rev.Sci.Instr. 27, 26 (1956).
3) G.Caglioti and F.P.Ricci, Nucl.Instr. and Meth. 15, 155 (1962).
4) B.O.Loopstra, Nucl.Instr. and Meth. 44, 181 (1966).
5) S.A.Werner and A.Arrott, Phys.Rev. 140, A675 (1965).
6) S.A.Werner, A.Arrott, J.S.King,and H.Kendrick, J.Appl.Phys. 37, 2343 (1966).

Chapter II

CALCULATION OF NEUTRON INTENSITY SCATTERED BY ORDERED SPIN SYSTEMS

2.1 Introduction

In the introduction of this thesis it has already been mentioned that neutron diffraction can be used to measure the amplitude and the propagation vector of each constituent Fourier component of a spin structure. In this chapter it will be shown how the directions in which neutrons are scattered and the intensity of this scattering are connected with the above mentioned quantities.

For the interpretation of neutron diffraction data it should be kept in mind that neutrons are scattered by both nuclear and magnetic forces in the crystal. In their classical paper on the magnetic scattering of neutrons Halpern and Johnson [1] have shown that the intensities resulting from magnetic and nuclear scattering are purely additive when the incident neutrons are unpolarized as is the case in our experiments. This means that the two types of scattering can be treated separately.

2.2 Nuclear scattering

It will be assumed that the crystallographic structure of the sample can be described on the basis of a unit cell with base vectors $\vec{a}$, $\vec{b}$, and $\vec{c}$. These vectors represent the periodicity of the crystallographic structure in three directions.

As the expressions for the intensity of elastic neutron scattering by the nuclei and for the directions in which this scattering occurs appear in several surveys (see for example Bacon [2]), the derivation of these expressions will not be given here and the results will merely be stated.

Nuclear scattering is appreciable only when the scattering vector $\vec{e}$ satisfies

$$\vec{e} = \vec{H} \text{ , where } \vec{H} = h\vec{a}^* + k\vec{b}^* + l\vec{c}^* \qquad (2.1)$$

$\vec{a}^*$, $\vec{b}^*$, and $\vec{c}^*$ being the base vectors of the lattice reciprocal to that defined by $\vec{a}$, $\vec{b}$, and $\vec{c}$.

The integrated intensity associated with the reciprocal lattice vector $\vec{H}$ is

$$I_{\vec{H}}^{nucl} = C\, F_{\vec{H}} F_{\vec{H}}^* L(\vec{H}) A(\vec{H}) \exp(-B|\vec{H}|^2/2) \text{ ,} \qquad (2.2)$$

where the structure factor $F_{\vec{H}}$ is given by

$$F_{\vec{H}} = \sum_{\nu} b_\nu \exp 2\pi i \vec{H} \cdot \vec{r}_\nu \text{ .} \qquad (2.3)$$

In these expressions C is an instrumental constant, $L(\vec{H})$ is the Lorentz factor, B the overall temperature factor, $A(\vec{H})$ the factor which accounts for the absorption in the sample, b_ν the scattering length of the ν-th atom in the unit cell and $\vec{r}_\nu$ its position vector in the cell. The sum in the expression $F_{\vec{H}}$ is taken over all atoms in the cell.

2.3 Magnetic scattering

The calculations for the magnetic scattering are complicated by the fact that, though all known ordered spin structures are periodic, this periodicity is not necessarily the same as that of the crystallographic structure. To treat the general case the formalism given by Lyon, Kaplan, Dwight, and Menyuk [3] will be used.

Let $\vec{R}_{n\nu}$ be the position of the ν-th atom in the n-th unit cell of the crystal. Then

$$\vec{R}_{n\nu} = \vec{R}_n + \vec{r}_\nu \text{ ,} \qquad (2.4)$$

where $\vec{R}_n = u\vec{a} + v\vec{b} + w\vec{c}$ (u,v,w integers) specifies the position of the n-th cell in the crystal and, as before, $\vec{r}_\nu$ that of the ν-th atom in the unit cell.

If the atom is magnetic, a vector $\vec{S}_{n\nu}$ can be assigned to it which gives the direction and magnitude (in Bohr magnetons) of the magnetic moment. Because of the periodicity of the spin structure, these vectors may be written as a Fourier series

$$\vec{S}_{n\nu} = \sum_{\vec{\tau}} \vec{Q}_\nu(\vec{\tau}) \exp 2\pi i\, \vec{\tau} \cdot \vec{R}_{n\nu} \quad , \tag{2.5}$$

where $\vec{Q}_\nu(\vec{\tau})$ is the Fourier component associated with the propagation vector $\vec{\tau}$. Because the positional periodicity of the magnetic atoms is that defined by the vectors $\vec{a}$, $\vec{b}$, and $\vec{c}$, the vectors $\vec{\tau}$ may be reduced to lie within the first Brillouin zone by adding or subtracting the vector $\vec{H}$ (2.1) an appropriate number of times.

Halpern and Johnson [1] have shown that for unpolarized neutrons the magnetic scattering intensity is proportional to

$$\sigma_{\vec{e}} = |\vec{P}(\vec{e})|^2 - |\hat{e} \cdot \vec{P}(\vec{e})|^2 \quad , \tag{2.6}$$

where

$$\vec{P}_{\vec{e}} = \left(\frac{e^2\gamma}{2mc^2}\right) \sum_{n,\nu} f_\nu(\vec{e}) \vec{S}_{n\nu} \exp 2\pi i\, \vec{e} \cdot \vec{R}_{n\nu} \quad . \tag{2.7}$$

Here e and m are the electron charge and the neutron mass, γ is the magnetic moment of the neutron in nuclear magnetons, c is the velocity of light ($\frac{e^2\gamma}{2mc^2} = 0.2695 \times 10^{-12}$cm), $f_\nu(\vec{e})$ is the formfactor which describes the effect of the spatial distribution of the unpaired electrons, and $\hat{e}$ is the unit vector in the direction of $\vec{e}$.

Substitution of (2.5) results in

$$\vec{P}(\vec{e})=\left(\frac{e^2\gamma}{2mc^2}\right) \sum_{\vec{\tau},\nu} f_\nu(\vec{e})\vec{Q}_\nu(\vec{\tau})\exp 2\pi i(\vec{\tau}+\vec{e})\cdot\vec{r}_\nu \sum_n \exp 2\pi i(\vec{\tau}+\vec{e})\cdot\vec{R}_n \cdot \quad \ldots\ldots (2.8)$$

From the nature of the vectors $\vec{R}_n$ it follows that the sum over n is small unless $\vec{\tau}+\vec{e}$ is very near to one of the reciprocal lattice vectors $\vec{H}$. As a consequence, the magnetic scattering is concentrated in certain directions associated with the scattering vectors $\vec{e} = \vec{H} - \vec{\tau}$.

The integrated intensity is, similarly to (2.2) given by

$$I^{magn}_{\vec{H}-\vec{\tau}} = C\, \sigma_{\vec{H}-\vec{\tau}}\, L(\vec{H}-\vec{\tau})A(\vec{H}-\vec{\tau})\exp(-B|\vec{H}-\vec{\tau}|^2/2), \qquad (2.9)$$

where, in accordance with (2.6),

$$\sigma_{\vec{H}-\vec{\tau}} = |\vec{P}_{\vec{H}-\vec{\tau}}|^2 - |\hat{e}\cdot\vec{P}_{\vec{H}-\vec{\tau}}|^2 \qquad (2.10)$$

and

$$\vec{P}_{\vec{H}-\vec{\tau}} = \left(\frac{e^2\gamma}{2mc^2}\right) \sum_\nu f_\nu(\vec{H}-\vec{\tau})\vec{Q}_\nu(\vec{\tau})\exp 2\pi i\vec{H}\cdot\vec{r}_\nu \ . \qquad (2.11)$$

This result means that in reciprocal space around each point $\vec{H}$ there is an additional number of scattering points equal to the number of nonzero Fourier components which describes the whole spin structure. Components with $\vec{\tau} = 0$, i.e. components with the same periodicity as the nuclear lattice, manifest themselves as scattering at the lattice points of the reciprocal lattice, i.e. in the same directions as the nuclear scattering.

The above formula describes the scattering of neutrons by any spin structure provided that it is periodic. In principle it is possible that for the description of the behaviour of the spin of each magnetic atom in the unit cell one or more Fourier components are needed. Most of the magnetic structures published up to now have the same periodicity as the underlying nuclear structure (only Fourier components with $\vec{\tau} = 0$), or a periodicity which is a simple multiple of it.

Spin structures with periodicities which are a simple multiple of that of the nuclear structure can also be considered as special cases of the general group of structures with periodicities which have no special relation to the repetition period of the nuclear structure. Though it can be advantageous occasionally to use the general description to survey the location of scattering points in reciprocal space, very often a magnetic unit cell is selected which is a multiple of the nuclear cell. No general rules can be given for the decision which choice is the better one because this is determined by the nature of the problem. Even then, it is very often more a matter of taste than of principle.

A smaller number can be described with one value for $\vec{\tau} \neq 0$. Nowadays only one group of spin structures, the antiphase-domain type structures, is known for the description of which one needs a larger number of propagation vectors.

For special cases the above given formula can be simplified considerably. Some examples of this, among which the structure types, met in the experimental work described in the chapters III, IV, and V will be given below.

2.3.1 Collinear spin structure with the same periodicity as the nuclear structure

In a collinear spin structure with the same periodicity as the nuclear structure, Fourier components with $\vec{\tau} \neq 0$ do not exist. The ν-th spin in the n-th unit cell is given by

$$\vec{S}_{n\nu} = \vec{Q}_{\nu}(0) = \pm \hat{z}\mu_{\nu}$$

where $\hat{z}$ is a unit vector parallel to the spin axis and μ_{ν} the moment of the ν-th atom in Bohr magnetons. Magnetic scattering occurs when

$$\vec{e} = \vec{H}$$

and

$$\vec{P}_{\vec{H}} = \left(\frac{e^2\gamma}{2mc^2}\right)\hat{z} \sum_{\nu} \pm \mu_{\nu} f_{\nu}(\vec{H}) \exp 2\pi i \vec{H}\cdot\vec{r}_{\nu}$$

$$\sigma_{\vec{H}} = \{|\hat{z}|^2 - |\hat{e}\cdot\hat{z}|^2\} \left[\left(\frac{e^2\gamma}{2mc^2}\right) \sum_{\nu} \pm \mu_{\nu} f_{\nu}(\vec{H}) \exp 2\pi i \vec{H}\cdot\vec{r}_{\nu}\right]^2$$

$$= \sin^2 \omega \left[\left(\frac{e^2\gamma}{2mc^2}\right) \sum_{\nu} \pm \mu_{\nu} f_{\nu}(\vec{H}) \exp 2\pi i \vec{H}\cdot\vec{r}_{\nu}\right]^2$$

where ω is the angle between $\hat{z}$ and $\vec{e}$.

When the sample is in powder form $\sigma_{\vec{H}}$ should be averaged over all equivalent reflections. It has been shown by Shirane [4] that $\langle\sigma_{\vec{H}}\rangle$ depends only on the angle ψ between $\hat{z}$ and the unique axis when the configurational symmetry of the spin structure is uniaxial (trigonal, tetragonal or hexagonal). Such a symmetry is characterized by the fact that for all crystallographically equivalent reflections the vectors $\vec{P}_{\vec{H}}$ are parallel, or antiparallel and equal in magnitude.

Then

$$\langle\sigma_{\vec{H}}\rangle = \left(\frac{1+\cos^2\eta}{2}\sin^2\psi + \sin^2\eta\cos^2\psi\right)$$

$$\times\left[\left(\frac{e^2\gamma}{2mc^2}\right)\sum_\nu \pm \mu_\nu f_\nu(\vec{H})\exp 2\pi i\vec{H}\cdot\vec{r}_\nu\right]^2 ,$$

where η is the angle between the scattering vector $\vec{e}$ and the unique axis.

When the configurational symmetry is cubic, $\langle\sin^2\omega\rangle$ is $\frac{2}{3}$. In this case it is impossible to determine the direction of the spin axis in the lattice.

2.3.2 Non-collinear spin structure with the same periodicity as the nuclear structure

In non-collinear spin structures with the same periodicity as the nuclear structures, there are as previously no components with $\vec{\tau} \neq 0$ and magnetic scattering occurs again only in directions associated with nuclear reciprocal lattice points i.e.

$$\vec{e} = \vec{H}.$$

In this case

$$\vec{S}_{n\nu} = \vec{Q}_\nu(0) = \hat{K}_\nu\mu_\nu$$

defining $\hat{K}_\nu$ as a unit vector in the direction of the ν-th spin.

Now

$$\vec{P}_{\vec{H}} = \left(\frac{e^2\gamma}{2mc^2}\right)\sum_\nu \hat{K}_\nu\mu_\nu f_\nu(\vec{H})\exp 2\pi i\vec{H}\cdot\vec{r}_\nu$$

$$\sigma_{\vec{H}} = \sin^2\omega\left|\left(\frac{e^2\gamma}{2mc^2}\right)\sum_\nu \hat{K}_\nu\mu_\nu f_\nu(\vec{H})\exp 2\pi i\vec{H}\cdot\vec{r}_\nu\right|^2$$

where ω is the angle between $\vec{P}_{\vec{H}}$ and $\vec{e}$.

For powder samples $\langle\sigma_{\vec{H}}\rangle$ has to be used averaged over all equivalent reflections.

When the configurational symmetry of the spin structure is uniaxial,

$$\langle\sigma_{\vec{H}}\rangle = \frac{1+\cos^2\eta}{2}\left|\left(\frac{e^2\gamma}{2mc^2}\right)\sum_\nu \vec{K}_\nu^{\perp}\,\mu_\nu f_\nu(\vec{H})\exp 2\pi i\vec{H}\cdot\vec{r}_\nu\right|^2 +$$

$$+\sin^2\eta\left|\left(\frac{e^2\gamma}{2mc^2}\right)\sum_\nu \vec{K}_\nu^{//}\,\mu_\nu f_\nu(\vec{H})\exp 2\pi i\vec{H}\cdot\vec{r}_\nu\right|^2,$$

where η is the angle between the unique axis and the scattering vector. $\vec{K}_\nu^{//}$ and $\vec{K}_\nu^{\perp}$ are the components of $\hat{K}_\nu$ parallel and perpendicular to the unique axis.

When the configurational symmetry is cubic, $\langle\sin^2\omega\rangle$ is $\frac{2}{3}$.

2.3.3 Spin structure with a periodicity not equal to that of the nuclear structure

Some examples will be given of spin structures with periodicities which have no special relation to those of the nuclear structure.

2.3.3.1 The magnetic spiral structure

In the magnetic spiral structure the ν-th spin in the n-th cell is given by

$$\vec{S}_{n\nu} = \mu_\nu\{\sin\beta_\nu\left[\hat{x}\cos(2\pi\vec{\tau}\cdot\vec{R}_{n\nu}+\phi_\nu)+\hat{y}\sin(2\pi\vec{\tau}\cdot\vec{R}_{n\nu}+\phi_\nu)\right]+\hat{z}\cos\beta_\nu\}$$

$$= \mu_\nu\left[\frac{\hat{x}-i\hat{y}}{2}\exp i\phi_\nu\exp 2\pi i\vec{\tau}\cdot\vec{R}_{n\nu}\right.$$

$$\left.+\frac{\hat{x}+i\hat{y}}{2}\exp(-i\phi_\nu)\exp(-2\pi i\vec{\tau}\cdot\vec{R}_{n\nu})\right] + \hat{z}\mu_\nu\cos\beta_\nu\,.$$

This expression represents a structure in which the spin lies on a cone with half-angle β_ν and the radial component rotates with a fixed periodicity in a given direction with propagation vector $\vec{\tau}$. Further ϕ_ν is the phase angle of the spin, and $\hat{x}$, $\hat{y}$, and $\hat{z}$ are unit vectors of an orthogonal coordinate system attached to the cone ($\hat{z}$ coincides with the cone axis). When $\beta_\nu = \pi/2$, there is no net moment.

In this case there are three nonzero Fourier components for the ν-th spin i.e.

$$\vec{Q}_\nu(0) = \hat{z}\mu_\nu \cos\beta_\nu \ ,$$

$$\vec{Q}_\nu(\vec{\tau}) = \frac{\hat{x}-i\hat{y}}{2}\,\mu_\nu \sin\beta_\nu \exp i\phi_\nu \ , \text{ and}$$

$$\vec{Q}_\nu(-\vec{\tau}) = \frac{\hat{x}+i\hat{y}}{2}\,\mu_\nu \sin\beta_\nu \exp(-i\phi_\nu).$$

The $\vec{\tau} = 0$ component produces magnetic intensities, commonly called "fundamentals", at the nuclear peak locations ($\vec{e} = \vec{H}$). The other components give rise to magnetic scattering for $\vec{e} = \vec{H} \mp \vec{\tau}$. These peaks are called "satellites".

The relevant magnetic scattering cross sections are given by

$$\sigma_{\vec{H}} = \left[1-(\hat{e}\cdot\hat{z})^2\right]\left[\left(\frac{e^2\gamma}{2mc^2}\right)\sum_\nu \mu_\nu f_\nu(\vec{H})\cos\beta_\nu \exp 2\pi i\vec{H}\cdot\vec{r}_\nu\right]^2$$

$$= \sin^2\omega\left[\left(\frac{e^2\gamma}{2mc^2}\right)\sum_\nu \mu_\nu f_\nu(\vec{H})\cos\beta_\nu \exp 2\pi i\vec{H}\cdot\vec{r}_\nu\right]^2 \ ,$$

$$\sigma_{\vec{H}-\vec{\tau}} = \frac{1}{4}\{|\hat{x}-i\hat{y}|^2-|\hat{e}\cdot(\hat{x}-i\hat{y})|^2\}$$

$$\times \left[\left(\frac{e^2\gamma}{2mc^2}\right)\sum_\nu \mu_\nu f_\nu(\vec{H}-\vec{\tau})\sin\beta_\nu \exp\, i(2\pi\vec{H}\cdot\vec{r}_\nu+\phi_\nu)\right]^2$$

$$= \frac{1+(\hat{e}\cdot\hat{z})^2}{4}\left[\left(\frac{e^2\gamma}{2mc^2}\right)\sum_\nu \mu_\nu f_\nu(\vec{H}-\vec{\tau})\sin\beta_\nu \exp\, i(2\pi\vec{H}\cdot\vec{r}_\nu+\phi_\nu)\right]^2$$

$$= \frac{1+\cos^2\omega}{4}\left[\left(\frac{e^2\gamma}{2mc^2}\right)\sum_\nu \mu_\nu f_\nu(\vec{H}-\vec{\tau})\sin\beta_\nu \exp\, i(2\pi\vec{H}\cdot\vec{r}_\nu+\phi_\nu)\right]^2 ,$$

$$\sigma_{\vec{H}+\vec{\tau}} = \frac{1+\cos^2\omega}{4}\left[\left(\frac{e^2\gamma}{2mc^2}\right)\sum_\nu \mu_\nu f_\nu(\vec{H}+\vec{\tau})\sin\beta_\nu \exp\, i(2\pi\vec{H}\cdot\vec{r}_\nu-\phi_\nu)\right]^2 ,$$

where ω is the angle between the cone axis $\hat{z}$ and $\vec{e}$.

When the configurational symmetry of the magnetic structure is uniaxial and the sample is in powder form, these scattering cross sections have to be averaged over the appropriate reflections. For the fundamental reflections this results in

$$\langle\sigma_{\vec{H}}\rangle = \left(\frac{1+\cos^2\eta}{2}\sin^2\psi + \sin^2\eta\cos^2\psi\right)$$

$$\times \left[\left(\frac{e^2\gamma}{2mc^2}\right)\sum_\nu \mu_\nu f_\nu(\vec{H})\cos\beta_\nu \exp 2\pi i\vec{H}\cdot\vec{r}_\nu\right]^2 ,$$

where ψ is the angle between $\hat{z}$ and the unique axis, and η the angle between the scattering vector $\vec{e}$ and the unique axis.

For the satellite reflections this averaging is necessary only when the wave vector $\vec{\tau}$ is parallel to the unique axis.

Then

$$\langle \sigma_{\vec{H}\pm\vec{\tau}} \rangle = \left(\frac{1}{4} + \frac{\sin^2\eta}{8}\sin^2\psi + \frac{\cos^2\eta}{4}\cos^2\psi\right) \times \left[\left(\frac{e^2\gamma}{2mc^2}\right)\sum_\nu \mu_\nu f_\nu(\vec{H}\pm\vec{\tau})\sin\beta_\nu \exp i(2\pi\vec{H}\cdot\vec{r}_\nu \mp \phi_\nu)\right]^2 .$$

2.3.3.2 The modulated amplitude type of structure

The modulated amplitude structure is a spin structure in which the magnitude of a single component varies sinusoidally with distance along the propagation vector. In such a structure the ν-th spin in the n-th unit cell can be written as

$$\vec{S}_{n\nu} = \hat{z}\mu_\nu^o \cos(2\pi\vec{\tau}\cdot\vec{R}_{n\nu}+\phi_\nu)$$

$$= \frac{\hat{z}}{2}\mu_\nu^o \exp i\phi_\nu \exp 2\pi i\vec{\tau}\cdot\vec{R}_{n\nu} + \frac{\hat{z}}{2}\mu_\nu^o \exp(-i\phi_\nu)\exp(-2\pi i\vec{\tau}\cdot\vec{R}_{n\nu})$$

where μ_ν^o is the amplitude of the sinusoidal variation of the moment of the ν-atom. Again, ϕ_ν is the phase angle of the ν-th spin and $\hat{z}$ is a unit vector in the direction of the varying spin component.

The nonzero Fourier components for the ν-th spin are

$$\vec{Q}_\nu(\vec{\tau}) = \frac{\hat{z}}{2}\mu_\nu^o \exp i\phi_\nu \text{ and}$$

$$\vec{Q}_\nu(-\vec{\tau}) = \frac{\hat{z}}{2}\mu_\nu^o \exp(-i\phi_\nu) .$$

In this type of structures the varying spin components manifest themselves as scattering in satellite peaks equally spaced in reciprocal space from nuclear lattice points.

The magnetic scattering cross sections are

$$\sigma_{\vec{H}-\vec{\tau}} = \frac{1}{4}\{|\hat{z}|^2 - |\hat{e}\cdot\hat{z}|^2\}\left|\left(\frac{e^2\gamma}{2mc^2}\right)\sum_\nu \mu_\nu^o f_\nu(\vec{H}-\vec{\tau})\exp i(2\pi\vec{H}\cdot\vec{r}_\nu+\phi_\nu)\right|^2 =$$

$$= \frac{\sin^2\omega}{4}\left|\left(\frac{e^2\gamma}{2mc^2}\right)\sum_\nu \mu_\nu^o f_\nu(\vec{H}-\vec{\tau})\exp i(2\pi\vec{H}\cdot\vec{r}_\nu+\phi_\nu)\right|^2 ,$$

$$\sigma_{\vec{H}+\vec{\tau}} = \frac{\sin^2\omega}{4}\left|\left(\frac{e^2\gamma}{2mc^2}\right)\sum_\nu \mu_\nu^o f_\nu(\vec{H}+\vec{\tau})\exp i(2\pi\vec{H}\cdot\vec{r}_\nu-\phi_\nu)\right|^2 ,$$

where ω is the angle between $\hat{z}$ and $\vec{e}$.

When the configurational symmetry of the structure is uniaxial and the wave vector $\vec{\tau}$ is parallel to the unique axis, the averaged scattering cross sections for powder samples are

$$\langle\sigma_{\vec{H}\pm\vec{\tau}}\rangle = \left(\frac{1+\cos^2\eta}{8}\sin^2\psi + \frac{\sin^2\eta}{4}\cos^2\psi\right) \times$$

$$\left|\left(\frac{e^2\gamma}{2mc^2}\right)\sum_\nu \mu_\nu^o f_\nu(\vec{H}\pm\vec{\tau})\exp i(2\pi i\vec{H}\cdot\vec{r}_\nu \mp\phi_\nu)\right|^2 ,$$

where ψ and η are the angles the unique axis makes with $\hat{z}$ and $\vec{e}$ respectively.

2.3.3.3 The antiphase domain type of structure

In the antiphase domain type structure the moment at a certain position in the unit cell is parallel to a certain direction in several adjacent unit cells and antiparallel to this direction in the next several unit cells. The resulting structure can be ferrimagnetic or antiferromagnetic.

The periodicity of this structure type is in general equal to an integral number N times the periodicity of the crystallographic structure.

If the wave vector of the crystallographic structure in the direction of the modulation of the spin structure is $\vec{k}$, then the wave vectors of the Fourier components of the spin structure are 0, $\vec{\tau}$, $2\vec{\tau}$, . . . $(N-1)\vec{\tau}$ where $\vec{\tau}=\vec{k}/N$.

The moment distribution for each set of sites is

$$\vec{S}_{n\nu} = \sum_{p} \vec{Q}_{\nu}(p\vec{\tau}) \exp 2\pi i p\vec{\tau}\cdot\vec{R}_{n\nu}$$

where p is an integer ($0 \leq p \leq N-1$) and $\vec{Q}_{\nu}(p\vec{\tau})$ are the Fourier components given by

$$\vec{Q}_{\nu}(p\vec{\tau}) = \frac{1}{N} \sum_{n} \vec{S}_{n\nu} \exp(-2\pi i p\vec{\tau}\cdot\vec{R}_{n\nu}) \; ; \quad (1 \leq n \leq N) \; .$$

A general relation is

$$\vec{Q}_{\nu}[(N-p)\vec{\tau}] = [\vec{Q}_{\nu}(p\vec{\tau})]^{*} \exp(-2\pi i\vec{k}\cdot\vec{r}_{\nu}) \; .$$

If all spins are parallel or antiparallel to a direction given by a unit vector $\hat{z}$, then

$$\vec{Q}(p\vec{\tau}) = \hat{z} Q_{\nu p} \exp i\phi_{\nu p}$$

where $Q_{\nu p}$ and $\phi_{\nu p}$ are the modulus and the phase angle of the Fourier component with wave vector $p\vec{\tau}$.

Magnetic scattering can occur in reciprocal lattice points $\vec{H} - p\vec{\tau}$. These points form rows parallel to $\vec{k}$ and are spaced from each other by $\vec{k}/N$.

For the magnetic scattering cross sections we obtain

$$\sigma_{\vec{H}-p\vec{\tau}} = \sin^2\omega \left[\left(\frac{e^2\gamma}{2mc^2}\right) \sum_{\nu} f_{\nu}(\vec{H}-p\vec{\tau}) Q_{\nu p} \exp i(2\pi\vec{H}\cdot\vec{r}_{\nu}+\phi_{\nu p}) \right]^2 ,$$

where ω is the angle between $\hat{z}$ and $\vec{e}$.

When the configurational symmetry of the structure is uniaxial and $\vec{\tau}$ is parallel to the unique axis, the cross sections for powder samples are

$$\langle \sigma_{\vec{H}-p\vec{\tau}} \rangle = \left(\frac{1+\cos^2\eta}{2} \sin^2\psi + \sin^2\eta \cos^2\psi\right) \times \left[\left(\frac{e^2\gamma}{2mc^2}\right) \sum_\nu f_\nu(\vec{H}-p\vec{\tau}) Q_{\nu p} \exp i(2\pi\vec{H}\cdot\vec{r}_\nu + \phi_{\nu p})\right]^2 ,$$

ψ and η having the same meaning as in the preceding sections.

It should be emphasized that, in this type of structure it is not a priori excluded that magnetic scattering occurs in nuclear reciprocal lattice points $\vec{H}$. Whether this scattering is present or not depends only on the value of the constant terms $\vec{Q}_\nu(0)$ in the Fourier series.

2.4 Discussion

In section 2.3, it has been deduced how the magnetic scattering from a certain spin structure will be distributed over the different points in reciprocal space. It has been demonstrated that all Fourier components with the same propagation vector $\vec{\tau}$ manifest themselves as scattering in the reciprocal lattice points $\vec{H} - \vec{\tau}$ with an intensity proportional to

$$\left[\sum_\nu f_\nu(\vec{H}-\vec{\tau}) \vec{Q}_\nu(\vec{\tau}) \exp 2\pi i \vec{H}\cdot\vec{r}_\nu\right]^2 .$$

By measuring the intensity of the scattering for different vectors $\vec{H}$, as many relations between the vectors $\vec{Q}_\nu(\vec{\tau})$ with the same $\vec{\tau}$ will be obtained as measurements, making it in principle possible to determine the values of $|\vec{Q}_\nu(\vec{\tau})|$ for all ν and relative values for the phase angles $\phi_\nu(\vec{\tau})$.

From the intensities on the reciprocal lattice points $\vec{H} - \vec{\tau}'$ information is obtained about the absolute values and the relative phase angles of the components $\vec{Q}_\nu(\vec{\tau}')$ etc. From neutron diffraction intensities it is not possible to obtain information about the relative phases of Fourier components with different wave vectors.

To synthesize the complete spin structure one needs the relative phases of all Fourier components as well as their amplitudes. In general it will not be possible to derive a unique model for the structure from diffraction data alone when more than one wave vector occurs in the spin arrangement and when no relations between the phases of these wave vectors are known.

However, when other information is available, for example when the approximate values of the individual moments are known, it may be possible to derive a unique model for the spin arrangement.

References

1. O.Halpern and M.H.Johnson,Jr., Phys.Rev. 55, 898 (1939).
2. G.E.Bacon, Neutron Diffraction, Clarendon Press, Oxford (1962).
3. D.H.Lyons, F.A.Kaplan, K.Dwight, and N.Menyuk, Phys. Rev. 126, 540 (1962).
4. G.Shirane, Acta Cryst. 12, 282 (1959).

Chapter III

THE MAGNETIC STRUCTURE OF CoO

3.1 Introduction

The compound MnO, FeO, CoO, and NiO have been the subject of many investigations. All of them become antiferromagnetic at sufficiently low temperatures. Above the Néel-temperature, T_N, their crystal structures are cubic of the NaCl type. In the antiferromagnetic state these oxides are no longer cubic, but a distortion occurs [1,2] which causes MnO and NiO to become rhombohedral with $\alpha > 60^\circ$; FeO becomes rhombohedral with $\alpha < 60^\circ$ and CoO tetragonal with $c/a < 1$. This tetragonal distortion of CoO has been studied by Greenwald [3].

The first neutron diffraction experiments on these compounds were carried out by Shull, Strauser, and Wollan [4]. The diffraction patterns in the antiferromagnetic state show that no magnetic intensity is scattered in directions associated with the crystallographic reciprocal lattice, which means that in the spin structure there is no Fourier component with propagation vector $\vec{\tau} = 0$. All peaks of magnetic origin could be indexed by doubling the pseudo cubic unit-cell sides in all three directions, apart from the above-mentioned crystallographic distortion. The reflection condition, h, k, l all odd, for the magnetic intensities shows immediately that in the magnetic structure each spin has antiparallel partners at vector distances $(0,0,\frac{1}{2})$, $(0,\frac{1}{2},0)$, $(\frac{1}{2},0,0)$. This provided the first direct experimental proof of the existence of a superexchange interaction between two metal-ions through an intermediate oxygen ion as first postulated by Kramers [5]. It follows that there are also parallel partners at $(\frac{1}{2},\frac{1}{2},0)$, $(\frac{1}{2},0,\frac{1}{2})$, $(0,\frac{1}{2},\frac{1}{2})$ and a antiparallel one at $(\frac{1}{2},\frac{1}{2},\frac{1}{2})$. If we call such an antiferromagnetic set of spins a submotive, the 32 spins in the magnetic unit cell form four submotives.

The relative orientation of these four submotives, has to be deduced from the intensities of the magnetic reflections.

It has been shown by Li [6] that for a single-spin-axis (or collinear) arrangement, in which all moments are parallel or antiparallel to a given direction, there are two different ways in which the four face-centered submotives can be combined in order to conserve the concept of antiparallel coupling between next-nearest neighbours.

These two possibilities are model A and model B, as designated by Li in his paper. In type A the four submotives are correlated such that on each (111) plane the spins are parallel with antiparallel coupling between spins on adjacent (111) planes; in type B such ferromagnetic planes are absent. The configurational symmetry of the spins in model A is compatible with a rhombohedral deformation in the antiferromagnetic state, while in model B it is compatible with a tetragonal deformation.

From their neutron diffraction data Shull et al. [4] concluded that in all four oxides the spin structure was according to model A. They reported the spin axis in MnO, CoO, and NiO to be parallel to [100] and in FeO parallel to [111].

Having re-examined these magnetic structures with a better experimental arrangement, Roth [7] also concluded that the spin ordering should be described with model A, but with different directions for the spin axes. His conclusions were: (a) in MnO and NiO the spin axis is in the (111) plane; (b) in FeO the spin axis is along the [111] axis; (c) in CoO the spin axis is parallel to $[11\bar{7}]$ thus making an angle of 11.5° with the tetragonal c axis. Evidently the arrangement of moments in MnO, FeO, and NiO is consistent with the crystal deformation below the Néel-point in the sense that the unique crystal axis is perpendicular to the ferromagnetically coupled sheets.

This correlation is absent in the case of CoO, a fact which drew the attention of various workers in this field. In general two possible mechanisms for the deformation in the antiferromagnetic state were distinguished by the various authors: (a) magnetostriction related to the anisotropy energy and depending on the orientation of the magnetic moments in the crystal lattice, and (b) exchange-striction related to the exchange energies as a function of the interionic distances and thus depending on the relative arrangement of the magnetic moments only and not on their orientation in the lattice.

Greenwald and Smart [8,9] based their discussion on the exchange interactions and proposed a model for the magnetic structure of CoO that explained the tetragonal deformation. However, in this model moments on next-nearest cobalt ions are coupled ferromagnetically, but this is immediately contradicted by the neutron diffraction data. Li [6] adopted the point of view that the deformation is a result of the anisotropy magnetostriction and he proposed for the magnetic structure of CoO three alternative models: the collinear models A and B, mentioned above, with spin axes along the tetragonal c axis and a model C in which two different spin axes, [100] and [010], occur. In a neutron powder diagram in which the tetragonal splitting is not resolved, these three models would yield the same intensities. However, Roth's [7] diffraction study ruled out these three models.

The most extensive theoretical treatment of the magnetic properties of FeO and CoO has been given by Kanamori [10]. He computed the anisotropy energies considering them to originate from four sources: (a) magnetic dipole-dipole interactions, (b) spin-orbit interactions, (c) orbit-orbit interactions, and (d) the anisotropy energy arising from deformation. His conclusion was that the magnetostrictive anisotropy energy (d) is the most effective in CoO and that this energy causes the tetragonal deformation.

Furthermore, the deformation dependent anisotropy energy overcomes the other anisotropy energies ((a), (b), and (c)) and this causes the magnetic moments to align themselves along the tetragonal axis. However, if the moments are arranged according to model A, as he assumed to be the case, there is another competing action: the trigonal dipolar anisotropy which tends to order the magnetic moments in the (111) plane. Thus, the direction of the spin axis will be determined by a balancing of the cubic and of the trigonal anisotropies characterized by the constants K and T respectively.

The total anisotropy energy can then be written [10] as:

$$E = K(\alpha^2\beta^2 + \beta^2\gamma^2 + \alpha^2\gamma^2) + T(\alpha\beta + \beta\gamma + \alpha\gamma),$$

where α, β, and γ are the direction cosines of the spin axis. Kanamori estimated K and T to be 20 and 1 cm^{-1} respectively and concluded that the spin axis should deviate about 2^o from the tetragonal axis *).

This theory was modified by Nagamiya and Motizuki [11] who discussed the possibility that in CoO the quantities T and K are different from the values estimated by Kanamori. They concluded that K may be as low as 10 cm^{-1} and T as large as 3 cm^{-1}. With these values the angle of deviation of the spin axis of CoO in model A should be 10^o according to Kanamori's theory. This agreed well with the value of 11.5^o reported by Roth [7].

The interpretation by Roth of his neutron diffraction data was complicated by the fact that, due to the limited resolving power of his neutron powder diffractometer, he was able to measure the total intensity of the cubic forms $\{hkl\}_c$ only, but he recognized that additional information might be obtained if it were possible to measure the intensities of the tetragonal forms $\{hkl\}_t$ and $\{hlk\}_t$ separately.

- - - - - - - - - -

*) See section 3.4.3 for the application of Kanamori's theory to unit-cell deformation.

As the resolving power of the powder diffractometer at the High Flux Reactor at Petten is high enough to separate these reflections, a new investigation of CoO had been undertaken. This investigation will be described in section 3.2. In addition, neutron diffraction measurements were carried out on single crystals of CoO which will be presented in section 3.3.

3.2 Neutron diffraction investigation of a powder sample of CoO

3.2.1 Experimental

The powder sample used in this investigation was prepared from Merck's CoO by heating to 950°C in a nitrogen atmosphere. Chemical analysis showed the composition to be $CoO_{0.97}$*. Neutron diffraction data were collected with the powder diffractometer at the High Flux Reactor. The sample, at liquid-nitrogen temperature, was contained in a cylindrical aluminium sample holder with a diameter of 20 mm and a wall thickness of 0.05 mm.

A monochromatic beam of neutrons with a wave-length of 1.273 Å was obtained from the (111) reflection of a copper monochromating crystal with a thickness of 7 mm. The crystal slab was placed in the symmetrical transmission position with a take-off angle $2\theta_M = 35.5°$. Soller slits with a nominal angular divergence, defined as width divided by full length, of $\alpha_1 = 5.5'$ were mounted between the reactor and the monochromator. The slits in front of the BF_3-counter had a nominal angular divergence of $\alpha_3 = 5'$. No collimator was placed between monochromator and sample. Two different sets of data were taken, one with a sample to counter distance of 74 cm, the other with a distance of 107 cm.

- - - - - - -

*) Thanks are due to Dr.Ir.E.H.P.Cordfunke of the Chemistry Department of R.C.N. for the preparation and analysis of the sample.

3.2.2 Indexing

The peaks in the diagrams were indexed on the basis of a tetragonal unit cell deduced from the cubic unit cell of the paramagnetic state by doubling the cell edges in all directions and a subsequent deformation. The cell parameters obtained by means of a least squares fit of the calculated to the observed scattering angles $2\theta_B$ were

$a = b = (8.530 \pm 0.012)\text{Å}$,
$c = (8.428 \pm 0.012)\text{Å}$,
$c/a = 0.988 \pm 0.003$.

Although in the diagram the separation of the peaks $\{hkl\}_t$ and $\{hlk\}_t$ is not complete, apart from the $\{400\}_t$ and the $\{004\}_t$ which are completely separated, it was still possible to obtain the separate intensities and positions of the peaks by means of the following computer program.

In this program *), it is assumed that the peak shapes can be described with a Gaussian (an assumption which is found to be correct from an analysis of single peaks) and that the full width at half height of both constituent peaks is the same. The program performs a least squares fit of the calculated to the observed peak profile by adjusting the height and position of the constituent peaks and their full width at half height. Examples of peak separations carried out with this program are given in figs. 3.1 and 3.2.

3.2.3 Nuclear scattering

The structure factor for the nuclear intensities (h,k,l all even) can be written for the magnetic unit cell which contains 32 CoO units, i.e.

- - - - - - - - - -

*) This program "PIEKAN" has been written by Ir.H.P.Struch of the Physics Department of R.C.N.

$$F_{hkl} = 32\,(b_{Co} + b_O) \text{ if } h+k+l = 4n\,, \qquad (3.1a)$$

$$F_{hkl} = 32\,(b_{Co} - b_O) \text{ if } h+k+l = 4n+2\,, \qquad (3.1b)$$

$$F_{hkl} = 0 \qquad \text{for all other conditions}\,. \qquad (3.1c)$$

It should be noted that the calculation of the structure factors for the nuclear structure has been carried out on the basis of the magnetic unit cell. This has been done to treat, in the following sections, the magnetic structure as one with a periodicity equal to the nuclear structure.

The intensity of the nuclear peaks is then given by (see section 2.2)

$$I^{nucl}_{hkl} = C\, j_{hkl}\, F^2_{hkl}\, L\{hkl\}A\{hkl\}\, \exp\left(\frac{-B}{2d^2_{hkl}}\right)\,, \qquad (3.2)$$

j_{hkl} being the multiplicity of the reflection {hkl}.

The total removal cross sections σ_T of Co and O at the wave-length used are 31.8×10^{-24} cm^2 and 4.0×10^{-24} cm^2 [12] respectively. The ratio ρ'/ρ between the measured density of the powder sample and the calculated specific density of CoO was 0.33. From these figures it was calculated that the linear absorption coefficient μ of the sample was $\mu = 0.62$ cm^{-1} and hence $\mu R = 0.62$, R being the radius of the sample.

The tabulated values of the absorption factor A(hkl) was obtained from [13]. They range from 0.358 at $\theta=0^o$ to 0.373 at $\theta=30^o$.

By plotting $\ln(I_{obs}/jF^2_{hkl}LA\{hkl\})$ vs $1/2d^2_{hkl}$, for the nuclear reflections the value $B = 0.74\,\text{Å}^2$ was deduced.

The scattering lengths used for the calculation of F are $b_{Co} = 0.245 \times 10^{-12}$ cm and
$b_O = 0.577 \times 10^{-12}$ cm.

For both diagrams the instrumental constant C was calculated. Both quantities B and C are needed to place the observed magnetic intensities on an absolute basis. A comparison of the calculated and observed nuclear intensities is given in table 3.I.

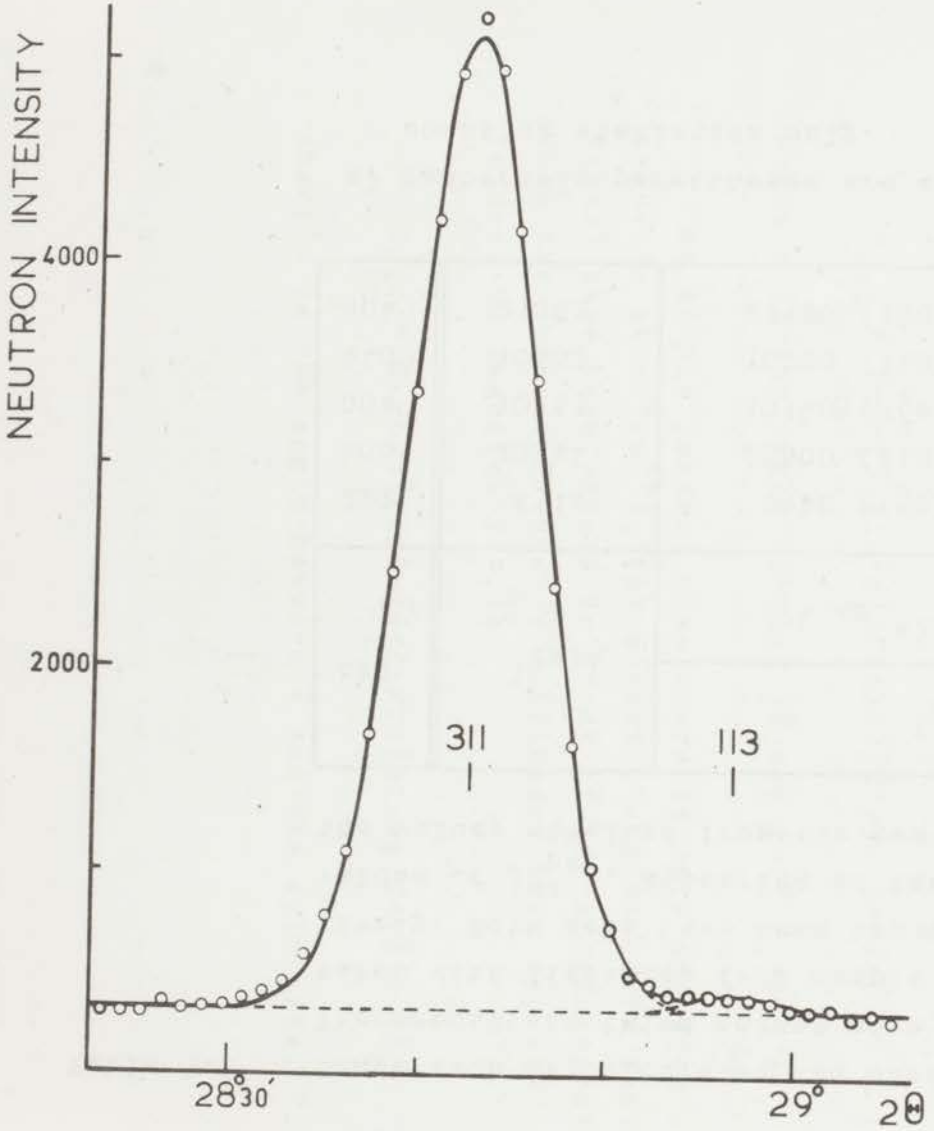

Fig. 3.1
Neutron powder diffraction peaks
$\{311\}_t$ and $\{113\}_t$.

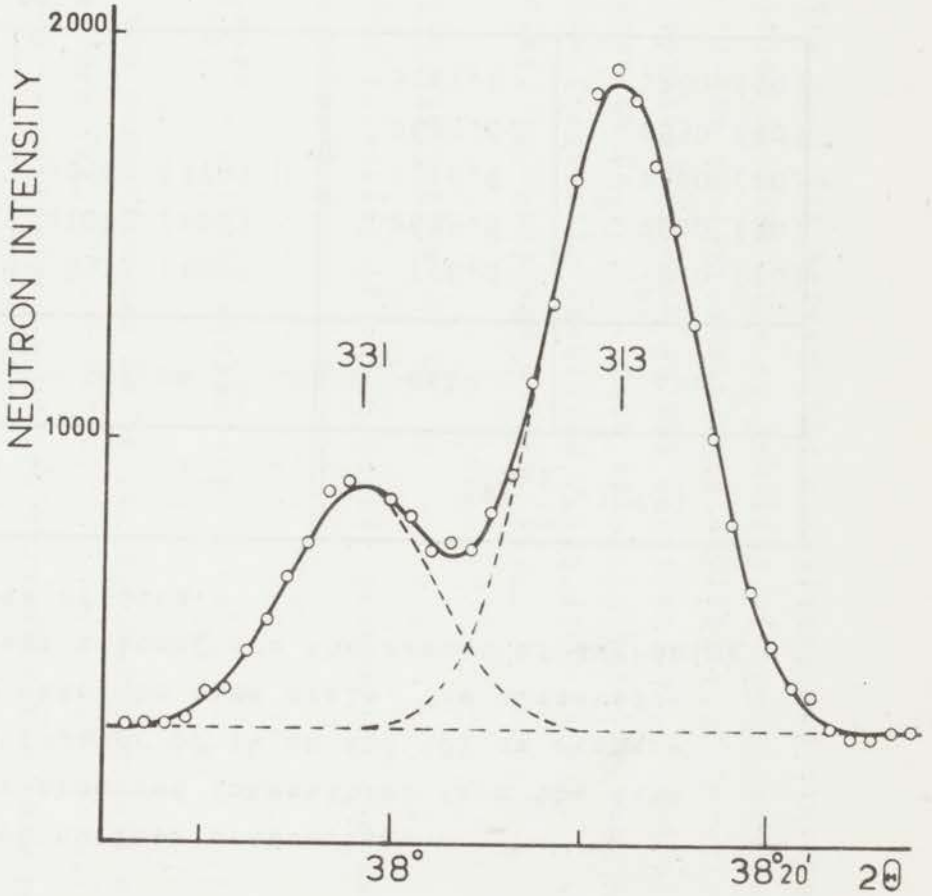

Fig. 3.2
Neutron powder diffraction peaks
$\{331\}_t$ and $\{313\}_t$.

Table 3.I Comparison of calculated and observed nuclear scattering.
The second and third column give the observed intensities from the data taken with distances from sample to counter of 74 cm and 107 cm respectively. Both sets have been brought onto the same scale. The observed values of jF^2_{hkl}, appearing in the last column, are the result of averaging the values obtained from the two sets of data.

hkl	I_{calc}	I_{obs}		$jF^2_{hkl}(\times 10^{24})$	
		74 cm [a]	107 cm [a]	calc	obs [a]
222	8314	8440 (150)	8312 (100)	796.8	810 (20)
400	20744	20500 (210)	21083 (220)	2633.6	2600 (30)
004	10153	10140 (160)	10109 (170)	1316.8	1320 (20)
440	10652	10700 (140)		2633.6	2650 (40)
404	21083	21120 (180)		5267.2	5280 (50)

a) Numbers in parentheses are estimated standard deviations based on counting statistics only.

The good fit between the calculated and observed scattering confirms the reliability of the above-mentioned value of the nuclear scattering amplitude of Co which was first reported by Roth in his paper on CoO [7] and also in his paper on Co_3O_4 [14]. This value is considerably smaller than the frequently tabulated value of 0.28×10^{-12} cm determined by Shull and Wollan [15].

3.2.4 Magnetic scattering

The intensity of the magnetic scattering can be written (see section 2.3)

$$I^{magn}_{hkl} = CL\{hkl\}\, A\{hkl\}\, \exp(-B/2d^2_{hkl}) \sum \sigma_{hkl} \qquad (3.3)$$

where the summation has to be carried out over all members of the form {hkl}.

For an arbitrary spin structure with the same periodicity as the nuclear spin structure (section 2.3.2)

$$\sigma_{hkl} = \left(\frac{e^2\gamma}{2mc^2}\right)^2 \sin^2\omega \left| \mu f\{hkl\} \sum_\nu \hat{K}_\nu \exp 2\pi i \vec{H}\cdot\vec{r}_\nu \right|^2 \qquad (3.4)$$

where ω is the angle between $\sum_\nu \hat{K}_\nu \exp 2\pi i \vec{H}\cdot\vec{r}_\nu$ and $\vec{e}$.

As in the present case there is only one kind of magnetic atom (Co^{++}), the moment μ and the form factor f{hkl} have been placed in front of the summation sign. When the spin structure is collinear, this expression reduces to (section 2.3.1)

$$\sigma_{hkl} = 0.2695^2 \sin^2\omega \left[\mu f\{hkl\} \sum_\nu \pm \exp 2\pi i \vec{H}\cdot\vec{r}_\nu\right]^2 \qquad (3.5)$$

where ω is the angle between $\vec{e}$ and the spin axis.

As has been discussed in section 3.1, it can be concluded from the reflection condition, h,k,l all odd, for the magnetic reflections that the magnetic structure consists of four antiferromagnetic submotives. Thus the spin-structures can be described fully by giving the orientation of four spins each belonging to a different submotive.

In the following these four atoms had been placed, arbitrarely, at $(0,0,0)$; $(\frac{1}{4},0,\frac{1}{4})$; $(\frac{1}{4},\frac{3}{4},\frac{1}{2})$; $(0,\frac{3}{4},\frac{3}{4})$. This means that for any reflection fulfilling the above-mentioned reflection conditions the scattering cross section can be written as

$$\sigma_{hkl} = 0.2695^2 \sin^2 \omega \left| \{8\mu_{Co^{++}} f_{Co^{++}}\{hkl\} [\hat{K}_1 + \hat{K}_2 \exp 2\pi i \frac{h+l}{4} + \hat{K}_3 \exp 2\pi i \frac{h+3k+2l}{4} + \hat{K}_4 \exp 2\pi i \frac{3k+3l}{4}]\} \right|^2 \qquad (3.6)$$

where $\hat{K}_j$ is the unit vector in the direction of the moment of the j-th independent atom, and $\mu_{Co^{++}}$ and $f_{Co^{++}}\{hkl\}$ respectively are the moment of the Co^{++}-ion in Bohr magnetons and the value of the Co^{++}-form factor appropriate to the reflection {hkl}.

Using the values of the scaling factor C and the temperature factor B obtained from the intensities of the nuclear scattering (section 3.2.3), each observed magnetic intensity I^{magn}_{hkl} can be reduced to $\sum \sigma_{hkl}$. Finding the spin arrangement then becomes equivalent to finding the directions of the four unit vectors $\hat{K}_i$ such that the quantities $\sum \sigma_{hkl}$ calculated by means of (3.6) fit the observed values.

Firstly this will be tried by means of a collinear spin arrangement, secondly by a non-collinear model.

3.2.4.1 Collinear model

For a collinear arrangement of the moments, expression (3.6) can be written as

$$\sigma_{hkl} = 0.2695^2 \sin^2\omega \{8\mu_{Co^{++}} f_{Co^{++}}\{hkl\}|k_1 + k_2 \exp 2\pi i\frac{h+l}{4} + k_3 \exp 2\pi i\frac{h+3k+2l}{4} + k_4 \exp 2\pi i\frac{3k+3l}{4}|\}^2 \qquad (3.7)$$

where k_j is a scalar with the values ± 1 depending on whether the moment on the j-th atom is parallel or antiparallel to the spin axis.

As mentioned in section 3.1, Li [6] deduced that there are only two possibilities for combining the four submotives. These two possibilities, model A and model B, are shown in fig.3.3.

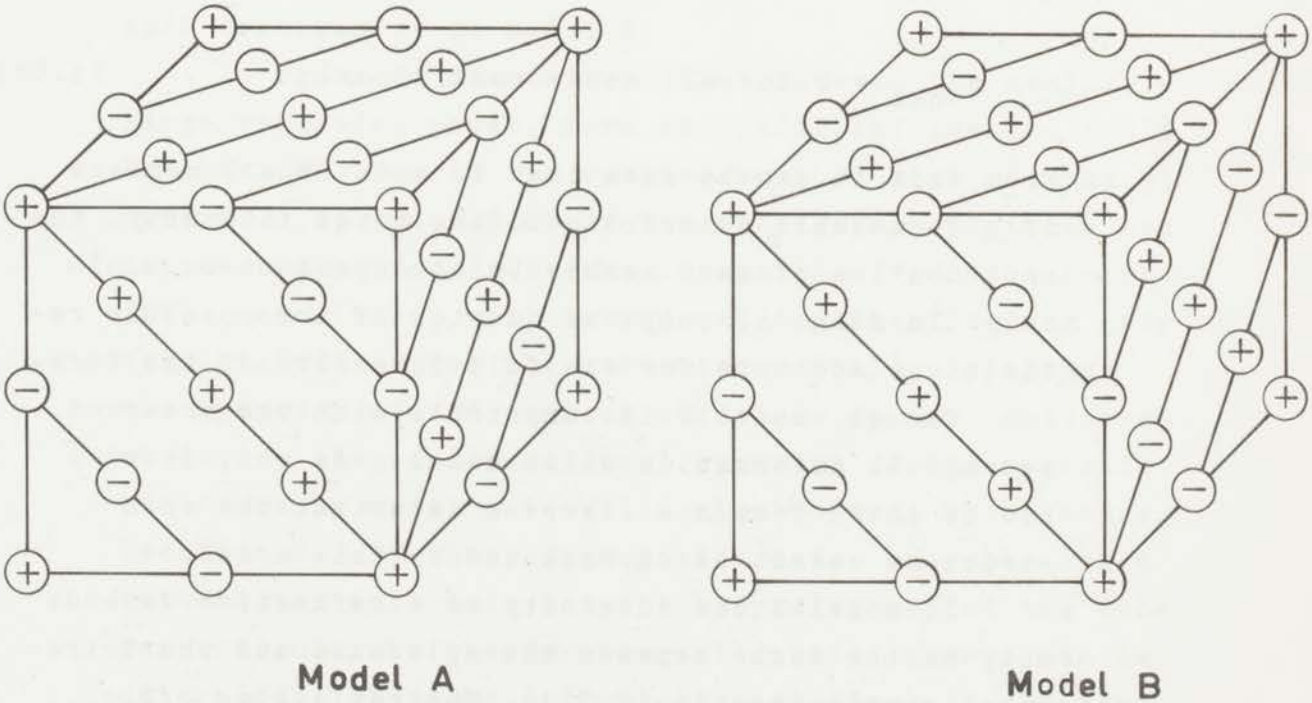

Fig.3.3
The two possibilities for combining the four magnetic submotives subject to the restriction that the spins are parallel or antiparallel to a single magnetic axis.

In model A k_1, k_2, k_3, and k_4 respectively are +1, -1, -1, -1, and in model B +1, -1, +1, -1.

The corresponding expressions for the magnetic scattering cross section (in $10^{-24}cm^2$) for a reflection (hkl) are in model A

$$\sigma_{hkl} = 0.2695^2 \left[64\mu^2_{Co^{++}} f^2_{Co^{++}}\{hkl\}\right] 16 \sin^2\omega$$

for h,k,l all odd and h+k, k+l, h+l = 4n+2, (3.8a)

$$\sigma_{hkl} = 0 \quad \text{for all other conditions} \qquad (3.8b)$$

in model B

$$\sigma_{hkl} = 0.2695^2 \left[64\mu^2_{Co^{++}} f^2_{Co^{++}}\{hkl\}\right] 4 \sin^2\omega$$

for h,k,l all odd, (3.8c)

$$\sigma_{hkl} = 0 \text{ for all other conditions.} \qquad (3.8d)$$

From this it can be seen that in model B all members of a form $\{hkl\}_c$ contribute to the total intensity, the contribution of each member being dependent on $\sin^2\omega$ only. In model A, only one quarter of the possible reflections accounts for the full intensity of the form.

Though model B is compatible with the observed tetragonal deformation while model A is not, it will now be shown from the observed data that the spin structure cannot be represented by this model.

In model B the intensity of a reflection depends only on the angle between the spin axis and the tetragonal c axis (section 2.3.1). The ratio $\Sigma_t\sigma_{311}/\Sigma_t\sigma_{113}$ (Σ_t represents the summation over all reflections in a tetragonal form) is independent of the value of $\mu_{Co^{++}}$ and practically independent of the form factor as the angular difference between the two peaks amounts to only

14' in 2θ. Calculating this ratio for different orientations of the spin axis showed that, when the angle between the spin axis and the c axis varies from 0° to 90°, the ratio $\Sigma_t\sigma_{311}/\Sigma_t\sigma_{113}$ varies gradually from 10.2 to 1.2.

This should be compared with the observed value of this ratio. In fig. 3.1 the peaks $\{311\}_t$ and $\{113\}_t$ are shown. Because the intensity of $\{113\}_t$ is very small, it has to be corrected for the contribution of the nuclear $\{226\}_t$ reflection caused by the second order contamination with $\lambda = 0.637$ Å, in the primary neutron beam. Calculation shows that the observed intensity of $\{113\}_t$ for at least 50% is due to this second order contamination. With this correction it is found that $\Sigma_t\sigma_{311}/\Sigma_t\sigma_{113} > 100$. This immediately rules out model B as a possible model for the spin arrangement.

Therefore the only other possibility for a collinear spin arrangement is model A.

In order to demonstrate that, due to the available large resolving power, more essential information could be obtained then in the earlier work of Roth [7], the data will be treated as if the tetragonal splitting had not been observed, i.e. the intensities from the forms $\{hkl\}_t$ and $\{hlk\}_t$ will be grouped together leaving only the intensities for the cubic forms $\{hkl\}_c$. Although the symmetry of the nuclear structure is now considered as cubic, the configurational symmetry of the magnetic structure in model A is still rhombohedral which means (section 2.3.1) that, from powder data, only the angle between the spin axis and the body diagonal of the cube perpendicular to the ferromagnetic (111) planes can be determined. This had not yet been realized at the time of the investigation by Roth. He assumed, intuitively, that the spin axis lay in the $(1\bar{1}0)$ plane and determined the deviation angle ψ from the c axis by trial and error.

For the observable magnetic reflections, (3.8a) may be written in the form

$$\mu^2_{Co^{++}} = \frac{\Sigma_c \sigma_{hkl}}{\Sigma_c \sin^2\omega} \times \frac{1}{64 f^2_{Co^{++}}\{hkl\} 16 \times 0.2695^2} . \qquad (3.9)$$

When it is assumed with Roth that the spin axis lies in the plane $(1\bar{1}0)$, $\sin^2\omega$ for each reflection may be written as a function of the deviation angle ψ between spin axis and tetragonal axis. Thus, if the form factor $f_{Co^{++}}\{hkl\}$ is also known, each observed $\Sigma_c \sigma_{hkl}$ may be used to calculate $\mu^2_{Co^{++}}$ for every assumed ψ.

Using the formfactor obtained for $KCoF_3$ by Scatturin, Corliss, Elliott, and Hastings [16], curves were obtained for three reflections which are shown in fig.3.4. It may be noted at once that the curves are symmetrical around $\psi = 35.3^\circ$. This corresponds to a spin axis in the (111) plane, showing once more that only the angle between spin axis and rhombohedral axis can be determined.

The correct value of ψ should now correspond to that point on the three curves in fig.3.4 which yield the same value for $\mu^2_{Co^{++}}$ within the limits of accuracy. It is seen, however, that it is hardly possible to select a satisfactory value due to the following circumstances:

a) as the curves are rather flat in the region of interest, the point of intersection of the three curves is difficult to determine,
b) for each value ψ there is a value $70.5-\psi$ which fits as well,
c) the result will be strongly dependent on the choice of form factor.

It is, therefore, necessary to obtain more information.

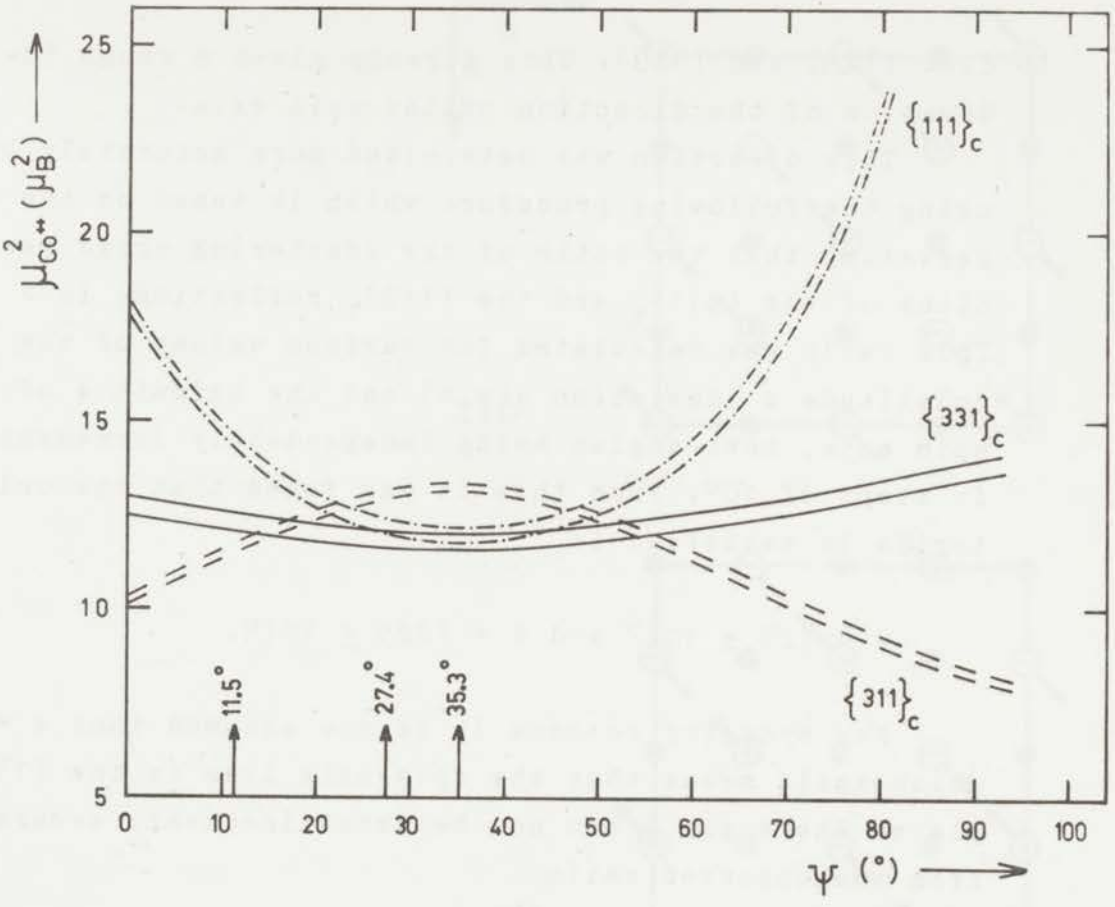

Fig. 3.4
The magnetic moment of the cobalt ion calculated from three observed intensities $\{hkl\}_c$ as a function of the deviation angle ψ, assuming that the spin axis is in the $(1\bar{1}0)$ plane. The width of the bands represent the estimated standard deviation based on counting statistics only.

In the following it will be shown that this may be achieved by measuring the intensities of $\{hkl\}_t$ and $\{hlk\}_t$ separately.

As has been mentioned previously, a salient feature in the neutron diagram is the almost complete absence of the $\{113\}_t$ peak. In model A this can only be explained by a spin axis which is almost perpendicular to those members of the form $\{113\}_t$ for which $h+k, k+l, h+l = 4n\pm2$,

i.e. $(\bar{1}\bar{1}3)$ and $(11\bar{3})$. This already gives a rough indication of the direction of the spin axis.

This direction was determined more accurately by using the following procedure which is based on the observation that the ratio of the scattering cross sections of the $\{311\}_t$ and the $\{113\}_t$ reflections is > 100. This ratio was calculated for various values of the colatitude ψ (deviation angle) and the azimuth ϕ of the spin axis, both angles being independently incremented in steps of 10°. From this it was found that the criterion is satisfied if

$$\psi = (25 \pm 10)^\circ \text{ and } \phi = (225 \pm 15)^\circ.$$

For symmetry reasons it is now assumed that $\phi = 225^\circ$ which again means that the spin axis lies in the $(1\bar{1}0)$ plane. The angle ψ can now be determined very accurately from the observed ratio

$$\Sigma_t\sigma_{331}/\Sigma_t\sigma_{313} = 0.367 \pm 0.008$$

and hence $\psi = (27.4 \pm 0.5)^\circ$. The corresponding direction cosines of the spin axis are $\alpha = \beta = -0.325$, $\gamma = +0.888$. The resulting spin structure is shown in fig.3.5.

The determination of ψ from $\Sigma_t\sigma_{331}/\Sigma_t\sigma_{313}$ is shown in fig.3.6. From this figure the sensitivity of this determination is clearly seen. It should be noted that Roth's value of $\psi = 11.5^\circ$ leads to $\Sigma_t\sigma_{331}/\Sigma_t\sigma_{313} = 0.64$ which is far outside the limits of accuracy of the observation.

A survey of the calculated and observed ratios is given in table 3.II.

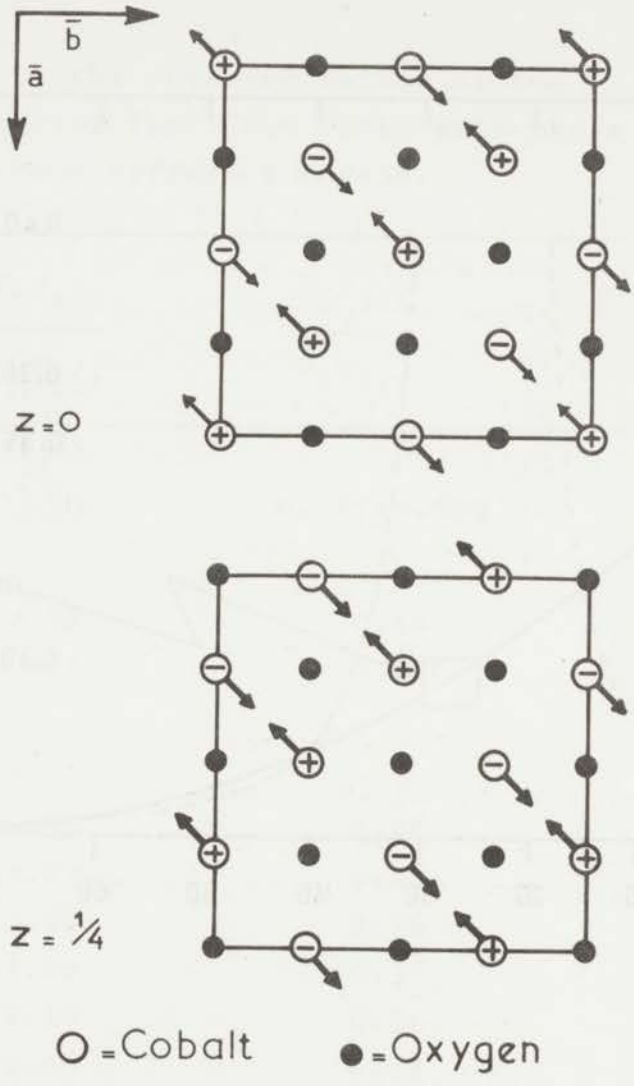

Fig.3.5
Collinear spin structure (model A) of CoO. The plus or minus signs designate the up or down direction into the paper of the z components of the spins. The arrows represent the projection of the spins on the a-b plane. The layers $z = \frac{1}{2}$ and $z = \frac{3}{4}$ can be constructed by reversing the spin directions in the layers $z = 0$ and $z = \frac{1}{4}$ respectively.

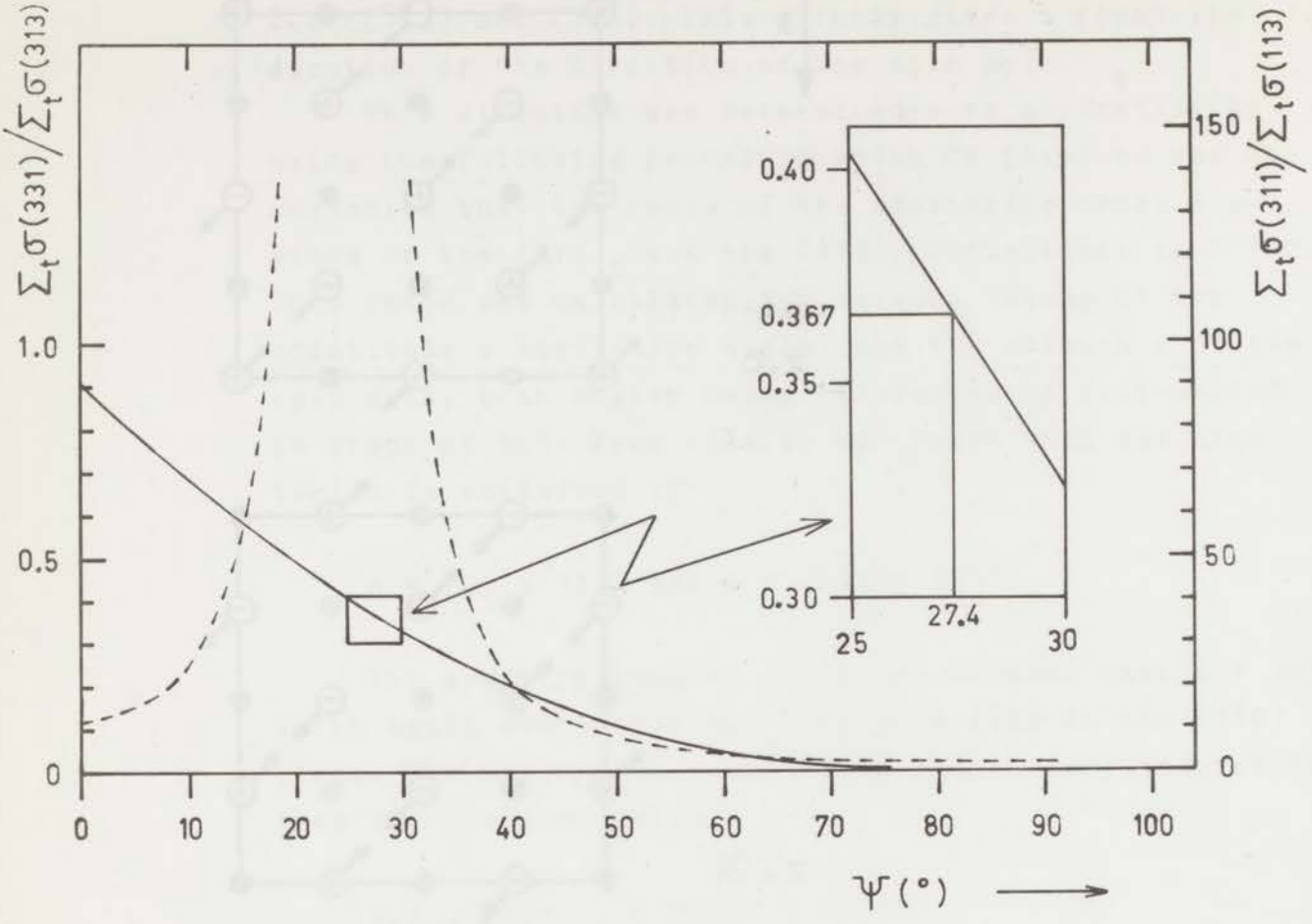

Fig.3.6
The quantities $\Sigma_t\sigma_{331}/\Sigma_t\sigma_{313}$ (drawn line-left hand ordinate) and $\Sigma_t\sigma_{311}/\Sigma_t\sigma_{113}$ (broken line-right hand ordinate) calculated as a function of the deviation angle ψ (spin axis in $(1\bar{1}0)$ plane).

Table 3.II Comparison of the observed ratios of the intensities from {hkl} and {hlk} with those calculated from different models.

	$\frac{\Sigma_t \sigma_{311}}{\Sigma_t \sigma_{113}}$	$\frac{\Sigma_t \sigma_{331}}{\Sigma_t \sigma_{313}}$
Observed	>50	0.367±0.008
Collinear model A:		
$\psi = 11.5^\circ$	32	0.64
$\psi = 27.4^\circ$	158	0.366
Multispin models proposed by Roth:		
I	0.55	0.86
J	1.99	0.03
K	1.20	0.36
R	1.20	0.36
T	1.20	0.36
U	2.06	0.88
V	2.15	0.82
Multispin model proposed in this chapter	158	0.366

It should be noted that in this collinear model for the spin arrangement the direction of the spin axis can also be deduced uniquely from powder data, although the spin structure has a rhombohedral configurational symmetry. This seems to be contradictory to the statement that in such a structure only the angle between the spin axis and the unique axis ([111]) can be determined from powder data (section 2.3.1). That this statement is not valid is due to the tetragonal splitting of the intensities which can be seen as a splitting of the powder lines of the rhombohedral forms into two groups.

As has been shown above, the only assumption necessary for the determination of the spin structure is that the form factor is isotropic. For the determination of the magnetic moment the form factor must be known.

Again using the value given by Scatturin, Corliss, Elliott, and Hastings [16], the moment is calculated to be

$$\mu_{Co^{++}} = (3.52 \pm 0.12)\mu_B \text{ at } T = 78^{\circ}K.$$

In the stated uncertainty of this value, the uncertainty in the form factor has not been taken into account, because it is very difficult to estimate its effect. However, it seems to be safe to assign to $\mu_{Co^{++}}$, in CoO at $T = 78^{\circ}K$, the value $(3.5 \pm 0.2)\mu_B$.
This is somewhat less than the value of $3.80\ \mu_B$ reported by Roth [7], who obtained this result from averaged data over runs at 77 and $4.2^{\circ}K$.

A comparison of the calculated and observed magnetic intensities is given in table 3.III. The agreement in general is very good.

Table 3.III Comparison of calculated and observed magnetic scattering intensities. The third and the fourth column give the observed intensities from the data taken with distances from sample to counter of 74 cm and 107 cm respectively. Both sets have been brought onto the same scale. The observed values of $\Sigma_t \sin^2\eta$, appearing in the last column, are the results of averaging the values from the two sets of data.

hkl	I_{calc}		I_{obs} 74 cm [a]		I_{obs} 107 cm [a]		$\Sigma_t \lvert\sigma_{hkl}/(0.2695^2 \times 64 \mu^2_{Co^{++}} f^2_{Co^{++}}\{hkl\})\rvert$ calc		$\Sigma_t \lvert\sigma_{hkl}/(0.2695^2 \times 64 \mu^2_{Co^{++}} f^2_{Co^{++}}\{hkl\})\rvert$ obs [a]	
111	61006		61711 (1050)		59120 (640)		31.4		32.1 (7)	
311	18645	18761	19860 (280)		19054 (170)		50.7	51.0	50.1 (10)	
113	116						0.3			
331	2855	10586	2670 (90)	9894 (210)	2797 (60)	10366 (150)	18.3	68.4	18.5 (4)	68.9(14)
313	7731		7224 (130)		7569 (90)		50.1		50.4 (10)	
511	5039						61.4			
333	2559	8799	9226 (230)		8524 (120)		31.4	107.6	106.0 (20)	
115	1201						14.9			
531	3146						63.9			
513	1207	5145	5149 (170)		4647 (100)		24.6	104.8	109.0 (40)	
315	792						16.3			

a) Numbers in parentheses are estimated standard deviations in units of the last given decimals based on counting statistics only.

Nevertheless, the objection still holds that this model does not explain the observed tetragonal deformation. Furthermore, in order to explain the angle of deviation of 27.4° by means of the theory of Nagamija and Motizuki [11], a value of 0.55 for the ratio T/K has to be assumed. This would seem to strain beyond acceptable limits the assumptions basic to the theory. Therefore it was tried to find a model that is in accord with this deformation. Such a model should necessarily be non-collinear.

3.2.4.2 Non-collinear model

To conform with the tetragonal symmetry of CoO in the antiferromagnetic state, Roth, in a more recent publication [17], discusses seven multi-spin-axis models, i.e. models in which the spin axes of the four sublattices have different directions. In these seven models, (designated by Roth I, J, K, R, T, U, and V), the different spin axes are all located in the a-b plane or perpendicular to it.

Roth concluded that all these models, except J and V, are consistent with his powder diffraction data due to uncertainties in the Co^{++} form factor. From the present data, however, it is found that all these models must be rejected since they give too low a value for the ratio $\Sigma_t \sigma_{311} / \Sigma_t \sigma_{113}$ (table 3.II).

For a more general approach, one should consider the full range of values for the direction cosines α_i, β_i, and γ_i ($i=1,2,3,4$) of the spins at $(0,0,0)$; $(\frac{1}{4},0,\frac{1}{4})$; $(\frac{1}{4},\frac{3}{4},\frac{1}{2})$; $(0,\frac{3}{4},\frac{3}{4})$, subject to $\alpha_i^2 + \beta_i^2 + \gamma_i^2 = 1$. However, the number of intensities determined in this investigation is insufficient to allow a unique solution. Therefore the following approach has been attempted.

The agreement between observed and calculated intensities given in table 3.III is very good. Thus it seems reasonable to require that the intensities calculated for any non-collinear (multi-spin-axis) model should be equal to those calculated for the collinear (model A) structure discussed in the previous section. Analysis shows (see appendix of this chapter) that there is only one model that fulfils this requirement. This model is given by

$$\alpha_1 = +\alpha \quad , \quad \beta_1 = +\beta \quad , \quad \gamma_1 = +\gamma \quad ,$$
$$\alpha_2 = -\alpha \quad , \quad \beta_2 = +\beta \quad , \quad \gamma_2 = -\gamma \quad ,$$
$$\alpha_3 = -\alpha \quad , \quad \beta_3 = -\beta \quad , \quad \gamma_3 = +\gamma \quad ,$$
$$\alpha_4 = +\alpha \quad , \quad \beta_4 = -\beta \quad , \quad \gamma_4 = -\gamma \quad , \quad \text{where}$$

α, β, γ are the direction cosines of the spin axis in the collinear arrangement ($\alpha=\beta$). The numerical values for these quantities in the multi-spin-axis structure are given in table 3.IV.

Table 3.IV Multi-spin-axis structure of CoO.

atom	direction cosines of spins α_i	β_i	γ_i
1. 0,0,0	-0.325	-0.325	+0.888
2. $\frac{1}{4},0,\frac{1}{4}$	+0.325	-0.325	-0.888
3. $\frac{1}{4},\frac{3}{4},\frac{1}{2}$	+0.325	+0.325	+0.888
4. $0,\frac{3}{4},\frac{3}{4}$	-0.325	+0.325	-0.888

As fig.3.7 shows, the structure found by this procedure does conform to the tetragonal deformation.

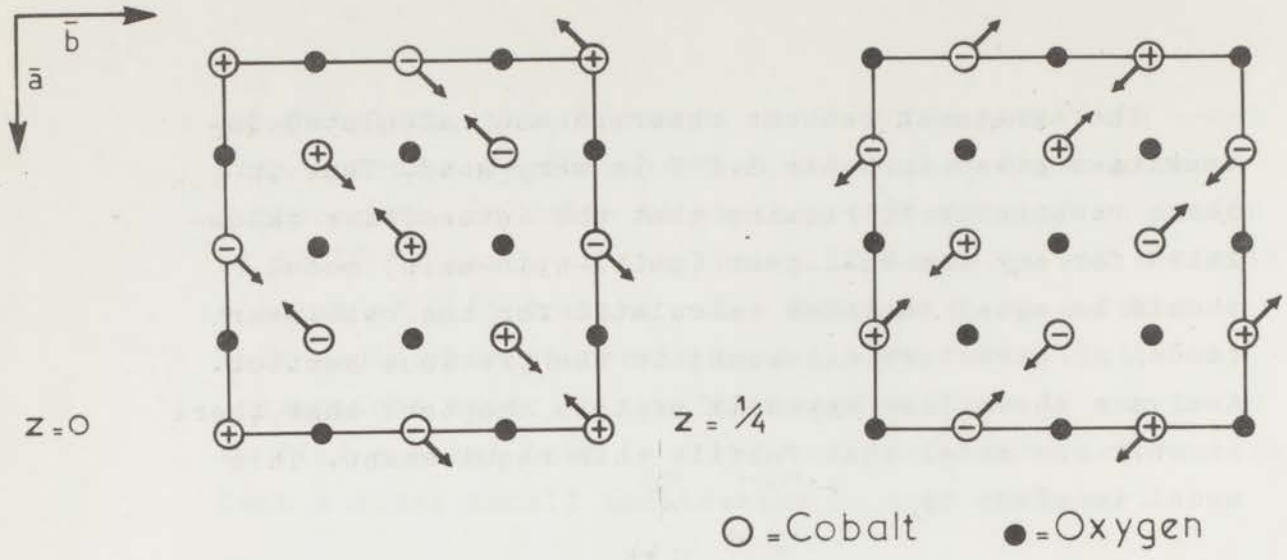

Fig.3.7
Multi-spin-axis structure of CoO. The plus or minus signs designate the up or down direction into the paper of the z components of the spins. The arrows represent the projection of the spins on the a-b plane. The layers $z = \frac{1}{2}$ and $z = \frac{3}{4}$ can be constructed by reversing the spin directions in the layers $z = 0$ and $z = \frac{1}{4}$ respectively.

It should be noted that, while the multi-spin model gives exactly the same intensity for all members of the form $\{hkl\}_t$, in model A one quarter of the possible reflections accounts for the full intensity.

The obtained multi-spin-axis structure is related to Li's [6] model B (section 3.1) in the sense that the z components of the moments are arranged according to this model.

3.3 Neutron diffraction investigations of CoO single crystals *)

As has been mentioned in the previous section, the collinear and the multi-spin-axis model give exactly the same powder neutron-diffraction intensities. This makes it impossible to distinguish between these models on powder data only.

With a single crystal, the multi-spin model leads to the same intensities for the four magnetic reflections (hkl), ($\bar{h}\bar{k}$l), ($\bar{h}$kl), and (h$\bar{k}$l), while in the collinear model only one of these intensities is nonzero, i.e.the one that accounts for the full powder intensity of the form $\{hkl\}_t$. Therefore, an investigation of single crystals of CoO was undertaken as soon as they became available.

3.3.1 Experimental

The crystals used were kindly furnished by Mr. J.Mareschal of the CENG. Having been cut from an ingot grown by the Verneuil-method, they were annealed for 48 h at 1000°C and cooled down slowly in a stream of argon.

Measurements were carried out on two different crystals which we shall designate A and B. Crystal A had been ground to a size of 5.25 × 2.50 × 2.50 mm^3, thus having a perfectly square prismatic shape; crystal B was not reshaped after the cleavage and measured 4.52 × 3.40 × 3.56 mm^3.

In general CoO shows crystallographic twinning below the Néel point, as there are three possible directions for the tetragonal axis when the crystal becomes antiferromagnetic. Uchida et al. [18] have described a method to obtain an almost untwinned antiferromagnetic single crystal. Following this method, the crystal was mounted in a liquid-nitrogen cryostat. During cooling a temperature gradient was set up across the crystal while a small pressure in the vertical direction was applied (fig.3.8).

- - - - - - - - - - - - - -

*) The work described in this section has been carried out at the Centre d'Etudes Nucléaires de Grenoble (CENG), Grenoble, France in cooperation with Mr.J.Schweizer and Mr.R.Lemaire.

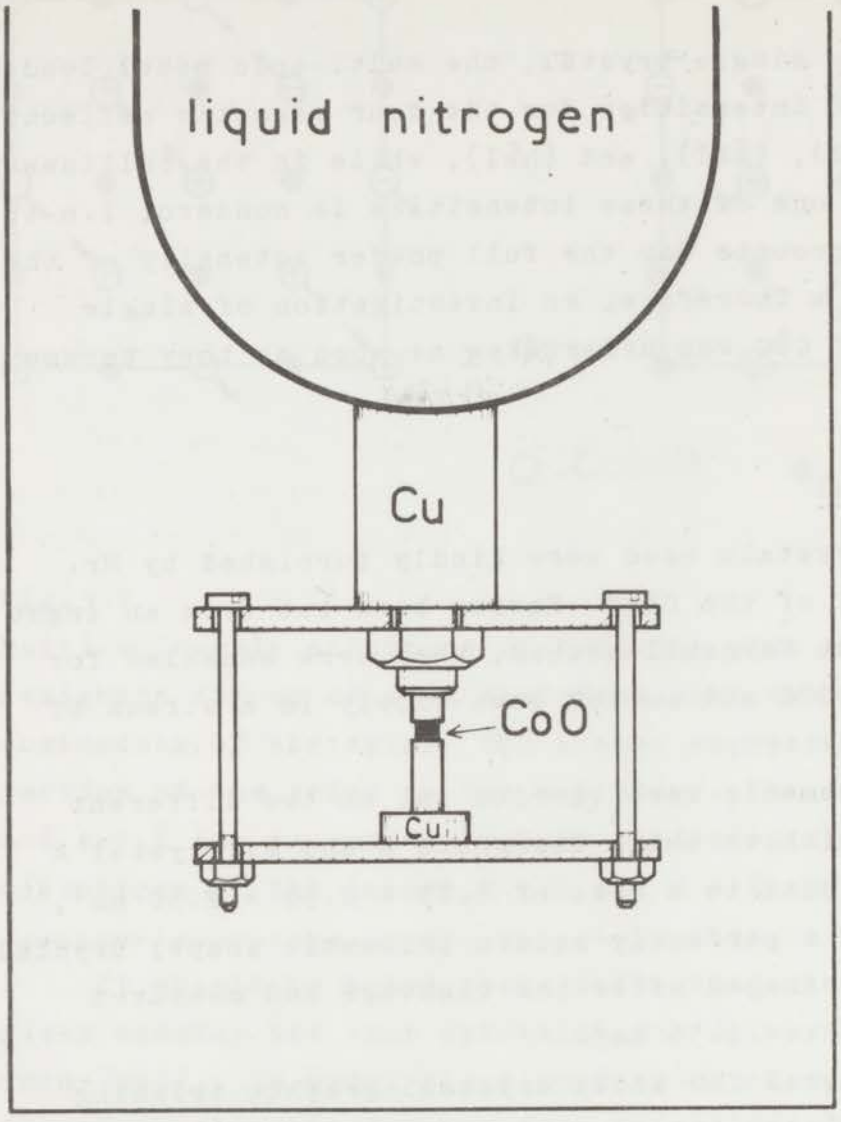

Fig.3.8
Mounting of the crystal in the cryostat, permitting it to cool down in a temperature gradient and under a small vertical pressure.

The whole cryostat was mounted on a goniometer head.

Since it was impossible to rotate the sample around any other axis than the vertical one, the only possibility to collect the intensity data was by using a rotating crystal method with the counter arm tilted at the desired angle.

This facility is available at the DN2 diffractometer, located at the Melusine reactor of the CENG. The monochromator used was a Ge crystal [(113) plane] giving a neutron wavelength of 1.127 Å.

It should be noted that it was only the intention to compare intensities in a group (hkl), ($\bar{h}\bar{k}$l), (h$\bar{k}$l), and ($\bar{h}$kl). The sum of these intensities is known from the powder work (section 3.2).

Intensities from crystal A have been recorded once, but those of crystal B three times with intermediate heating to above the Néel point and recooling.

3.3.2 Twinning

The observed intensities in each group of four reflections are practically equal (table 3.V). We designate as p,q, and r the volume fractions of the crystal tetragonalized along the three possible directions. The values of p,q, and r can be measured at the (440) and (4$\bar{4}$0) reflections. In these reflections the angular separation of the reflections due to the different twins is large enough to separate the intensities quite accurately (fig.3.9). For crystal A this resulted in: p=0.83, q=0, r=0.17; for crystal B in each of the three series of measurements p was greater than 0.98, thus this crystal can be considered as practically untwinned. The two spin models will now be discussed separately.

Table 3.V Observed intensities from CoO single crystals in the antiferromagnetic state. The intensities are given as fractions of the sum of the intensities of the reflections (hkl), $(\bar{h}\bar{k}l)$, $(\bar{h}kl)$, and $(h\bar{k}l)$. The stated uncertainties are calculated from statistical counting errors. For crystal B, data are given for successive cooling and reheating cycles.

(hkl)	crystal A	crystal B 1st cycle	2nd cycle	3rd cycle
040	0.256±0.004	0.253±0.002		
400	0.245	0.245		
$0\bar{4}0$	0.253	0.257		
$\bar{4}00$	0.246	0.245		
440	0.254±0.005	0.252±0.002		
$\bar{4}\bar{4}0$	0.249	0.255		
$\bar{4}40$	0.249	0.247		
$4\bar{4}0$	0.248	0.246		
222	0.260±0.006	0.252±0.004		
$\bar{2}\bar{2}2$	0.260	0.254		
$\bar{2}22$	0.235	0.246		
$2\bar{2}2$	0.245	0.248		
622		0.248±0.005		
$\bar{6}\bar{2}2$		0.253		
$\bar{6}22$		0.251		
$6\bar{2}2$		0.248		
262		0.252±0.005		
$\bar{2}\bar{6}2$		0.252		
$\bar{2}62$		0.250		
$2\bar{6}2$		0.246		
111	0.251±0.002	0.260±0.002	0.262±0.004	0.255±0.004
$\bar{1}\bar{1}1$	0.251	0.248	0.244	0.251
$\bar{1}11$	0.248	0.250	0.250	0.251
$1\bar{1}1$	0.251	0.242	0.244	0.244
311	0.253±0.004	0.267±0.003	0.268±0.005	0.263±0.006
$\bar{3}\bar{1}1$	0.252	0.250	0.248	0.257
$\bar{3}11$	0.248	0.251	0.255	0.246
$3\bar{1}1$	0.247	0.232	0.229	0.235
131	0.246±0.004	0.233±0.003		0.234±0.005
$\bar{1}\bar{3}1$	0.250	0.252		0.251
$\bar{1}31$	0.248	0.254		0.247
$1\bar{3}1$	0.256	0.262		0.269
331	0.250±0.010	0.247±0.005		0.243±0.007
$\bar{3}\bar{3}1$	0.253	0.252		0.260
$\bar{3}31$	0.245	0.241		0.244
$3\bar{3}1$	0.252	0.261		0.253

Table 3.V (continued)

(hkl)	crystal A	1st cycle	crystal B 2nd cycle	3rd cycle
$\bar{5}11$	0.254±0.010	0.264±0.005		0.266±0.009
$\bar{5}\bar{1}1$	0.255	0.254		0.250
$5\bar{1}1$	0.238	0.248		0.243
$5\bar{1}\bar{1}$	0.254	0.235		0.240
$\bar{1}51$	0.249±0.010	0.256±0.005		0.262±0.009
$\bar{1}\bar{5}1$	0.248	0.247		0.242
$1\bar{5}1$	0.258	0.252		0.258
$1\bar{5}\bar{1}$	0.245	0.244		0.239
$\bar{3}13$	0.237±0.010	0.239±0.005		
$\bar{3}\bar{1}3$	0.264	0.239		
$3\bar{1}3$	0.233	0.249		
$3\bar{1}\bar{3}$	0.260	0.272		
$\bar{1}\bar{3}3$	0.235±0.010	0.261±0.005		
$\bar{1}3\bar{3}$	0.254	0.246		
$1\bar{3}3$	0.235	0.248		
$1\bar{3}\bar{3}$	0.277	0.245		
$\bar{3}\bar{3}3$	0.245±0.010	0.271±0.005		
$\bar{3}3\bar{3}$	0.254	0.241		
$3\bar{3}3$	0.232	0.248		
$3\bar{3}\bar{3}$	0.269	0.240		

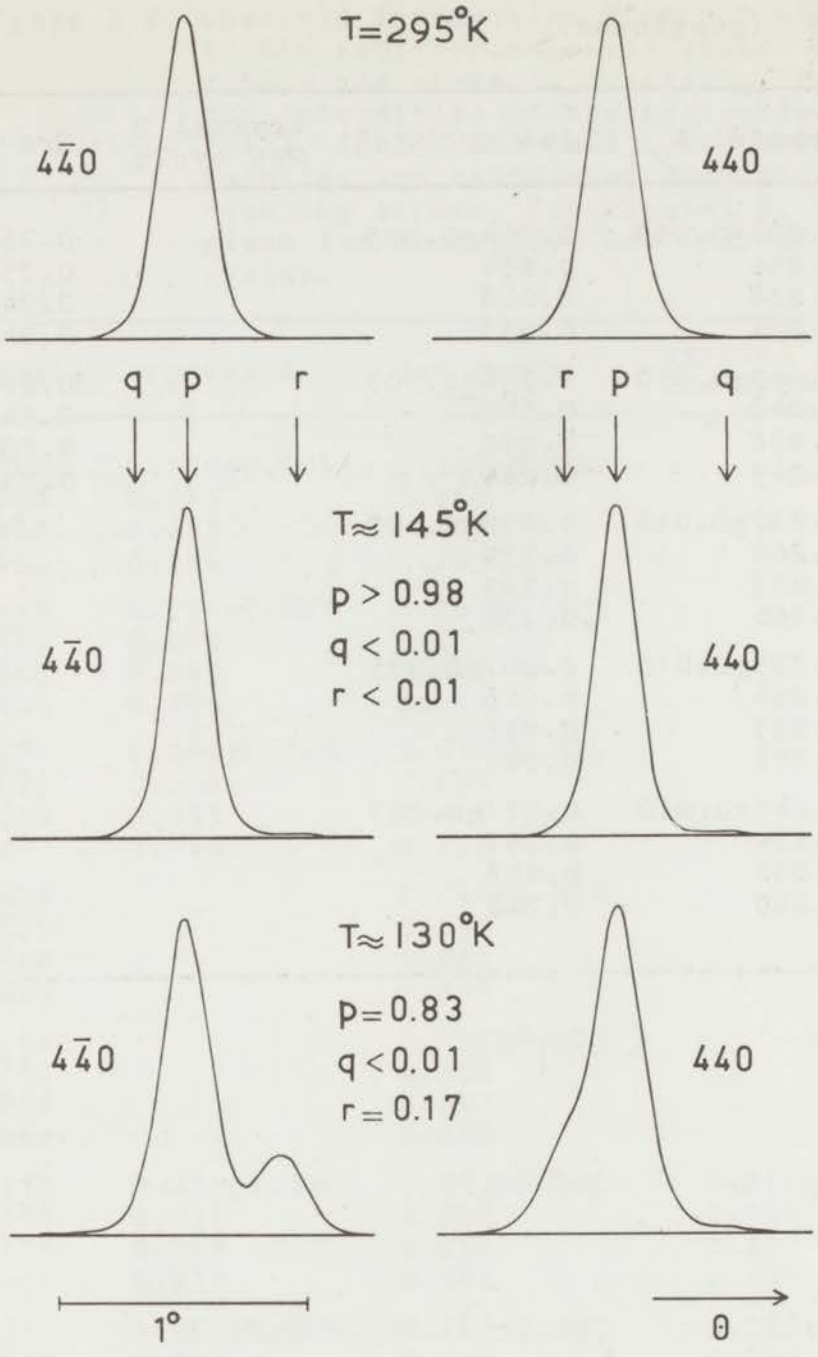

Fig.3.9
Peak shapes of the (440) and the (4$\bar{4}$0)reflections from a crystal at room temperature, crystal B (T≈145°K, practically untwinned) and crystal A (T≈130°K, partially twinned) respectively. The arrows, marked p, q, and r, indicate the calculated positions of the peak due to the different crystallographic twins.

3.3.3 Collinear model

In this model we have to consider the possibility of the existence of four antiferromagnetic domains with different directions of the antiferromagnetic axis in each tetragonal twin p, q, and r. Such an antiferromagnetic domain may be defined as a region in a crystal in which the antiferromagnetic pattern of magnetic moments is triply periodic throughout the volume. The fractions of these domains in part p are denoted by a_p, b_p, c_p, and d_p, etc. When the magnetic domain a_p is in reflection position for reflection (hkl), the intensity is given by

$$I^{magn}_{hkl} \propto \{p\left[a_p\sigma_{hkl} + b_p\sigma_{\bar{k}hl} + c_p\sigma_{\bar{h}\bar{k}l} + d_p\sigma_{k\bar{h}\bar{l}}\right] +$$

$$+ q\left[a_q\sigma_{klh} + b_q\sigma_{l\bar{k}h} + c_q\sigma_{kl\bar{h}} + d_q\sigma_{l\bar{k}\bar{h}}\right] +$$

$$+ r\left[a_r\sigma_{lhk} + b_r\sigma_{\bar{h}lk} + c_r\sigma_{lh\bar{k}} + d_r\sigma_{\bar{h}l\bar{k}}\right]\}.$$

In this expression σ_{hkl} denotes the scattering cross section calculated for domain a_p.

From the results on crystal A the magnetic domain distribution in each twin was calculated by means of a least-squares method. This resulted in

$$a_p = 0.256\pm0.006\ ,\quad a_r = 0.22\pm0.03\ ,$$
$$b_p = 0.246\pm0.006\ ,\quad b_r = 0.23\pm0.03\ ,$$
$$c_p = 0.247\pm0.006\ ,\quad c_r = 0.28\pm0.03\ ,$$
$$d_p = 0.251\pm0.006\ ,\quad d_r = 0.27\pm0.03\ .$$

For crystal B

$$a_p = 0.260\pm0.004\ ,$$
$$b_p = 0.241\pm0.004\ ,$$
$$c_p = 0.246\pm0.004\ ,$$
$$d_p = 0.253\pm0.004\ .$$

These last values deviate slightly from 0.25, but the fact that the measurements, when repeated after a heating and cooling cycle, could be reproduced within statistical counting errors proves that the deviations are not due to a nonequal distribution of the domains, but that absorption effects and small systematic errors only are responsible for them.

Thus the results show clearly that, if the collinear model is correct, it is necessary to assume that in each crystallographic twin any of the four possible antiferromagnetic domains occupy equal volumes.

3.3.4 Multi-spin-axis model

In this model the intensity of a reflection (hkl) is given by

$$I_{hkl}^{magn} \propto \left[p\sigma_{hkl} + q\sigma_{klh} + r\sigma_{lhk}\right].$$

From this expression it is seen that for the multi-spin model the intensity is always equal for the four reflections (hkl), $(\bar{h}k\bar{l})$, $(\bar{h}kl)$, and $(h\bar{k}l)$. This is true even when the crystal is crystallographically twinned. Therefore it is not necessary to assume a completely homogeneous distribution of the antiferromagnetic domains in order to obtain a good fit with the experimental data.

3.4 Discussion

In the sections 3.2 and 3.3 it has been shown that the neutron diffraction data from powder and single-crystal samples can be explained equally well by two different models for the arrangement of the magnetic moments:

a) a collinear model in which all magnetic moments are parallel or antiparallel to a certain direction, i.e. the spin axis. This spin axis lies in the $(1\bar{1}0)$plane and the deviation angle between this axis and the tetragonal c axis is $(27.4\pm0.5)^\circ$. This model is essentially the same as the models proposed earlier by Roth [7] (neutron diffraction) and Nagimija and Motizuki [11] (theoretical calculations based on Kanamori's [10] work), apart from the deviation angle which is given by these authors as 11.5° and 10° respectively. To explain the single-crystal data it has to be assumed that in each crystallographic twin the four possible antiferromagnetic domains have exactly the same volume.

b) a non-collinear (multi-spin-axis) model in which the spin axes of the four antiferromagnetic submotives make an angle of $(27.4\pm0.5)^\circ$ with the c axis, but are not parallel to each other. With this model no further assumptions regarding the distribution of the antiferromagnetic domains have to be made in order to explain the single-crystal data.

It should be emphasized that these two models are the only possibilities compatible with the diffraction data.

During and after the completion of the diffraction work, several other papers on the magnetic structure of CoO were published. For the sake of completeness, some of the results reported in these papers (all obtained with methods other than neutron diffraction) will now be summarized and compared with the above results.

3.4.1 Anisotropy measurements on single crystals

Magnetic anisotropy measurements on CoO single crystals have been published by Uchida et al. [18]. More details have been given in ref. [19]. In these experiments torque measurements were performed on single crystals. To obtain untwinned antiferromagnetic single crystals, the crystals were cooled down either with a temperature gradient along [001] or with a stress applied in the same direction. It was assumed that crystallographically the crystal was almost untwinned ($p \approx 1$, $q = r \approx 0$).

Assuming that only one antiferromagnetic domain is present ($a_p = 1$, $b_p = c_p = d_p = 0$) and that the collinear model is correct, the torques, in sufficiently weak magnetic fields, for rotations around the three crystallographic axes are

$$T_{[001]} = A\left[(\beta^2-\alpha^2)\sin 2\phi_1 + 2\alpha\beta \cos 2\phi_1\right]$$

$$= A \frac{(\beta^2-\alpha^2)}{\cos 2\varepsilon_1} \sin 2(\phi_1+\varepsilon_1),$$

$$T_{[100]} = A\left[(\gamma^2-\beta^2)\sin 2\phi_2 + 2\beta\gamma \cos 2\phi_2\right]$$

$$= A \frac{(\gamma^2-\beta^2)}{\cos 2\varepsilon_2} \sin 2(\phi_2+\varepsilon_2),$$

$$T_{[010]} = A\left[(\alpha^2-\gamma^2)\sin 2\phi_3 + 2\alpha\gamma \cos 2\phi_3\right]$$

$$= A \frac{(\alpha^2-\gamma^2)}{\cos 2\varepsilon_3} \sin 2(\phi_3+\varepsilon_3).$$

Here ϕ_1, ϕ_2, and ϕ_3 are the rotation angles defined as the angles between the magnetic field direction and the reference direction [100], [010], and [001] respectively; α, β, and γ are the direction cosines of the spin axis in the lattice and $A = -\frac{1}{2}(\chi_\perp - \chi_{//})H^2$.

The phase constants ε_1, ε_2, and ε_3 are equal to arctan (α/β), arctan (β/γ), and arctan (γ/α), respectively.

Assuming the existence of four antiferromagnetic domains with a neglegible interaction, the torques are given by

$$T_{[001]} = A\left[(\beta^2-\alpha^2)\sin 2\phi_1+2(a-b+c-d)\alpha\beta \cos 2\phi_1\right] ,$$

$$T_{[100]} = A\left[(\gamma^2-\beta^2)\sin 2\phi_2+2(a-b-c+d)\beta\gamma \cos 2\phi_2\right] ,$$

$$T_{[010]} = A\left[(\alpha^2-\gamma^2)\sin 2\phi_3+2(a+b-c-d)\alpha\gamma \cos 2\phi_3\right] ,$$

where a, b, c, and d are the volume fractions of the antiferromagnetic domains with the spin axis along $\alpha\beta\gamma$, $\alpha\bar{\beta}\gamma$, $\bar{\alpha}\bar{\beta}\gamma$, and $\bar{\alpha}\beta\gamma$ respectively.

When the crystal is not completely untwinned and the three crystallographic twins occur with volume fractions p, q, and r respectively, then

$$\begin{aligned} T_{[001]} = A\{&\left[(p-r)\beta^2+(q-p)\alpha^2+(r-q)\gamma^2\right]\sin 2\phi_1 + \\ &+2\left[p(a_p-b_p+c_p-d_p)\alpha\beta + q(a_q+b_q-c_q-d_q)\alpha\gamma + \right. \\ &\left. + r(a_r-b_r-c_r+d_r)\beta\gamma\right]\cos 2\phi_1\} , \end{aligned}$$

$$\begin{aligned} T_{[100]} = A\{&\left[(p-r)\gamma^2+(q-p)\beta^2+(r-q)\alpha^2\right]\sin 2\phi_2 + \\ &+2\left[p(a_p-b_p-c_p+d_p)\beta\gamma + q(a_q-b_q+c_q-d_q)\alpha\beta + \right. \\ &\left. + r(a_r+b_r-c_r-d_r)\alpha\gamma\right]\cos 2\phi_2\} , \end{aligned}$$

$$\begin{aligned} T_{[010]} = A\{&\left[(p-r)\alpha^2+(q-p)\gamma^2+(r-q)\beta^2\right]\sin 2\phi_3 + \\ &+2\left[p(a_p+b_p-c_p-d_p)\alpha\gamma + q(a_q-b_q-c_q+d_q)\beta\gamma + \right. \\ &\left. + r(a_r-b_r+c_r-d_r)\alpha\beta\right]\cos 2\phi_3\} . \end{aligned}$$

Uchida et al.[18] and Nagamija et al.[19] report that they have observed the following torque curves

a) $T_{[001]} \propto \cos 2(\phi_1+\varepsilon_1)$ with $\varepsilon_1 = \pm 10^{\circ}$,

b) $T_{[100]} = -T_{[010]} \propto \sin 2(\phi_2+\varepsilon_2)$ with $\varepsilon_2 = -3^{\circ}$.

These observations can be explained by assuming that the crystallographic twin with the c axis along the vertical direction predominates and that the other two are present in about equal amounts ($p \gg q \approx r$). Furthermore, the assumption has to be made that in each twin the magnetic domains are not equally represented, an assumption which is contradictory to the results of the neutron diffraction single crystal work (section 3.3). It should be realized that these investigations have been carried out on different samples from different origins, but nevertheless such a different behaviour is hard to understand.

For the multi-spin-axis model the formulae for the torque curves become independent from the domain distribution, i.e.

$$T_{[001]} = A\left[(p-r)\beta^2+(q-p)\alpha^2+(r-q)\gamma^2\right]\sin 2\phi_1 ,$$

$$T_{[100]} = A\left[(p-r)\gamma^2+(q-p)\beta^2+(r-q)\alpha^2\right]\sin 2\phi_2 ,$$

$$T_{[010]} = A\left[(p-r)\alpha^2+(q-p)\gamma^2+(r-q)\beta^2\right]\sin 2\phi_3 .$$

It is clearly seen that it is not possible to describe the observed torque curves with these expressions.

3.4.2 Anisotropy measurements on single-crystal films

Greiner, Berkowitz, and Weidenborner [20] studied the properties of single-crystal CoO films, 3 to 30 μ thick, which were grown epitaxially on MgO by halide decomposition.

Torque curves were taken with these CoO-films after cooling them down in a magnetic field of 20 k Oe. They concluded that, although the distribution of the crystallographic twins had not been affected by this treatment, the distribution of the magnetic domains had been altered.

The toque measurements made on (111) CoO-films (films grown on MgO (111) planes) cooled in a field along $[1\bar{1}0]$, $[01\bar{1}]$, and $[\bar{1}01]$ were consistent with the single- and the multi-spin-axis model. However, the torque data for (001) films cooled in a field along $[\bar{1}10]$ showed that the torque vanished in directions other than $[100]$ and $[010]$. This was inconsistent with the multi-spin-axis model. The data could be interpreted on the basis of the collinear model when two assumptions were made:

a) the crystallographic twins with the tetragonal axis along $[100]$ and $[010]$ were present in equal amounts,
b) the magnetic domains with spin axes most perpendicular to the cooling field were favoured with respect to those with spin axes most parallel to this field.

This experiment, which seems rather conclusive, rules out the multi-spin-axis model and leaves the collinear model, with a spin axis making an angle of 27.4° with the c axis (α=-0.325, β=-0.325, γ=+0.888)as the only possible arrangement of moments in CoO (fig.3.4). This in spite of the rather large value of 0.55 for T/K, required by the theory of Nagamija and Motizuki [11], to explain this model.

3.4.3 Low temperature X-ray diffraction

After the publication [21,22] of the work described in sections 3.2 and 3.3, Saito, Nakahigashi, and Shimomura [23] reported a low temperature (123°K) X-ray diffraction study on CoO single crystals. In their paper they criticized the deduced value of 27.4° for the deviation angle and they concluded that their data can be explained better with the previously deduced value of 11.5°. For this reason their results and conclusions will be discussed more extensively below.

In their X-ray diffraction experiment the incident beam was monochromatized by a LiF or a Ge single crystal and line slits were placed between the X-ray source (NiKα) and the monochromator, and between the monochromator and the specimen. In this way a very high angular resolution was obtained.

With this experimental arrangement, oscillation photographs were taken of the {422} reflections. On these photographs the separation of the reflections $\{422\}_t$ and $\{224\}_t$ was very pronounced and corresponded to a c/a ratio of 0.989. Moreover, it could be observed that both lines were split into doublets. Each doublet consisted of a broad and a narrow line. In order to explain the existence of these doublets, it was assumed that the tetragonal cell underwent a small deformation described by shear strains e_{xy} and $e_{yz} = e_{zx}$ (for the definition of these quantities see, for example, ref. [24]). Saito et al. concluded that the doublets could be indexed when

$$e_{xy} = + 6 \times 10^{-4},$$

$$e_{yz} = e_{zx} = \pm 6 \times 10^{-4}.$$

This means that a slight rhombohedral deformation has been superimposed on the tetragonal cell and it also implies that it is no longer necessary for the spin structure to conform to tetragonal symmetry. The unit-cell parameters at T = 123°K of the deformed NaCl-type structure have been given by Saito et al. as

$$a = b = 4.26\ \text{Å}, \quad c = 4.22\ \text{Å},$$
$$\alpha = \beta = \gamma = 89°58' \text{ with } 4 \text{ CoO per cell.}$$

The magnetic unit cell has been obtained by doubling the a, b, and c edges.

This description has the advantage that the resemblance with the NaCl-type cubic structure of the paramagnetic state has been conserved. It should, however, be realized that the symmetry is now monoclinic and should be described in the monoclinic space group C 2/m (C_{2h}^3) with two CoO units per cell and 2 Co in 2(a): 0,0,0; $\frac{1}{2},\frac{1}{2},0$,
2 O in 2(d): $0,\frac{1}{2},\frac{1}{2}$; $\frac{1}{2},0,\frac{1}{2}$.
The cell parameters at T = 123°K then become

$$a = 5.18^3\ \text{Å}, \quad b = 3.01^5\ \text{Å}, \quad c = 3.01^7\ \text{Å},$$
$$\beta = 125°34'.$$

The edge vectors $\vec{a}_M$, $\vec{b}_M$, and $\vec{c}_M$ of the crystallographic monoclinic cell are related to the edge vectors $\vec{a}_T$, $\vec{b}_T$, and $\vec{c}_T$ of the crystallographic face-centered deformed tetragonal unit cell in the following way:

$$\vec{a}_M = -\tfrac{1}{2}\vec{a}_T - \tfrac{1}{2}\vec{b}_T \pm \vec{c}_T,$$
$$\vec{b}_M = -\tfrac{1}{2}\vec{a}_T + \tfrac{1}{2}\vec{b}_T,$$
$$\vec{c}_M = +\tfrac{1}{2}\vec{a}_T + \tfrac{1}{2}\vec{b}_T.$$

To obtain the monoclinic magnetic unit cell, the c_M-edge has to be doubled.

How this unit cell has to be oriented with respect to the spin arrangement, or, in other words, whether the sign of $\vec{c}_T$ in the expression for $\vec{a}_M$ is plus or minus depends on whether $e_{yz} = e_{zx} = +e_{xy}$ or $e_{yz} = e_{zx} = -e_{xy}$. To distinguish between these two possibilities, a comparison has been made by Saito et al. between the observed deformations and those calculated on the basis of Kanamori's [10] theory.

As has been mentioned in section 3.1, two possible mechanisms for the deformation on the cubic unit cell are considered in this theory:

a) magnetostriction which depends on the direction of the magnetic moments in the lattice. The deformation is given by

$$e_{ii}(M) = B_1\left[\tfrac{1}{3} - \alpha_i^2\right]/(c_{11}-c_{12}) ,$$

$$e_{ij}(M) = -B_2\alpha_i\alpha_j/c_{44} , \quad (i,j = x, y, z) ,$$

where B_1 and B_2 are the magneto-elastic coupling constants, c_{ij} the elastic stiffness constants, and α_i the direction cosines α, β, γ of the spin axis. Using the stiffness constants of MgO (as these data for CoO are not available), Kanamori arrives at

$$e_{ii}(M) = +2.01 \times 10^{-2}\left[\tfrac{1}{3} - \alpha_i^2\right] ,$$

$$e_{ij}(M) = -1.36 \times 10^{-3}\,\alpha_i\alpha_j .$$

The tetragonal contraction is given by

$$(a-c)/a = (e_{xx} - e_{zz})/(1 + e_{xx}).$$

b) exchange striction which depends on the relative orientation of the moments only and not on the direction of the spin axis. The deformation due to the exchange striction is purely rhombohedral and is given by

$$e_{xy}(E) = e_{yz}(E) = e_{zx}(E) = -B_3/c_{44} ,$$

where B_3 is a factor proportional to $-\partial|J|/\partial r$, the dependence of the absolute value of the exchange integral J between nearest neighbour ions on their distance r.
Having made proper estimations for different coefficients, Kanamori arrives at

$$e_{xy}(E) = e_{yz}(E) = e_{zx}(E) = -3 \times 10^{-4} .$$

The total deformation of the cubic cell is then given by

$$e_{ij} = e_{ij}(M) + e_{ij}(E).$$

Saito et al. treat the two possible explanations of the observed deformation separately and as follows.

a) The exchange- and magnetostriction combine in such a way that

$$e_{xy}(E) + e_{xy}(M) = +6 \times 10^{-4} ,$$

$$e_{yz}(E) + e_{yz}(M) = e_{zx}(E) + e_{zx}(M) = -6 \times 10^{-4} .$$

Using the relations $e_{xy}(M)/e_{yz}(M) = \alpha/\gamma$ and $e_{yz}(M) = e_{zx}(M)$, separate values for exchange- and magnetostriction are obtained. These values depend on the assumed value of the angle between spin axis and tetragonal c axis.

For $\alpha_z = 0.985$ (deviation angle of 10°), one obtains

$$e_{xy}(M) \sim 1 \times 10^{-4} ,$$

$$e_{yz}(M) = e_{zx}(M) \sim -(10 \sim 12) \times 10^{-4} ,$$

$$e_{xy}(E) = e_{yz}(E) = e_{zx}(E) \sim +(5 \sim 6) \times 10^{-4} .$$

For $\alpha_z = 0.888$ (deviation angle 27.4°),

$$e_{xy}(M) = \sim 3 \times 10^{-4} ,$$

$$e_{yz}(M) = e_{zx}(M) \sim -9 \times 10^{-4},$$

$$e_{xy}(E) = e_{yz}(E) = e_{zx}(E) \sim +3 \times 10^{-4} .$$

Comparing these results with the values calculated for both cases with Kanamori's theory (given in table 3.VI), Saito et al. reject this alternative.

b) Both strictions combine in such a way that

$$e_{xy}(E) + e_{xy}(M) = +6 \times 10^{-4} ,$$

$$e_{yz}(E) + e_{yz}(M) = e_{zx}(E) + e_{zx}(M) = +6 \times 10^{-4} .$$

In this case it is not possible to obtain separate values for exchange- and magnetostriction. However, Saito et al. conclude arbitrarely that

$$e_{xy}(M) \leq 1 \times 10^{-4} ,$$

$$e_{yz}(M) = e_{zx}(M) \leq 1 \times 10^{-4} ,$$

$$e_{xy}(E) = e_{yz}(E) = e_{zx}(E) \sim +6 \times 10^{-4}.$$

Table 3.VI Values for the coefficients describing the deformation of the cubic unit cell of CoO calculated with Kanamori's theory for two values of the angle between the spin axis and the tetragonal c axis.

	deviation angle	
	10°	27.4°
$\alpha_x = \alpha_y$	-0.122	-0.325
α_z	+0.985	+0.888
$e_{xy}(M)$	-0.2×10^{-4}	-1×10^{-4}
$e_{yz} = e_{zx}(M)$	$+1.6 \times 10^{-4}$	$+4 \times 10^{-4}$
$e_{xx} = e_{yy}(M)$	$+0.64 \times 10^{-2}$	$+0.46 \times 10^{-2}$
$e_{zz}(M)$	-1.28×10^{-2}	-0.92×10^{-2}
(a-c)/a	+1.9 %	+1.4 %
$e_{xy}=e_{yz}=e_{zx}(E)$	-3×10^{-4}	-3×10^{-4}
Total values:		
e_{xy}	-3.2×10^{-4}	-4×10^{-4}
$e_{yz} = e_{zx}$	-1.4×10^{-4}	$+1 \times 10^{-4}$

They claim that the values for the exchange striction agree in order of magnitude with those calculated by Kanamori and that the values for the magnetostriction agree better with the values calculated for a deviation angle of 10° than with those calculated for an angle of 27.4°. It is recognized that the sign of the exchange striction is different in theory and experiment, which means that the theory predicts a compression along the rhombohedral axis while experimentally an elongation has been found. This discrepancy can be removed by changing the sign of $\partial|J|/\partial r$.

It may be noted that this interpretation by Saito et al. of their X-ray data is rather arbitrary.

First of all, it is very difficult to justify the assumption that the sign of $\partial|J|/\partial r$ has to be reversed while the absolute value remains the same. This would mean that the interaction between nearest neighbour ions increases with increasing distance, contrary to the assumption made in the theory.

Furthermore, the observed values

$$e_{xy} = + 6 \times 10^{-4} \quad \text{and}$$

$$e_{yz} = e_{zx} = \pm 6 \times 10^{-4} \quad ,$$

should be compared directly with the total values $(e_{ij}(E) + e_{ij}(M))$ calculated with Kanamori's theory for the two values of the deviation angle given in table 3.VI. This comparison shows beyond doubt that the X-ray data do not permit a choice between the two possibilities.

This means that it is not possible to determine uniquely the direction of the spin axis in the monoclinic unit cell given by Saito et al. and that their conclusion, that the observed deformation should be explained on the basis of Kanamori's theory and the magnetic structure found by Roth [7], is not correct.

It may be added that the observed compression along the c axis of 1.2% is far better explained with a deviation angle of 27.4° then with an angle of 10°. It is doubtful, however, whether it is justified to attach any significance to this fact. It must be concluded that the experimental results of Saito et al. do not provide any conclusive evidence with regard to the magnitude of the deviation angle.

Appendix Chapter III

The aim of the following analysis is to show that there is only one non-collinear model for the spin structure of CoO giving exactly the same powder intensities as the collinear (model A) structure discussed in section 3.2.4.1.

It has been mentioned (section 3.2.4) that the scattering cross section for any reflection with h,k,l all odd can be written as

$$\sigma_{hkl} = \left(\frac{e^2\gamma}{2mc^2}\right)^2 \sin^2\omega \left| 8\mu_{Co^{++}} f_{Co^{++}}\{hkl\}\left[\hat{K}_1 + \right.\right.$$

$$\left.\left. + \hat{K}_2 \exp 2\pi i \frac{h+l}{4} + \hat{K}_3 \exp 2\pi i \frac{h+3k+2l}{4} + \hat{K}_4 \exp 2\pi i \frac{3k+3l}{4}\right]\right|^2 .$$

It will be assumed that the value of the Co^{++} moment in the non-collinear model is the same as in the collinear arrangement which means that this parameter has not to be considered. We now introduce

$$\sigma'_{hkl} = \sin^2\omega |\vec{K}_r|^2 \qquad \text{(A1a)}$$

where

$$\vec{K}_r = \hat{K}_1 + \hat{K}_2 \exp 2\pi i \frac{h+l}{4} + \hat{K}_3 \exp 2\pi i \frac{h+3k+2l}{4} + \hat{K}_4 \exp 2\pi i \frac{3k+3l}{4} =$$

$$= \sum_{j=1}^{4} \hat{K}_j \exp 2\pi i \, \vec{H}\cdot\vec{r}_j \qquad \text{(A1b)}$$

and ω is the angle between $\vec{K}_r$ and $\vec{e} = h\vec{a}^* + k\vec{b}^* + l\vec{c}^*$.

Therefore,

$$\sin^2\omega = 1 - \left[\frac{\vec{e}\cdot\vec{K}_r}{|\vec{e}||\vec{K}_r|}\right]^2 \qquad \text{(A1c)}$$

and

$$\sigma'_{hkl} = |\vec{K}_r|^2 - \left[\frac{\vec{e}\cdot\vec{K}_r}{|\vec{e}|}\right]^2 . \qquad \text{(A1d)}$$

The direction cosines of the moments on the four submotives are defined as

ion	direction cosines		
1. 0, 0, 0	α_1	β_1	γ_1
2. $\frac{1}{4}$, 0, $\frac{1}{4}$	α_2	β_2	γ_2
3. $\frac{1}{4}$, $\frac{3}{4}$, $\frac{1}{2}$	α_3	β_3	γ_3
4. 0, $\frac{3}{4}$, $\frac{3}{4}$	α_4	β_4	γ_4

with $\alpha_j^2 + \beta_j^2 + \gamma_j^2 = 1$.

These direction cosines are proportional to the magnitudes of the components of $\hat{K}_j$ along $\vec{a}$, $\vec{b}$, and $\vec{c}$. In the collinear model A the following relations exist

$$\alpha_1 = -\alpha_2 = -\alpha_3 = -\alpha_4 = \alpha \ , \qquad \text{(A2a)}$$

$$\beta_1 = -\beta_2 = -\beta_3 = -\beta_4 = \beta \ , \qquad \text{(A2b)}$$

$$\gamma_1 = -\gamma_2 = -\gamma_3 = -\gamma_4 = \gamma \ . \qquad \text{(A2c)}$$

To simplify the following discussion, the convention has been adopted that +h, +k, +l refer to those indices of the form $\{hkl\}_t$ for which h+k, k+l, and h+l = 4n+2. The values of the function $\exp 2\pi i \vec{H}\cdot\vec{r}_j$ for all the members of the form are then

	$\exp 2\pi i \vec{H}\cdot\vec{r}_j$			
j →	1.	2.	3.	4.
hkl	+1	-1	-1	-1
$\bar{h}$kl	+1	+1	+1	-1
h$\bar{k}$l	+1	-1	+1	+1
$\bar{h}\bar{k}$l	+1	+1	-1	+1
khl	+1	-1	-1	-1
$\bar{k}$hl	+1	+1	+1	-1
k$\bar{h}$l	+1	-1	+1	+1
$\bar{k}\bar{h}$l	+1	+1	-1	+1

The values for the other eight members can be found by realizing that (hkl) is equivalent to $(\bar{h}\bar{k}\bar{l})$. The magnitudes of the components of $\vec{K}_r$ along $\vec{a}$, $\vec{b}$, and $\vec{c}$ ($\vec{K}_{ra}$, $\vec{K}_{rb}$, $\vec{K}_{rc}$) for a reflection (hkl) are now

$$\vec{K}_{ra} = \sum_{j=1}^{4} \alpha_j \exp 2\pi i \, \vec{H}\cdot\vec{r}_j \, ,$$

$$\vec{K}_{rb} = \sum_{j=1}^{4} \beta_j \exp 2\pi i \, \vec{H}\cdot\vec{r}_j \, ,$$

$$\vec{K}_{rc} = \sum_{j=1}^{4} \gamma_j \exp 2\pi i \, \vec{H}\,\vec{r}_j \, .$$

The condition that $\Sigma_t \sigma'_{hkl}$ for the multi-spin-axis structure should be the same as for model A leads to the following equation

$$\begin{aligned}
&2\Big[(+\alpha_1-\alpha_2-\alpha_3-\alpha_4)^2+(+\beta_1-\beta_2-\beta_3-\beta_4)^2+(+\gamma_1-\gamma_2-\gamma_3-\gamma_4)^2 + \\
&\quad (+\alpha_1+\alpha_2+\alpha_3-\alpha_4)^2+(+\beta_1+\beta_2+\beta_3-\beta_4)^2+(+\gamma_1+\gamma_2+\gamma_3-\gamma_4)^2 + \\
&\quad (+\alpha_1-\alpha_2+\alpha_3+\alpha_4)^2+(+\beta_1-\beta_2+\beta_3+\beta_4)^2+(+\gamma_1-\gamma_2+\gamma_3+\gamma_4)^2 + \\
&\quad (+\alpha_1+\alpha_2-\alpha_3+\alpha_4)^2+(+\beta_1+\beta_2-\beta_3+\beta_4)^2+(+\gamma_1+\gamma_2-\gamma_3+\gamma_4)^2\Big] + \\
&-\Big[(h^2+k^2)|\vec{a}^*|^2+l^2|\vec{c}^*|^2\Big]^{-1} \quad \times \\
&\Big[\{|\vec{a}^*|[h(+\alpha_1-\alpha_2-\alpha_3-\alpha_4)+k(+\beta_1-\beta_2-\beta_3-\beta_4)]+|\vec{c}^*|l(+\gamma_1-\gamma_2-\gamma_3-\gamma_4)\}^2 + \\
&\quad \{|\vec{a}^*|[h(-\alpha_1-\alpha_2-\alpha_3+\alpha_4)+k(+\beta_1+\beta_2+\beta_3-\beta_4)]+|\vec{c}^*|l(+\gamma_1+\gamma_2+\gamma_3-\gamma_4)\}^2 + \\
&\quad \{|\vec{a}^*|[h(+\alpha_1-\alpha_2+\alpha_3+\alpha_4)+k(-\beta_1+\beta_2-\beta_3-\beta_4)]+|\vec{c}^*|l(+\gamma_1-\gamma_2+\gamma_3+\gamma_4)\}^2 + \\
&\quad \{|\vec{a}^*|[h(-\alpha_1-\alpha_2+\alpha_3-\alpha_4)+k(-\beta_1-\beta_2+\beta_3-\beta_4)]+|\vec{c}^*|l(+\gamma_1+\gamma_2-\gamma_3+\gamma_4)\}^2 + \\
&\quad \{|\vec{a}^*|[k(+\alpha_1-\alpha_2-\alpha_3-\alpha_4)+h(+\beta_1-\beta_2-\beta_3-\beta_4)]+|\vec{c}^*|l(+\gamma_1-\gamma_2-\gamma_3-\gamma_4)\}^2 + \\
&\quad \{|\vec{a}^*|[k(-\alpha_1-\alpha_2-\alpha_3+\alpha_4)+h(+\beta_1+\beta_2+\beta_3-\beta_4)]+|\vec{c}^*|l(+\gamma_1+\gamma_2+\gamma_3-\gamma_4)\}^2 + \\
&\quad \{|\vec{a}^*|[k(+\alpha_1-\alpha_2+\alpha_3+\alpha_4)+h(-\beta_1+\beta_2-\beta_3-\beta_4)]+|\vec{c}^*|l(+\gamma_1-\gamma_2+\gamma_3+\gamma_4)\}^2 + \\
&\quad \{|\vec{a}^*|[k(-\alpha_1-\alpha_2+\alpha_3-\alpha_4)+h(-\beta_1-\beta_2+\beta_3-\beta_4)]+|\vec{c}^*|l(+\gamma_1+\gamma_2-\gamma_3+\gamma_4)\}^2\Big] =
\end{aligned}$$

$$= 2\left[(4\alpha)^2+(4\beta)^2+(4\gamma)^2\right]-\left[(h^2+k^2)|\vec{a}^*|^2+1^2|\vec{c}^*|^2\right]^{-1} \times$$
$$\left[\{|\vec{a}^*|\left[k(4\alpha)+h(4\beta)\right] + |\vec{c}^*|1(4\gamma)\}^2\right] \qquad \text{(A3)}$$

Equation (A3) must be valid for all possible combinations of h,k, and 1. This causes equation (A3) to be reduced to

$$\sum_{j=1}^{4} \gamma_j^2 = 4\gamma^2 \quad , \quad \sum_{j=1}^{4} (\alpha_j^2+\beta_j^2) = 4\alpha^2+4\beta^2 \quad , \qquad \text{(A4a)}$$

$$-\alpha_1\beta_3-\alpha_3\beta_1+\alpha_2\beta_4+\alpha_4\beta_2 = 4\alpha\beta \quad , \qquad \text{(A4b)}$$

$$-\alpha_1\gamma_2-\alpha_2\gamma_1+\alpha_3\gamma_4+\alpha_4\gamma_3+\beta_3\gamma_2+\beta_2\gamma_3-\beta_1\gamma_4-\beta_4\gamma_1 = 4(\alpha\gamma+\beta\gamma). \qquad \text{(A4c)}$$

Writing $p\gamma=\gamma_2$, $q\gamma=\gamma_1$, $r\gamma=\gamma_4$, $s\gamma=\gamma_3$, and realizing that in model A $\alpha=\beta$, the following set is obtained

$$p(-\alpha_1+\beta_3)+q(-\alpha_2-\beta_4)+r(+\alpha_3-\beta_1)+s(\alpha_4+\beta_2) = 8\alpha \quad , \qquad \text{(A5a)}$$

$$-\alpha_1\beta_3-\alpha_3\beta_1+\alpha_2\beta_4+\alpha_4\beta_2 = 4\alpha^2 \quad , \qquad \text{(A5b)}$$

$$\alpha_1^2 + \beta_1^2 + (1-2\alpha^2)q^2 = 1 \quad , \qquad \text{(A5c)}$$

$$\alpha_2^2 + \beta_2^2 + (1-2\alpha^2)p^2 = 1 \quad , \qquad \text{(A5d)}$$

$$\alpha_3^2 + \beta_3^2 + (1-2\alpha^2)s^2 = 1 \quad , \qquad \text{(A5e)}$$

$$\alpha_4^2 + \beta_4^2 + (1-2\alpha^2)r^2 = 1 \quad , \qquad \text{(A5f)}$$

$$p^2 + q^2 + r^2 + s^2 = 4. \qquad \text{(A5g)}$$

Summing (A5c), (A5d), (A5e), (A5f),

$$\sum_{j=1}^{4} (\alpha_j^2 + \beta_j^2) = 8\alpha^2 \qquad \text{(A5h)}$$

which is equivalent to (A4a).

From (A5b) and (A5h) * ,

$$(\alpha_1+\beta_3)^2 + (\alpha_3+\beta_4)^2 + (\alpha_2-\beta_4)^2 + (\alpha_4-\beta_2)^2 = 0. \qquad (A6)$$

Only non-complex values of the direction cosines are physically possible, i.e.

$$\alpha_1 = -\beta_3 , \qquad (A7a)$$

$$\alpha_3 = -\beta_1 , \qquad (A7b)$$

$$\alpha_2 = \beta_4 , \qquad (A7c)$$

$$\alpha_4 = \beta_2 . \qquad (A7d)$$

By substitution of (A7) into (A5a) and (A5b),

$$-2p\alpha_1 + 2r\alpha_3 - 2q\alpha_2 + 2s\alpha_4 = 8\alpha , \qquad (A8)$$

$$\alpha_1^2 + \alpha_2^2 + \alpha_3^2 + \alpha_4^2 = 4\alpha^2 . \qquad (A9)$$

From (A5g), (A8), and (A9), $(\alpha \neq 0)$,

$$(\alpha_1+p\alpha)^2 + (\alpha_2+q\alpha)^2 + (\alpha_3-r\alpha)^2 + (\alpha_4-s\alpha)^2 = 0. \qquad (A10)$$

This gives

$$\alpha_1 = -p\alpha \quad , \quad \beta_3 = +p\alpha \quad , \qquad (A11a)$$

$$\alpha_2 = -q\alpha \quad , \quad \beta_4 = -q\alpha \quad , \qquad (A11b)$$

$$\alpha_3 = +r\alpha \quad , \quad \beta_1 = -r\alpha \quad , \qquad (A11c)$$

$$\alpha_4 = +s\alpha \quad , \quad \beta_2 = +s\alpha \quad . \qquad (A11d)$$

- -

* The author is indebted to Mr.D.van Ligten for aid with the following discussion.

By substitution of (A11) in (A5c), (A5d), (A5e), and (A5g),

$$p^2\alpha^2 + r^2\alpha^2 + (1-2\alpha^2)q^2 = 1, \qquad \text{(A12a)}$$

$$q^2\alpha^2 + s^2\alpha^2 + (1-2\alpha^2)p^2 = 1, \qquad \text{(A12b)}$$

$$r^2\alpha^2 + p^2\alpha^2 + (1-2\alpha^2)s^2 = 1, \qquad \text{(A12c)}$$

$$s^2\alpha^2 + q^2\alpha^2 + (1-2\alpha^2)r^2 = 1. \qquad \text{(A12d)}$$

The determinant of this set of linear equations is $D = (1-2\alpha^2)^2(1-4\alpha^2)$. If $D \neq 0$, as is the case for $\alpha = -0.325$, the solution of (A12) is

$$p^2 = q^2 = r^2 = s^2 = 1. \qquad \text{(A13)}$$

This equation, together with

$$\alpha_1 = -p\alpha\ , \quad \beta_1 = -r\alpha\ , \quad \gamma_1 = +q\gamma\ ,$$
$$\alpha_2 = -q\alpha\ , \quad \beta_2 = +s\alpha\ , \quad \gamma_2 = +p\gamma\ ,$$
$$\alpha_3 = +r\alpha\ , \quad \beta_3 = +p\alpha\ , \quad \gamma_3 = +s\gamma\ ,$$
$$\alpha_4 = +s\alpha\ , \quad \beta_4 = -q\alpha\ , \quad \gamma_4 = +r\gamma\ ,$$

represents sixteen sets of direction cosines satisfying (A3) and thus describing arrangements of the magnetic moments that result in powder intensities equal to the intensities from model A, presented in section 3.2.4.1. It is easy to show that all combinations of p, q, r, s, satisfying $p+q+r+s = \pm 2$, represent this model A structure.

For example,

$-p = +q = -r = -s = +1$ results in

$$\alpha_1 = +\alpha\ , \quad \beta_1 = +\alpha\ , \quad \gamma_1 = +\alpha\ ,$$
$$\alpha_2 = -\alpha\ , \quad \beta_2 = -\alpha\ , \quad \gamma_2 = -\alpha\ ,$$
$$\alpha_3 = -\alpha\ , \quad \beta_3 = -\alpha\ , \quad \gamma_3 = -\alpha\ ,$$
$$\alpha_4 = -\alpha\ , \quad \beta_4 = -\alpha\ , \quad \gamma_4 = -\alpha\ .$$

On the other hand combinations of p, q, r, s, satisfying $p+q+r+s \neq \pm 2$, all result in the same non-collinear model for the arrangement of the moments. For example,

$-p = +q = -r = +s = 1$ results in

$$\alpha_1 = +\alpha\ , \quad \beta_1 = +\alpha\ , \quad \gamma_1 = +\gamma\ ,$$
$$\alpha_2 = -\alpha\ , \quad \beta_2 = +\alpha\ , \quad \gamma_2 = -\gamma\ ,$$
$$\alpha_3 = -\alpha\ , \quad \beta_3 = -\alpha\ , \quad \gamma_3 = +\gamma\ ,$$
$$\alpha_4 = +\alpha\ , \quad \beta_4 = -\alpha\ , \quad \gamma_4 = -\gamma\ .$$

References

1) H.P.Rooksby, Acta Cryst. 1, 226 (1948).
2) N.C.Tombs and H.P.Rooksby, Nature 165, 442 (1950).
3) S.Greenwald, Acta Cryst. 6, 396 (1953).
4) C.G.Shull, W.A.Strauser, and E.O.Wollan, Phys.Rev. 83, 333 (1958).
5) H.A.Kramers, Physica 1, 182 (1934).
6) Yin-Yuan Li, Phys.Rev. 100, 627 (1955).
7) W.L.Roth, Phys.Rev. 110, 1333 (1958).
8) S.Greenwald and J.S.Smart, Nature 166, 523 (1950).
9) J.S.Smart and S.Greenwald, Phys.Rev. 82, 113 (1951).
10) J.Kanamori, Progr.Theoret.Phys. (Japan) 17, 177 (1957); 17, 197 (1957).
11) T.Nagamiya and K.Motizuki, Rev.Mod.Phys. 30, 89 (1958).
12) BNL 325, Brookhaven National Lab. July 1958.
13) International Tables for X-Ray Crystallography, The Kynoch Press, England, 1959. Volume II, p.295.
14) W.L.Roth, J.Phys.Chem.Solids 25, 1 (1964).
15) C.G.Shull and E.O.Wollan, Phys.Rev. 81, 527 (1951).
16) V.Scatturin, L.Corliss, N.Elliott, and J.Hastings, Acta Cryst. 14, 19 (1961).
17) W.L.Roth, Phys.Rev. 111, 772 (1958).
18) E. Uchida, N.Fukuoka, H.Kondoh, T.Takeda, Y.Nakazumi, and T.Nagamiya, J.Phys.Soc. Japan 19, 2088 (1964).
19) T.Nagamija, S.Saito, Y.Shimomura, and E.Uchida, J.Phys. Soc. Japan 20, 1285 (1965).
20) J.H.Greiner, A.E.Berkowitz, and J.E.Weidenborner, J.Appl.Phys. 37, 2149 (1966).
21) B.van Laar, Phys.Rev. 128, A584 (1965).
22) B.van Laar, J.Schweizer, and R.Lemaire, Phys.Rev. 141, 538 (1966).
23) S.Saito, K.Nakahigashi, and Y.Shimomura, J.Phys.Soc. Japan 21, 850 (1966).
24) C.Kittel, Introduction to Solid State Physics, third edition, Wiley and Sons, 1966, p.112.

Chapter IV

THE MAGNETIC STRUCTURES OF Cr_5S_6

4.1 Introduction

It has been found by Jellinek [1] that in the Cr-S system six phases can be distinguished with compositions varying from $Cr_{1.05}S$ to $Cr_{0.66}S$, each with a very narrow homogeneity range. These six phases are:

Phase	Symmetry	Homogeneity range
CrS	Monoclinic	Probably $\sim Cr_{1.03}S$
Cr_7S_8	Trigonal	$Cr_{0.88}S$ - $Cr_{0.87}S$
Cr_5S_6	Trigonal	$Cr_{0.85}S$
Cr_3S_4	Monoclinic	$Cr_{0.79}S$ - $Cr_{0.76}S$
Cr_2S_3tr.	Trigonal	$Cr_{0.69}S$
Cr_2S_3rh.	Rhombohedral	$Cr_{0.67}S$

With the exception of CrS, the crystal structures [1] of these phases can be considered as NiAs type structures in which a number of Cr atoms has been replaced by vacancies. These vacancies, which are confined to every second metal layer, are statistically distributed within the layers in Cr_7S_8, while in the other phases with NiAs type structures they are ordered. In Cr_3S_4 this ordering is accompanied by a slight monoclinic distortion of the lattice.

The magnetic properties of Cr-S compounds were first investigated by Haraldsen and Neuber [2]. The most interesting magnetic behaviour is shown by the phase Cr_5S_6 ($Cr_{0.85}S$) which is ferrimagnetic over a limited temperature range. More detailed information on the crystallographic and magnetic properties of this phase will be given in the following sections.

The crystal structure of Cr_5S_6, as given by Jellinek [1], is

Trigonal, space group $P\bar{3}1c$ (D_{3d}^2),

2 Cr in 2(a) : $(0,0,\frac{1}{4};\ 0,0,\frac{3}{4})$,

2 Cr in 2(c) : $(\frac{1}{3},\frac{2}{3},\frac{1}{4};\ \frac{2}{3},\frac{1}{3},\frac{3}{4})$,

2 Cr in 2(b) : $(0,0,0;\ 0,0,\frac{1}{2})$,

4 Cr in 4(f) : $\pm(\frac{1}{3},\frac{2}{3},z;\ \frac{1}{3},\frac{2}{3},\frac{1}{2}-z)$, with $z=0$,

12 S in 12(i): $\pm(x,y,z;\ \bar{y},x-y,z;\ y-x,\bar{x},z;\ y,x,\frac{1}{2}+z;$

$x-y,\bar{y},\frac{1}{2}+z;\ \bar{x},y-x,\frac{1}{2}+z)$, with $x=\frac{1}{3}$, $y=0$, $z=\frac{3}{8}$.

The arrangement of the Cr atoms is shown in fig.4.1. This is an idealized structure with the z parameter of the Cr atoms in 4(f) and the x,y,and z parameters of the sulphur atoms corresponding to the ideal NiAs type structure. Jellinek deduced from his X-ray powder data that these parameters did not deviate largely from the ideal values.

The magnetic properties of Cr_5S_6 have been the subject of many studies [2-8]. The compound is antiferromagnetic below 168°K in the sense that there is no net magnetic moment, ferrimagnetic between 168 and 305°K, and paramagnetic above 305°K.

In fig.4.2 a magnetization versus temperature curve of a Cr_5S_6 sample in a magnetic field of 8530 Oe is shown. The most important feature of this graph is the steep change in magnetization at 168°K representing the transition from the ferrimagnetic to the antiferromagnetic state.

Fig.4.3 *) gives magnetization versus field data at three different temperatures. It may be noted that just above the transition temperature of 168°K the magnetization, extrapolated to zero field, amounts to about 0.11 Bohr magneton per Cr atom, while at T=4.2°K the magnetization extrapolated to H=0 is zero.

- -

*) Figs. 4.2 and 4.3 represent the results of magnetization measurements carried out by Drs.C.F.van Bruggen of the "Laboratorium voor Anorganische Chemie" at Groningen and Mr.J.F.Fast of the "Natuurkundig Laboratorium der N.V. Philips Gloeilampenfabrieken" at Eindhoven. The author is grateful for the permission to use these data.

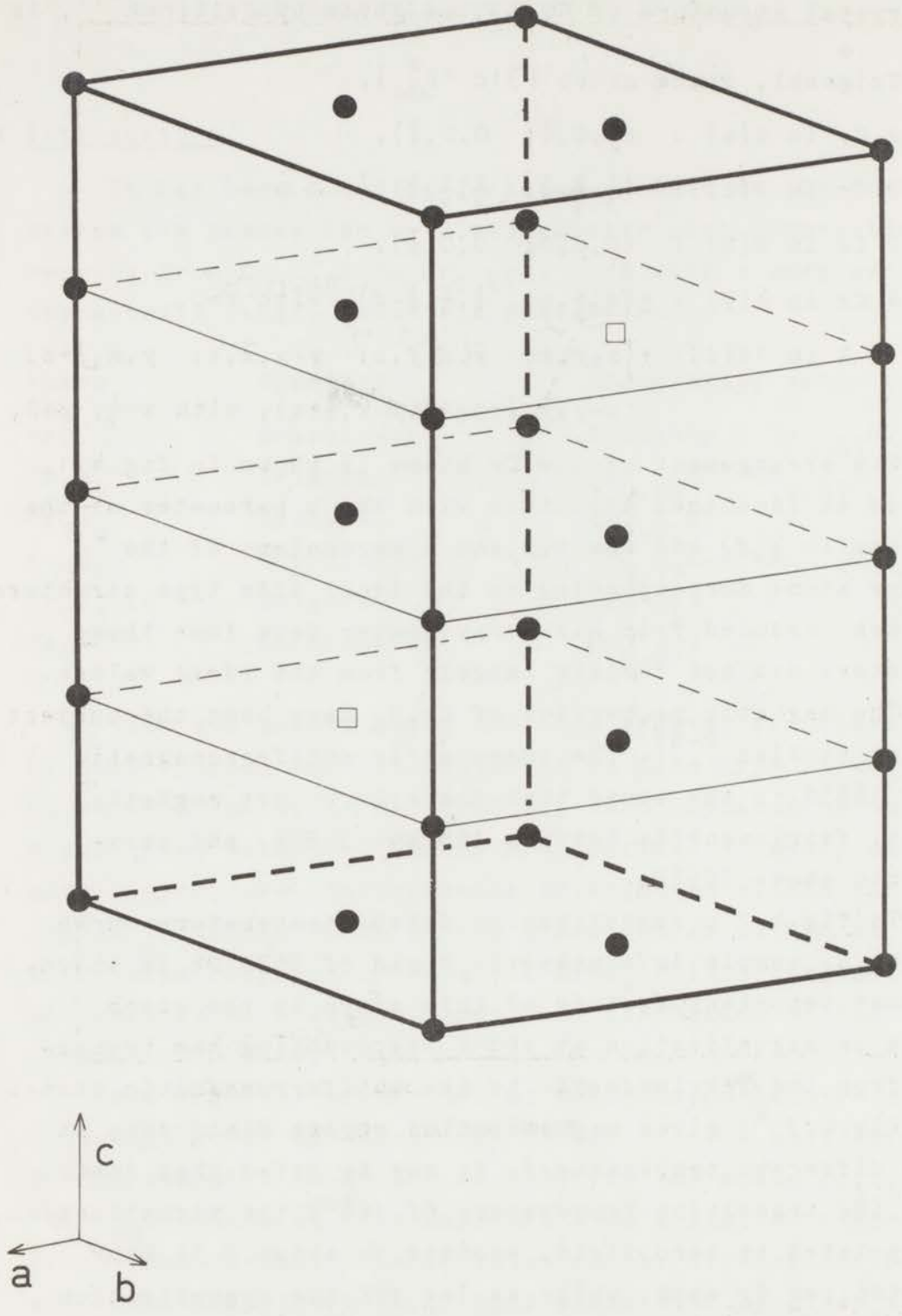

Fig.4.1
Lattice of chromium atoms in Cr_5S_6. The vacancies in the lattice are represented by open squares.

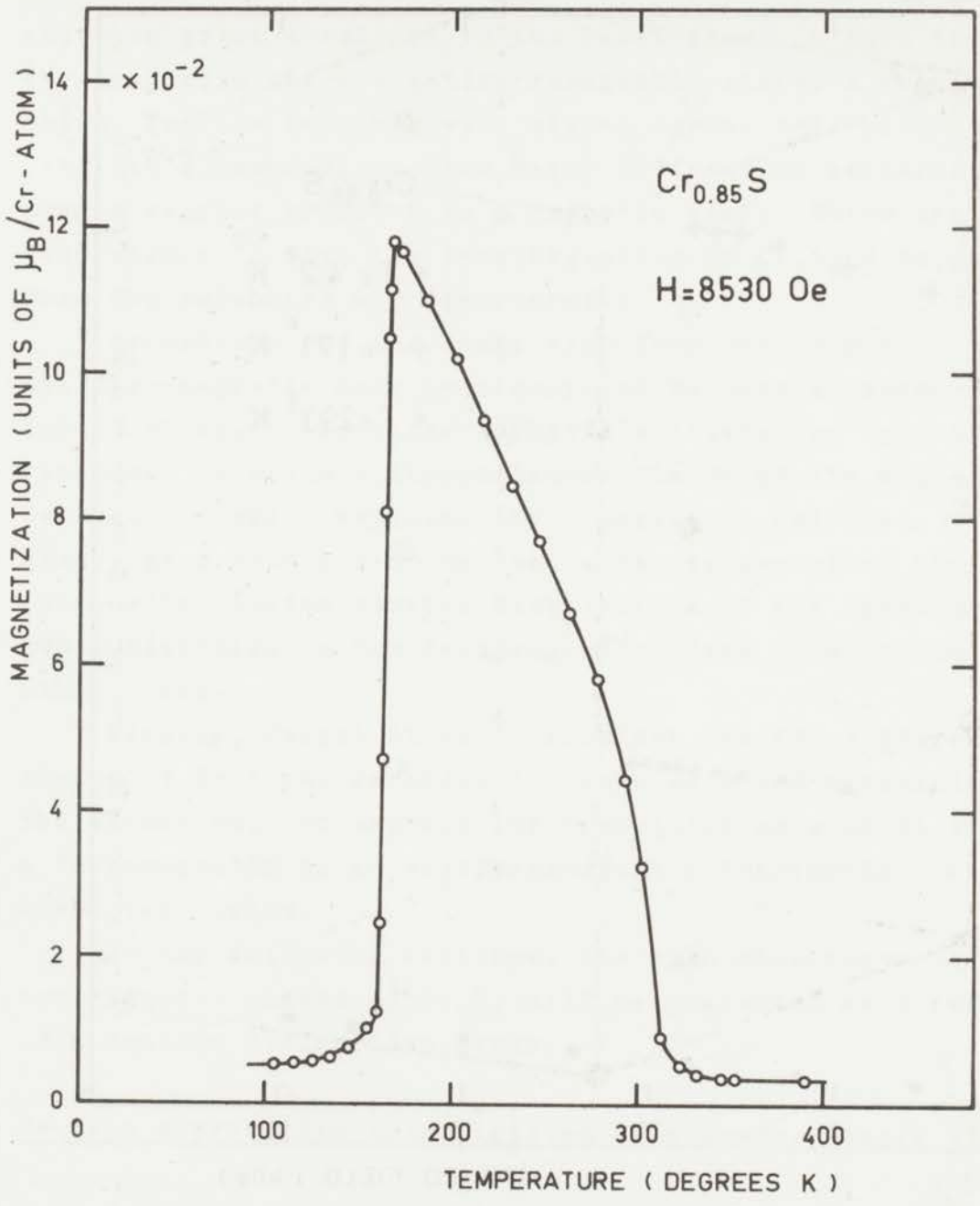

Fig.4.2
Magnetization versus temperature curve of Cr_5S_6.

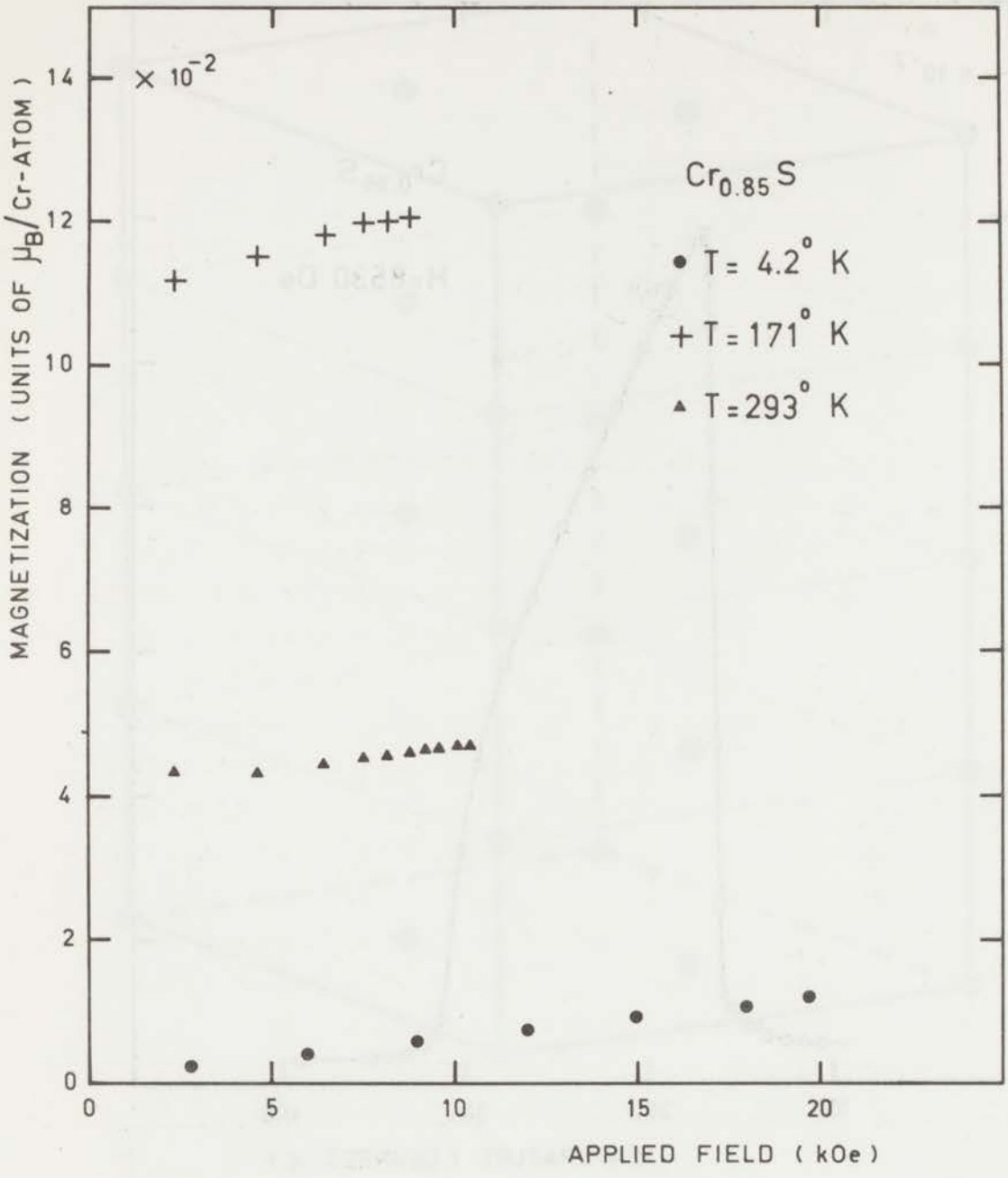

Fig.4.3
Magnetization versus applied field curves of Cr_5S_6.

Kamigaichi [4] showed from susceptibility measurements that the spins should be in the basal plane in both the ferrimagnetic and the antiferromagnetic state, a result which, for the ferrimagnetic state, agrees well with Jellinek's conclusions from X-ray diffraction patterns of powder samples oriented in a magnetic field. There are indications [5] that the ferrimagnetism in Cr_5S_6 disappears when the vacancies are disordered.

Mechanisms for the transition from ferrimagnetic to antiferromagnetic have been proposed by several authors. Yuzuri et al. [3] consider a possible triangular spin arrangement in which a discontinuous change of the angles between the spins explains the transition. Jellinek [1] gives, as a possible mechanism, a rearrangement of the spin order causing another distribution of the spins over two sublattices in the ferrimagnetic state than in the other state.

Finally, Dwight et al. [6] consider the two different chains of Cr ions, parallel to the c axis and containing the vacancies, and explain the transition as a shift from a ferromagnetic to an antiferromagnetic interaction between these two chains.

In the following sections, the spin structures of the two magnetic phases of Cr_5S_6 will be presented as a result of a neutron diffraction study.

4.2 Neutron diffraction investigation of a powder sample of Cr_5S_6

4.2.1 Experimental

The Cr_5S_6 sample was prepared at the University of Groningen by heating a mixture of chromium powder (99.99%) and sulphur (99.9999%) in evacuated quartz tubes for 48 h at 1000°C. The product was then cooled slowly, powdered, and tempered for several days at 300°C.

The total sample consisted of about 25 batches prepared in this way. Each batch was checked for homogeneity by X-ray diffraction and by measuring the magnetization versus temperature curve before it was added to the sample *). Only small traces of Cr_2O_3 were present in the specimen.

The lengths of the unit-cell edges at T=300°K were determined by means of X-ray diffraction (CuKα radiation) to be a=(5.9838±0.0005)Å and c=(11.518±0.001)Å. These values deviate slightly from those reported by Jellinek [1], i.e. a=(5.982±0.002)Å and c=(11.509±0.003)Å.

Neutron diffraction patterns were recorded at the Petten High Flux Reactor at temperatures of 4.2, 78, 208, and 370°K from a sample contained in a cylindrical vanadium sample holder with a diameter of 20 mm. The temperature of 208°K was obtained by filling the liquid nitrogen cryostat with a mixture of solid carbon-dioxide and ethanol. For the temperature of 370°K this cryostat was filled with boiling water. The sample temperature was measured by means of a copper-constantan thermocouple.

The neutron wavelength of 2.57 Å was obtained from the (111) reflection of a copper monochromator crystal. The Soller slits, which were placed between the reactor and the monochromator, had a horizontal angular divergence of 30'. The angular divergence of the slits in front of the BF_3 counter was 10' for the diagrams taken at He and N_2 temperatures, and 30' for the other diagrams. The diagrams obtained at 4.2, 208, and 370°K are shown in fig.4.4. As a second-order filter, a block of pyrolytic graphite with a thickness of 7.5 cm was employed, as described by Loopstra [9].

In order to study the transition from the antiferromagnetic to the ferrimagnetic state, two sections of the diagram were scanned repeatedly while the sample was allowed to warm up slowly from liquid-nitrogen temperature.

- -

*) The elaborate preparation and checking of the sample was performed by Miss A.Bruining and Drs.C.F.van Bruggen of the "Laboratorium voor Anorganische Chemie" at Groningen.

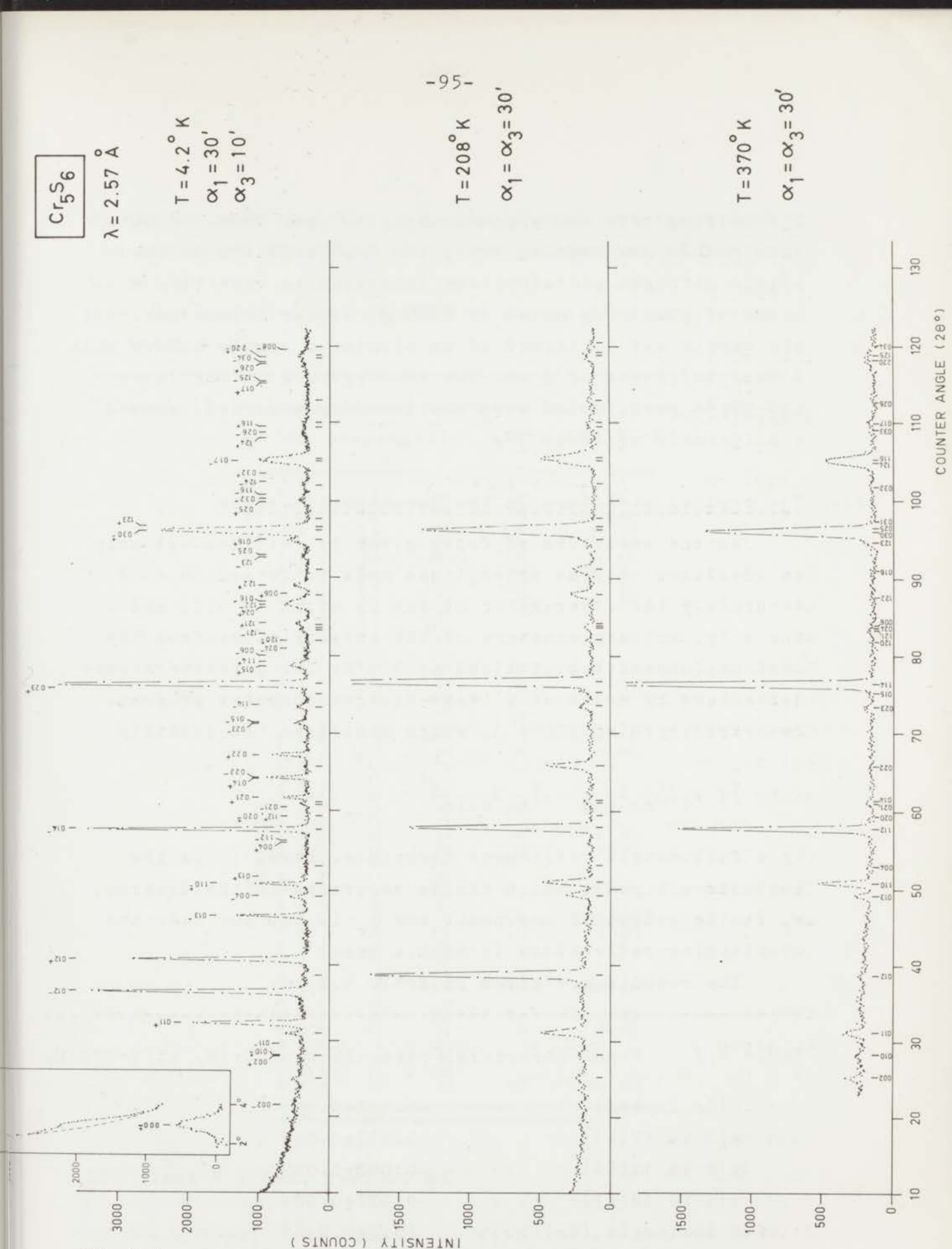

Fig.4.4

Neutron diffraction diagrams of Cr_5S_6 at three different temperatures. The indices in the lower diagram refer to the nuclear unit cell. The indices $hkl^{\pm}$ in the upper diagram correspond to the formalism as used in section 4.2.3.1. The $000^{\pm}$ peak (insert at T=4.2°K) has been properly scaled to conform with the main diagram.

The heating rate was approximately 10° per hour. To obtain this rather low heating rate, the heat capacity of the liquid nitrogen container was increased by inserting a block of aluminium metal of 8000 g. During this experiment the sample was contained in an aluminium sample holder with a wall thickness of 2 mm. The temperatures at the lower and upper part, which were continuously recorded, showed a difference of about 3°.

4.2.2 The crystal structure in the paramagnetic state

As the structure of Cr_5S_6 given by Jellinek was only an idealized one, an attempt was made to determine more accurately the z parameter of the Cr atoms in 4(f) and the x, y, and z parameters of the sulphur atoms from the neutron intensities obtained at 370°K. The parameters were determined by means of a least-squares computer program, described by Rietveld [10], which minimizes the quantity

$$\sum_i w_i \left(\sum_r I_{obs} - \sum_r I_{calc} \right)^2$$

by a full-matrix refinement technique. Here, $\sum_i$ is the sum over all peaks which can be separated in the diagram, w_i is the weight of one peak, and $\sum_r$ is the sum over the overlapping reflections in such a peak.

The results are given in table 4.I.

Table 4.I Final structural parameters of Cr_5S_6 at T=370°K.

z[Cr in 4(f)]	-0.007±0.001
x[S in 12(i)]	0.337±0.005
y[S in 12(i)]	-0.002±0.003
z[S in 12(i)]	0.377±0.002
B isotropic (Cr)	(1.2±0.2)Å^2
B isotropic (S)	(1.5±0.2)Å^2
R index	3.5%

It can be seen that the only significant deviation from the idealized structure is in the z parameter of the Cr in 4(f).

The observed and calculated intensities are listed in table 4.II.

Table 4.II Calculated and observed intensities of Cr_5S_6 in the paramagnetic state (T=370°K).

h	k	l	j	I_{calc}	$\sum_r I_{calc}$	$\sum_r I_{obs}$[a]
0	0	2	2	275	275	263 (62)
0	1	0	6	96	96	146 (61)
0	1	1	12	594	594	545 (70)
0	1	2	12	150	150	74 (66)
0	1	3	12	441	441	408 (61)
1	1	0	6	1283	1283	1312 (68)
0	0	4	2	3	3	64 (57)
1	1	2	6	3720		
1	1	$\bar{2}$	6	1467		
0	2	0	6	61	5248	5269 (120)
0	2	1	12	157		
0	1	4	12	93	250	231 (56)
0	2	2	12	58	58	0 (60)
0	2	3	12	249	249	0 (60)
0	1	5	12	48		
1	1	4	6	5366		
1	1	$\bar{4}$	6	4803	10217	10229 (125)
1	2	0	12	50	50	0 (60)
1	2	1	12	93		
1	2	$\bar{1}$	12	116		
0	2	4	12	21		
0	0	6	2	10	240	121 (63)
1	2	2	12	77		
1	2	$\bar{2}$	12	14	91	0 (60)
0	1	6	12	33	33	0 (60)
1	2	3	12	161		
1	2	$\bar{3}$	12	188		
0	3	0	6	6760		
0	2	5	12	43		
0	3	1	12	0	7151	7131 (125)
0	3	2	12	171	171	0 (60)
1	2	4	12	30		
1	2	$\bar{4}$	12	33		
1	1	6	6	570		
1	1	$\bar{6}$	6	1783	2416	2429 (93)
0	3	3	12	0		
0	1	7	12	252	252	263 (76)
0	2	6	12	31	31	0 (60)
2	2	0	6	481		
1	2	5	12	43		
1	2	$\bar{5}$	12	30		
0	3	4	12	18	571	599 (93)

[a] Numbers in parentheses are estimated standard deviations.

The final R index, defined as

$$R = \sum_i (|\sum_r I_{obs} - \sum_r I_{calc}|)/\sum_i \sum_r I_{obs},$$

was 3.5%.

The value for the coherent nuclear scattering amplitude of sulphur used in the refinement was 0.28×10^{-12} cm, as given by Menyuk, Dwight, and Wold [11]. Use of the value of 0.31×10^{-12} cm, listed in the International Tables for X-ray Crystallography, Vol.III, leads to an abnormally high value for the individual isotropic temperature factor of the sulphur atoms. For the chromium scattering amplitude, the value of 0.352×10^{-12} cm was used.

4.2.3 The magnetic structures

4.2.3.1 Antiferromagnetic state

In the diagrams, obtained with a sample temperature of 4.2 and 78°K, many extra peaks of magnetic origin were found. These could not be indexed satisfactorily on the basis of simple multiples of the nuclear cell, even considering a twenty-fivefold increase of its volume. This means that there is no simple relation between the periodicities of the magnetic and the nuclear structure.

No magnetic scattering has been observed in directions associated with nuclear reciprocal lattice points, which means that there is no Fourier component in the spin structure with the same periodicity as the nuclear structure (i.e. with propagation vector $\vec{\tau}=0$).

It was found that all peaks of magnetic origin could be indexed on the basis of

$$4\sin^2\theta/\lambda^2 = (h^2+hk+k^2)|\vec{a}^*|^2 + (l|\vec{c}^*|\pm|\vec{\tau}|)^2. \qquad (4.1)$$

With this formula a $000^{\pm}$ satellite should be expected. This satellite has actually been found. Intensity measurements with the sample at T=4.2°K and T=370°K were performed in the vicinity of the primary beam.

For these measurements the sample-counter distance was increased to 160 cm. The counting time on each point was 72 min. Subtraction of the two series revealed clearly the existence of the $000^{\pm}$ satellite (fig.4.4).

Thus it is seen that only two Fourier components are non-zero, one with propagation vector $+\vec{\tau}$ and one with propagation vector $-\vec{\tau}$ parallel with the c^* axis.

The existence of only two Fourier components immediately rules out the possibility of an antiphase domain type structure. Kamigaichi's observation [4] that the spins should be in the basal plane leaves a screw type spiral structure as the only remaining possibility. This then is a spiral structure with $\beta_\nu=\pi/2$ for all ν and $\psi=0$ (section 2.3.3.1).

In such an arrangement, the manner in which the spin component varies from one unit cell to the next is given by the propagation vector $\vec{\tau}$. The rotation angle α of the spiral between two adjacent Cr layers is defined as $\alpha = (|\vec{\tau}|/|\vec{c}^*|)\times(\pi/2)$. A phase angle ϕ_ν can be assigned to each magnetic atom, in any one unit cell which is taken as a reference.

For the satellite reflections, the scattering cross sections, averaged over equivalent reflections are (section 2.3.3.1)

$$\langle\sigma_{\vec{H}+\vec{\tau}}\rangle = \frac{1+\cos^2\eta}{4}\left[0.2695\sum_\nu \mu_\nu f_\nu(\vec{H}+\vec{\tau})\exp 2\pi i(\vec{H}\cdot\vec{r}_\nu-\phi_\nu)\right]^2, \quad (4.2a)$$

$$\langle\sigma_{\vec{H}-\vec{\tau}}\rangle = \frac{1+\cos^2\eta}{4}\left[0.2695\sum_\nu \mu_\nu f_\nu(\vec{H}-\vec{\tau})\exp 2\pi i(\vec{H}\cdot\vec{r}_\nu+\phi_\nu)\right]^2. \quad (4.2b)$$

In these expressions, $f_\nu(\vec{H}\pm\vec{\tau})$ is the magnetic form factor of the magnetic atom ν and μ_ν is its magnetic moment in Bohr magnetons.

The angle between the scattering vector and the c axis is indicated by η. The sum is taken over all magnetic atoms in the crystallographic unit cell.

From the observation that all satellites around reciprocal-lattice points with (h-k)=3n have very weak or zero intensity (except $000^{\pm}$ which is strongly enhanced by its high Lorentz factor), it was concluded that in each layer perpendicular to the c axis the vector sum of the moment approximates zero.

As the ionic picture, predicting Cr^{2+} and Cr^{3+} ions only, certainly is too simple and the Cr atoms are distributed over four crystallographic positions, four magnetic moments should be determined, one for each position. With these assumptions, it was found, by systematically considering all possibilities, that the only model able to explain the observed intensities is the one given in table 4.III.

Table 4.III Schematic representation of magnitude and relative phase angle of magnetic moments in the magnetic phases of Cr_5S_6. The values in the last column refer to the idealized structure (z=0). α is the rotation angle of the spiral between two adjacent Cr layers.

Position	x	y	z	Moment	Phase angle	Angle with moment at (0,0,0)
2(b)	0	0	0	μ_b	0°	0°
2(a)	0	0	$\frac{1}{4}$	μ_a	180°	180°+α
2(b)	0	0	$\frac{1}{2}$	μ_b	0°	+2α
2(a)	0	0	$\frac{3}{4}$	μ_a	180°	180°+3α
4(f)	$\frac{1}{3}$	$\frac{2}{3}$	z	μ_f	+φ	-φ
2(c)	$\frac{1}{3}$	$\frac{2}{3}$	$\frac{1}{4}$	μ_c	0°	+α
4(f)	$\frac{1}{3}$	$\frac{2}{3}$	$\frac{1}{2}$-z	μ_f	-φ	+2α+φ
4(f)	$\frac{2}{3}$	$\frac{1}{3}$	$\frac{1}{2}$+z	μ_f	+φ	+2α-φ
2(c)	$\frac{2}{3}$	$\frac{1}{3}$	$\frac{3}{4}$	μ_c	0°	+3α
2(f)	$\frac{2}{3}$	$\frac{1}{3}$	$\bar{z}$	μ_f	-φ	+φ

In addition to the phase angles of the different moments, the angles between these moments and the moment of the Cr atom at (0,0,0) are also given in this table.

In this model the magnetic parameters to be determined are the moments μ_a, μ_b, μ_c, μ_f, and a single phase angle ϕ. It was assumed that all chromium atoms had the same form factor and that this could be expressed analytically as

$$f(\vec{H}\pm\vec{\tau}) = a+(1-a)\exp(-b|\vec{H}\pm\vec{\tau}|^2) \quad , \qquad (4.3)$$

with the parameters a and b to be determined.

Evidently the "true" expression for the isotropic form factor is more complicated than this simple sum of a constant term and a Gaussian. Further, it is improbable that the form factor is isotropic and equal for the four crystallographic positions. However, because of the limited precision of the observation and the finite $\sin\theta/\lambda$ range ($0<\sin\theta/\lambda<0.35$), it seems justified to use this simple expression. As there is no reason to postulate that the structural parameters of Cr in 4(f) and of sulphur in 12(i) remain exactly the same as in the paramagnetic state, these parameters should also be refined from the nuclear intensities.

The refinement of both magnetic and structural parameters was carried out by a full-matrix least-squares program, especially written for this problem. This program minimizes the same quantity as that mentioned in section 4.2.2.

This refinement resulted in R indices of 2.9 and 4.7% for the data obtained at 4.2 and 78°K, respectively. At both temperatures, the form factor obtained was almost identical with the spherical form factor calculated by Watson and Freeman [12] for Cr^{2+}.

It should be mentioned that, in the refinement, rather large correlation factors appeared between the different magnetic parameters. As a result, the average moment is much better defined than the separate moments of the different positions. In table 4.IV, the final magnetic and structural parameters are listed, while the observed and calculated intensities are listed in table 4.V. The spin structure is shown in fig.4.5.

Table 4.IV Final structural and magnetic parameters of Cr_5S_6 in the magnetic states.

	Antiferromagnetic		Ferrimagnetic
	T=4.2°K	T=77°K	T=208°K
a	(5.962±0.003)Å	(5.962±0.001)Å	(5.974±0.012)Å
c	(11.509±0.011)Å	(11.506±0.005)Å	(11.509±0.028)Å
Spiral period	(49.77±0.56)Å	(53.25±0.32)Å	∞
Interlayer rotation angle α	(20.79±0.26)°	(19.45±0.13)°	0°
z[Cr in 4(f)]	-0.007±0.001	-0.005±0.001	-0.008±0.004
x[S in 12(i)]	0.331±0.003	0.328±0.003	0.329±0.008
y[S in 12(i)]	-0.002±0.002	-0.002±0.002	-0.009±0.007
z[S in 12(i)]	0.376±0.001	0.378±0.001	0.379±0.004
μ_a	(2.98±0.25)μ_B	(2.87±0.84)μ_B	(1.70±0.34)μ_B
μ_b	(2.77±0.12)μ_B	(2.66±0.56)μ_B	(2.12±1.86)μ_B
μ_c	(2.78±0.10)μ_B	(2.56±0.19)μ_B	(1.69±0.20)μ_B
μ_f	(2.57±0.11)μ_B	(2.34±0.32)μ_B	(1.01±1.67)μ_B
$\mu_{average}$	(2.73±0.04)μ_B	(2.55±0.06)μ_B	(1.51±0.33)μ_B
φ	(129.1±2.7)°	(131.2±9.2)°	180°
form factor constants:			
a	+0.20±0.04	-0.04±0.15	-0.50±1.58
b	(+4.54±0.51)Å^2	(+3.08±0.75)Å^2	(+1.42±1.93)Å^2
$B_{over-all}$	0 Å^2	(0.3±0.1)Å^2	(0.9±0.4)Å^2
R index	2.9%	4.7%	3.9%

Table 4.V Calculated and observed intensities of Cr_5S_6 in the antiferromagnetic state. The column s indicates whether the intensity is nuclear (s=0), or magnetic (s=±1). The column j gives the multiplicity of the reflection.

					$T=4.2°K$			$T=77°K$	
h	k	l	s	j	I_{calc}	$\sum_r I_{calc}$	$\sum_r I_{obs}$[a]	I_{calc}	$\sum_r I_{calc}$	$\sum_r I_{obs}$[a]
0	0	0	+1	2	6163	6163	6165 (400)			
0	0	2	−1	2	73	73	250 (150)	6	6	0 (60)
0	0	2	+0	2	722	722	614 (135)	435	435	490 (68)
0	0	2	+1	2	1			2		
0	1	0	+0	6	424			273		
0	1	0	−1	6	0			0		
0	1	0	+1	6	0	426	315 (130)	0	275	136 (60)
0	1	1	−1	12	278	278	190 (120)	107	107	0 (60)
0	1	1	+0	12	1696	1696	1659 (120)	862	862	774 (66)
0	1	1	+1	12	10846	10846	10530 (160)	4394	4394	4465 (100)
0	1	2	−1	12	20231	20231	20791 (250)	9140	9140	9119 (410)
0	1	2	+0	12	429	429	359 (100)	208	208	189 (52)
0	1	2	+1	12	15147	15147	14783 (170)	7150	7150	7164 (112)
0	1	3	−1	12	4597	4597	4972 (135)	1955	1955	1916 (68)
0	1	3	+0	12	1337	1337	1384 (110)	574	574	593 (59)
0	0	4	−1	2	47	47	40 (100)	19	19	0 (60)
1	1	0	+0	6	3756			1820		
1	1	0	−1	6	17			12		
1	1	0	+1	6	17	3790	3833 (120)	12	1843	1768 (70)
0	1	3	+1	12	226	226	327 (90)	75	75	95 (70)
0	0	4	+0	2	7	7	0 (70)	4	4	0(60)
0	0	4	+1	2	0	0	0 (70)	1	1	0(60)
1	1	2	−1	12	23	23	45 (80)	2	2	0 (60)
1	1	2	+0	6	11559			5432		
1	1	2	+0	6	4517	16076	15999 (170)	2235		
0	1	4	−1	12	10	10	0 (70)	2	7668	7563 (108)
1	1	2	+1	12	1	1	0 (70)	2		
0	2	0	+0	6	86	86	45 (70)	19		
0	2	0	−1	6	0			0		
0	2	0	+1	6	0	0	0 (70)	0	20	0 (60)
0	2	1	−1	12	38	38	30 (70)	14	14	0 (60)
0	2	1	+0	12	456			240		
0	1	4	+0	12	197	652	510 (90)	65	304	182 (47)
0	2	1	+1	12	1536	1536	1611 (95)	613	613	574 (47)
0	1	4	+1	12	8			2		
0	2	2	−1	12	3188	3196	3140 (115)	1405	1407	1395 (64)
0	2	2	+0	12	182	182	107 (85)	90	90	0 (60)
0	2	2	+1	12	2695	2695	2634 (110)	1214	1214	1133 (60)
0	2	3	−1	12	957	957	1001 (100)	382		
0	1	5	−1	12	5	5	0 (70)	4	386	493 (61)
0	2	3	+0	12	834	834	800 (110)	344		
1	1	4	−1	12	59	59	30 (60)	22	366	388 (57)
0	1	5	+0	12	134	134	380 (100)	101		
0	2	3	+1	12	54	54	30 (60)	16	117	139 (44)
1	1	4	+0	6	17089			8552		
1	1	4	+0	6	15879	32967	33121 (190)	7150	15702	16131 (470)
0	1	5	+1	12	1389			495	495	484 (60)
1	1	4	+1	12	0	1389	1500 (200)	1	1	0 (60)
0	0	6	−1	2	8	8	138 (80)	1	1	0 (60)
0	2	4	−1	12	3	3	0 (70)	0	0	0 (60)
1	2	0	+0	12	134			52		
1	2	0	−1	12	0			0		
1	2	0	+1	12	0	134	100 (70)	0	52	0 (60)
1	2	1	−1	24	27	27	20 (70)	8		
1	2	1	+0	12	288			153		
1	2	1	+0	12	390			189		
0	2	4	+0	12	178			131		
0	0	6	+0	2	45			7		
1	2	1	+1	24	1100	2000	1936 (120)	398	866	785 (80)
0	2	4	+1	12	3			0		
1	2	2	−1	24	2344			876		
0	1	6	−1	12	2118	4465	4447 (160)	766		
0	0	6	+1	2	3	3	0 (60)	1		
1	2	2	+0	12	98			14		
1	2	2	+0	12	168	266	300 (100)	147	1804	1893 (90)
1	2	2	+1	24	2052	2052	1836 (130)	769	769	931 (75)
0	1	6	+0	12	112	112	70 (50)	59	59	0 (60)
1	2	3	−1	24	770			249		
0	2	5	−1	12	2	772	758 (130)	1	250	220 (60)
0	1	6	+1	12	1302			471		
1	2	3	+0	12	551			231		
1	2	3	+0	12	677	2530	2676 (120)	269	972	981 (70)

Table 4.V (continued)

h	k	l	s	j	$T=4.2°K$ I_{calc}	$\sum_r I_{calc}$	$\sum_r I_{obs}$[a]	$T=77°K$ I_{calc}	$\sum_r I_{calc}$	$\sum_r I_{obs}$[a]
0	3	0	+0	6	23701			11029		
0	3	0	−1	6	2			1		
0	3	0	+1	6	2			1		
0	2	5	+0	12	139	23845	23755 (200)	92		
1	2	3	+1	24	46	46	40 (60)	10	11134	10888 (130)
0	3	1	+0	12	0	0	0 (70)	0	0	0 (60)
0	2	5	+1	12	581	581	700 (130)	159	159	125 (40)
0	3	2	−1	12	3	3	20 (60)	0	0	0 (60)
1	1	6	−1	12	22			2	2	0 (60)
0	3	2	+0	12	554	575	600 (130)	316	316	0(60)
1	2	4	−1	24	2	2	0 (70)	0	0	0 (60)
0	3	2	+1	12	0	0	0 (70)	0	0	0 (60)
1	2	$\bar{4}$	+0	12	135			77		
1	2	$\bar{4}$	+0	12	133			66		
1	1	6	+0	6	2277			902		
1	1	$\bar{6}$	+0	6	6424			3182		
0	1	7	−1	12	355	9325	9412 (140)	102	4328	4154 (110)
1	2	4	+1	24	3	3	0 (70)	0	0	0 (60)
0	2	6	−1	12	1031	1031	1206 (150)	269		
1	1	6	+1	12	10			2		
0	3	3	+0	12	0			0		
0	1	7	+0	12	961	971	847 (125)	349	620	442 (75)
0	2	6	+0	12	103	103	100 (60)	47	47	0 (60)
0	1	7	+1	12	39	39	30 (60)	7	7	0 (60)
1	2	5	−1	24	2	2	0 (70)	1	1	0 (60)
0	2	6	+1	12	729			178	178	40 (60)
0	3	4	−1	12	14			3	3	50 (60)
2	2	0	+1	6	1672			773		
2	2	0	−1	6	1			0		
2	2	0	+1	6	1			0		
1	2	5	+0	12	152			95		
1	2	$\bar{5}$	+0	12	93	2662	2480 (200)	70		
0	0	8	−1	2	7	7	0 (70)	1	940	800 (110)
0	3	4	+0	12	20	20	63 (85)	14	14	0 (60)
1	2	5	+1	24				130	130	0 (60)
0	3	4	+1	12				0	0	0 (60)
2	2	2	−1	12				0		
2	2	2	+0	6				1195		
2	2	$\bar{2}$	+0	6				2917		
0	0	8	+0	2				3634		
2	2	2	+1	12				0		
1	3	0	+0	12				134		
1	3	0	−1	12				0		
1	3	0	+1	12				0	7880	8073 (150)
1	3	1	+1	12				1		
1	3	1	+0	2				32		
0	1	8	−1	12				0	34	0 (60)

[a] Numbers in parentheses are estimated standard deviations.

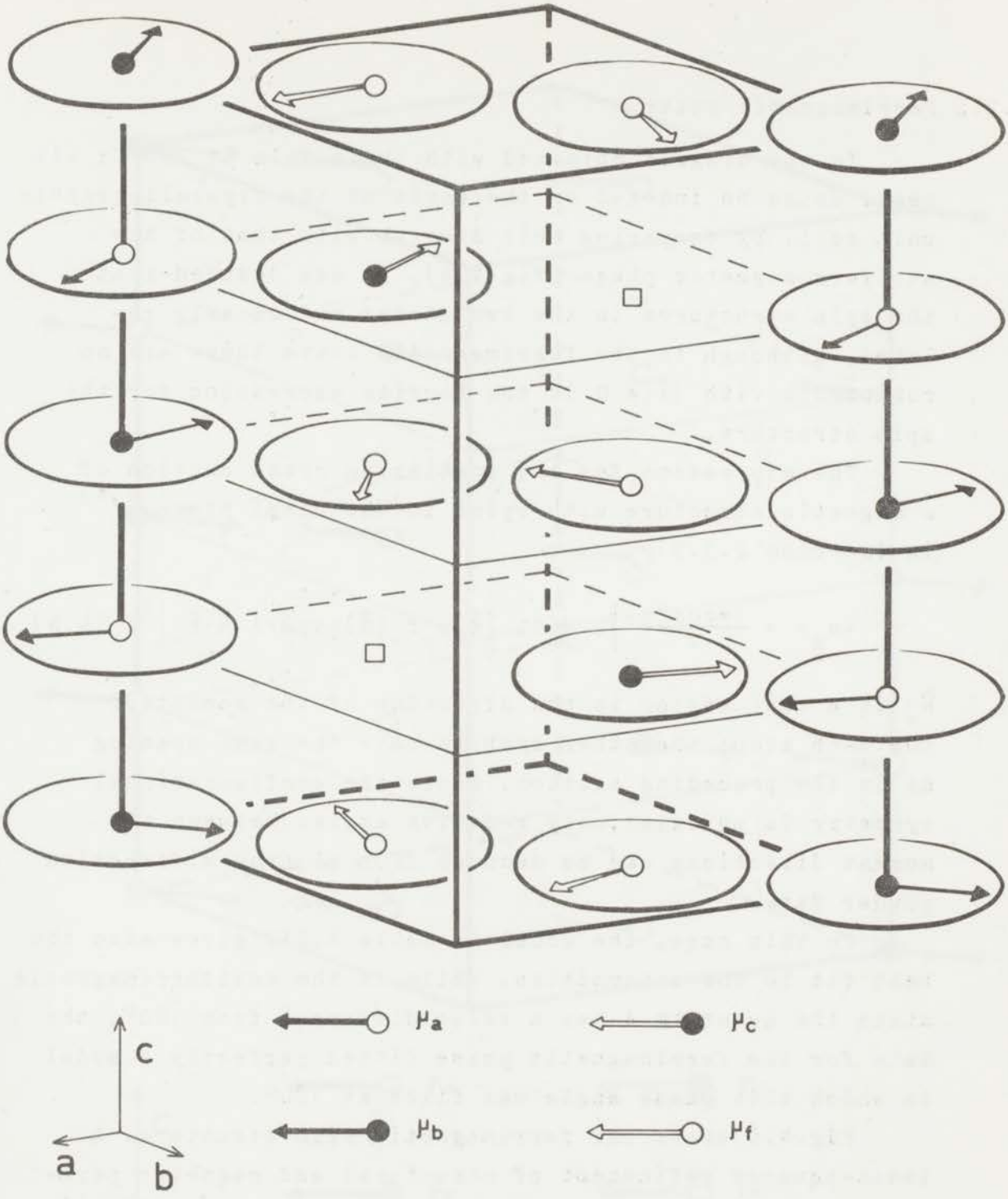

Fig.4.5 Antiferromagnetic spin arrangement in Cr_5S_6.

It may be noted that the structure is not antiferromagnetic, if this term is taken to mean that for each magnetic moment in the unit cell there is another one directed oppositely. The term helimagnetic, after French practice, is more appropriate.

4.2.3.2 Ferrimagnetic state

In the diagram obtained with the sample at 208°K, all peaks could be indexed on the basis of the crystallographic unit cell. By comparing this diagram with that of the antiferromagnetic phase (fig.4.4), it was deduced that the spin structures in the two states are closely related, although in the ferrimagnetic state there are no components with $|\vec{\tau}| \neq 0$ in the Fourier expression for the spin structure.

The expression for the scattering cross section of a magnetic structure with spins in the basal plane [1,4] is (section 2.3.2)

$$\langle \sigma_{\vec{H}} \rangle = \frac{1+\cos^2 n}{2} \left| 0.2695 \sum_{\nu} \hat{K}_\nu \mu_\nu f_\nu(\vec{H}) \exp 2\pi i \, \vec{H}\cdot\vec{r}_\nu \right|^2 . \quad (4.4)$$

$\hat{K}_\nu$ is a unit vector in the direction of the moment of the ν-th atom; the other symbols have the same meaning as in the preceding section. Since the configurational symmetry is uniaxial, only relative angles between the moment directions can be deduced from neutron diffraction powder data.

In this case, the model in table 4.III gives also the best fit to the intensities. While in the antiferromagnetic state the quantity ϕ has a value different from 180°, the data for the ferrimagnetic phase fitted perfectly a model in which this phase angle was fixed at 180°.

Fig.4.6 shows the ferrimagnetic spin structure. A least-squares refinement of structural and magnetic parameters resulted in an R index of 3.9%. The program for this refinement has also been written especially. The form factor, obtained from this refinement, was very close to the Cr^{3+} form factor of Watson and Freeman [12]. This would suggest that the moments are somewhat less spread out than in the antiferromagnetic state, but it is very doubtful whether such a quantitative interpretation is justified.

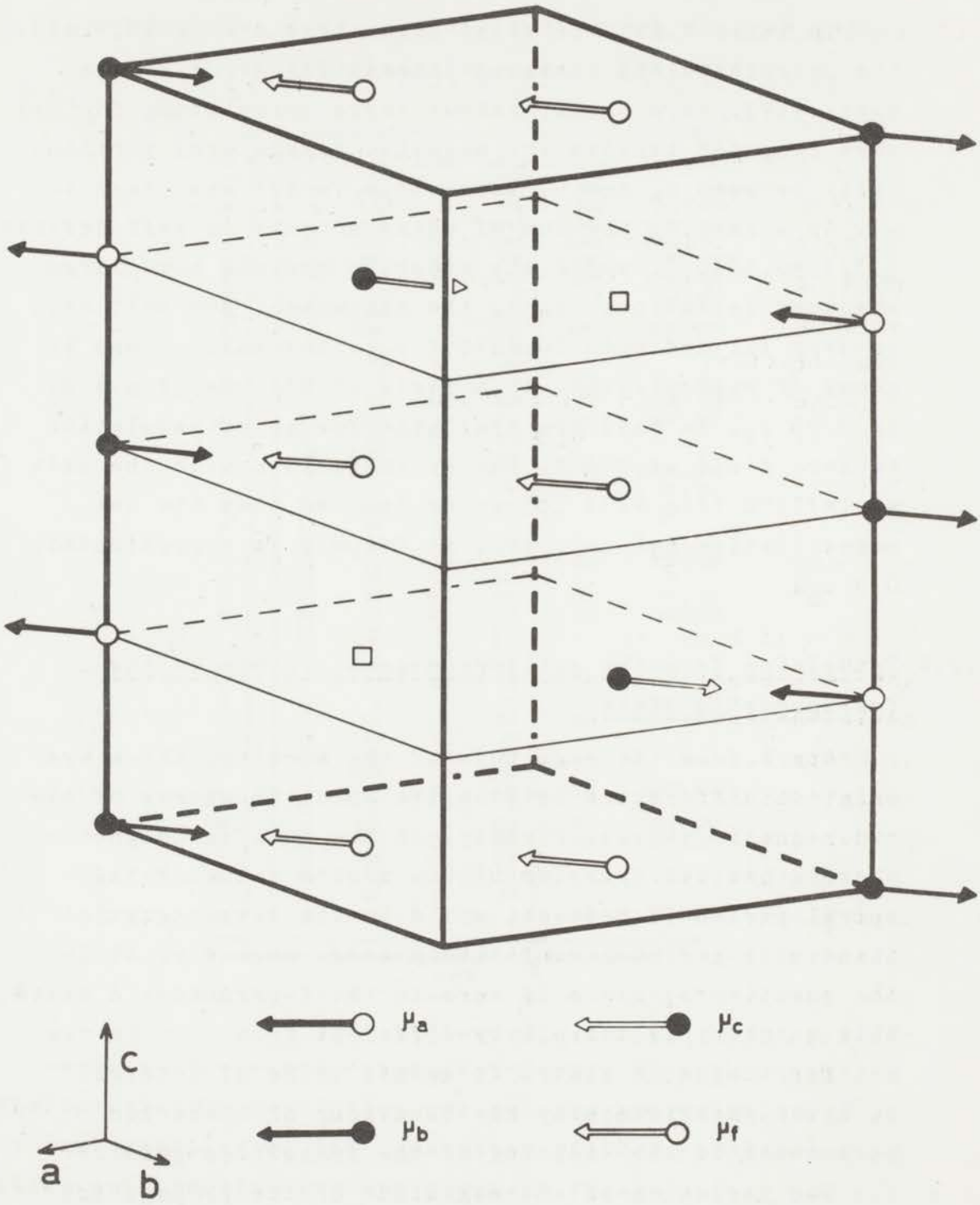

Fig.4.6
Ferrimagnetic spin arrangement in Cr_5S_6.

In table 4.IV, the final parameters are shown, and the calculated and observed intensities are given in table 4.VI. Here again, rather large correlation factors were computed between the magnetic parameters, particularly between μ_b and μ_f where this factor was close to -1. As a result, the sum of these moments is well defined $[(3.13\pm0.38)\mu_B]$, while the separate moments have large standard deviations. Also, the net moment per unit cell is very ill defined $[(0.2\pm10.7)\mu_B]$. The value found by means of magnetization in a field of 8530 Oe (fig.4.2) is 0.98 μ_B. No data are available for an extrapolation to zero field at 208°K, but by comparison with the data at T=171°K (fig.4.3) it can be deduced that the net magnetization per unit cell at T=208°K is approximately 0.9 μ_B.

4.2.4 Transition from the antiferromagnetic state to the ferrimagnetic state

Apart from the magnitude of the moments, there are only two differences between the spin structures of the two magnetic phases. Firstly, in the antiferromagnetic phase a helical ordering with a finite value of the spiral period is present, while in the ferrimagnetic phase this period is infinitely long. Secondly, while the quantity $\mu_f \sin\phi$ is zero in the ferrimagnetic state, this quantity is definitely different from zero in the antiferromagnetic state. It seemed to be of interest to study experimentally the behaviour of these two parameters in the vicinity of the transition point.

The variation of the magnitude of the propagation vector $\vec{\tau}$ as a function of temperature was studied by measuring continuously the (012^-) and (012^+) satellite peaks while warming up slowly. The angular distance between these two peaks provides a direct measure for $|\vec{\tau}|$.

Table 4.VI Calculated and observed intensities of Cr_5S_6 in the ferrimagnetic state (T=208°K).

h	k	l	j	I_n calc	I_m calc	I_{tot} calc	$\sum_r I_{tot}$ calc	$\sum_r I_{tot}$ obs[a]
0	0	2	2	307	1	309	309	239 (55)
0	1	0	6	130	45	174	174	222 (55)
0	1	1	12	655	587	1242	1242	1248 (70)
0	1	2	12	142	5901	6042	6043	6056 (100)
0	1	3	12	403	163	567	567	611 (50)
1	1	0	6	1230	0	1230	1230	1237 (65)
0	0	4	2	2	0	3	3	42 (50)
1	1	$\bar{2}$	6	1506	0	1506		
1	1	2	6	3598	0	3599	5105	4970 (100)
0	2	0	6	33	7	40	40	0 (60)
0	2	1	12	92	96	188		
0	1	4	12	71	21	92	279	198 (55)
0	2	2	12	57	1132	1189	1189	1255 (65)
0	2	3	12	355	39	394	394	430 (60)
0	1	5	12	22	131	153		
1	1	4	6	4562	0	4562		
1	1	$\bar{4}$	6	5577	0	5578	10293	10474 (125)
1	2	0	12	45	5	50	50	83 (40)
1	2	$\bar{1}$	12	163	34	197		
1	2	1	12	39	34	72		
0	2	4	12	48	6	54		
0	0	6	2	2	0	2	326	222 (50)
1	2	$\bar{2}$	12	39	403	442		
1	2	2	12	39	403	441	883	733 (70)
0	1	6	12	32	587	618	618	786 (75)
1	2	$\bar{3}$	12	296	14	311		
1	2	3	12	135	14	149		
0	3	0	6	6961	0	6962		
0	2	5	12	52	45	96		
0	3	1	12	0	0	0	7517	7403 (120)
0	3	2	12	204	0	204	204	340 (80)
1	2	4	12	36	2	39		
1	2	$\bar{4}$	12	36	2	39		
1	1	$\bar{6}$	6	1958	0	1958		
1	1	6	6	569	0	569	2604	2627 (90)
0	3	3	12	0	0	0		
0	1	7	12	344	6	351	351	339 (80)
0	2	6	12	28	221	249	249	273 (60)
2	2	0	6	478	0	478		
1	2	$\bar{5}$	12	5	18	23		
1	2	5	12	76	18	93		
0	3	4	12	8	0	8	602	581 (70)

[a] Numbers in parentheses are estimated standard deviations.

The temperature resolution per run was approximately 3°. Typical examples of the separation of these peaks at four different temperatures are given in fig.4.7.

In fig.4.8 the resulting curve of $|\vec{\tau}|$ versus temperature is given. This figure shows that $|\vec{\tau}|$ decreases monotonously to zero when the temperature approaches the transition point. In other words, the higher the temperature, the more the helix unwinds until at T=168°K the period of the helix becomes infinite. Then, a net moment develops and the transition to the ferrimagnetic state occurs.

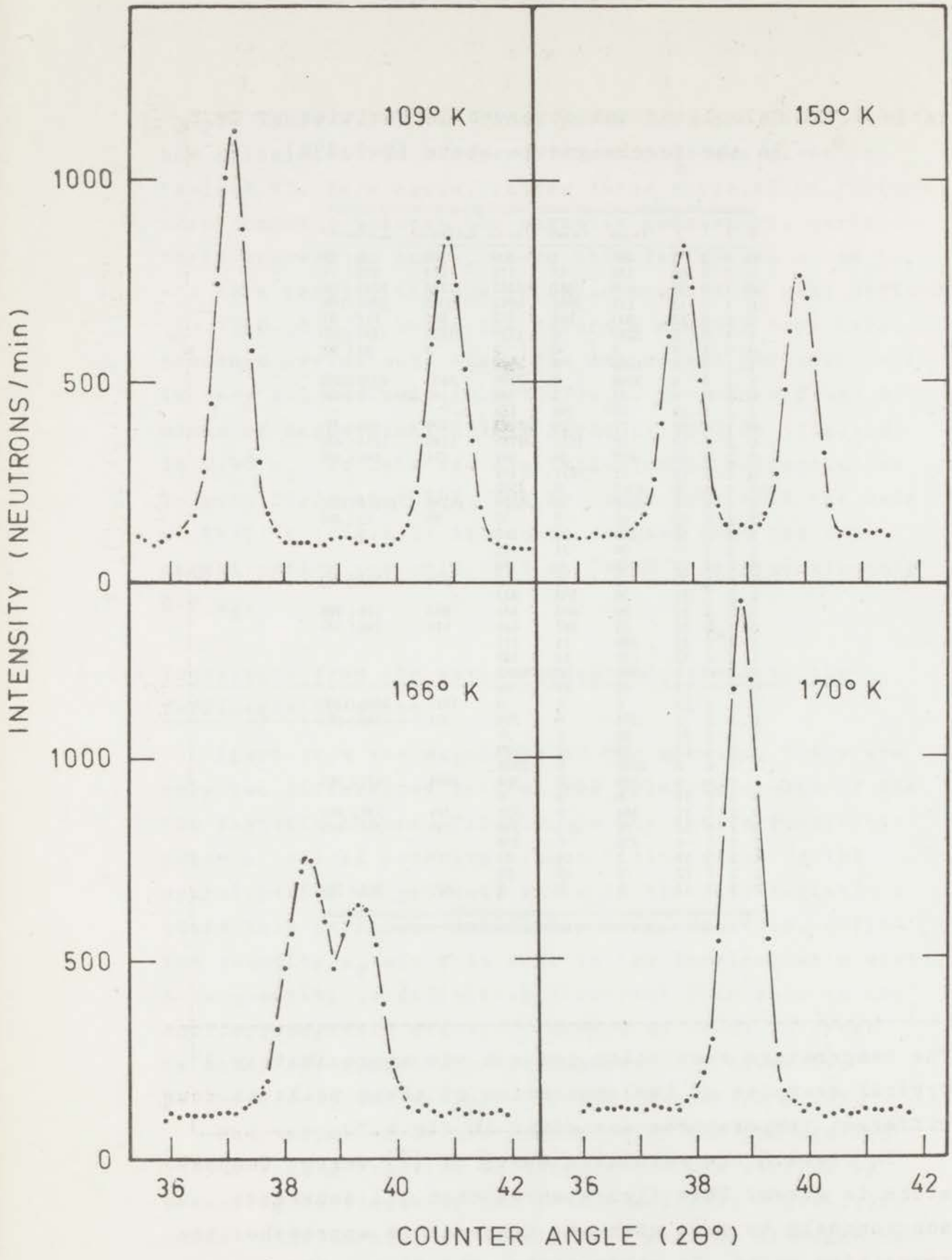

Fig.4.7
Typical examples of the angular separation of the (012^-) and (012^+) peaks at four different temperatures in Cr_5S_6.

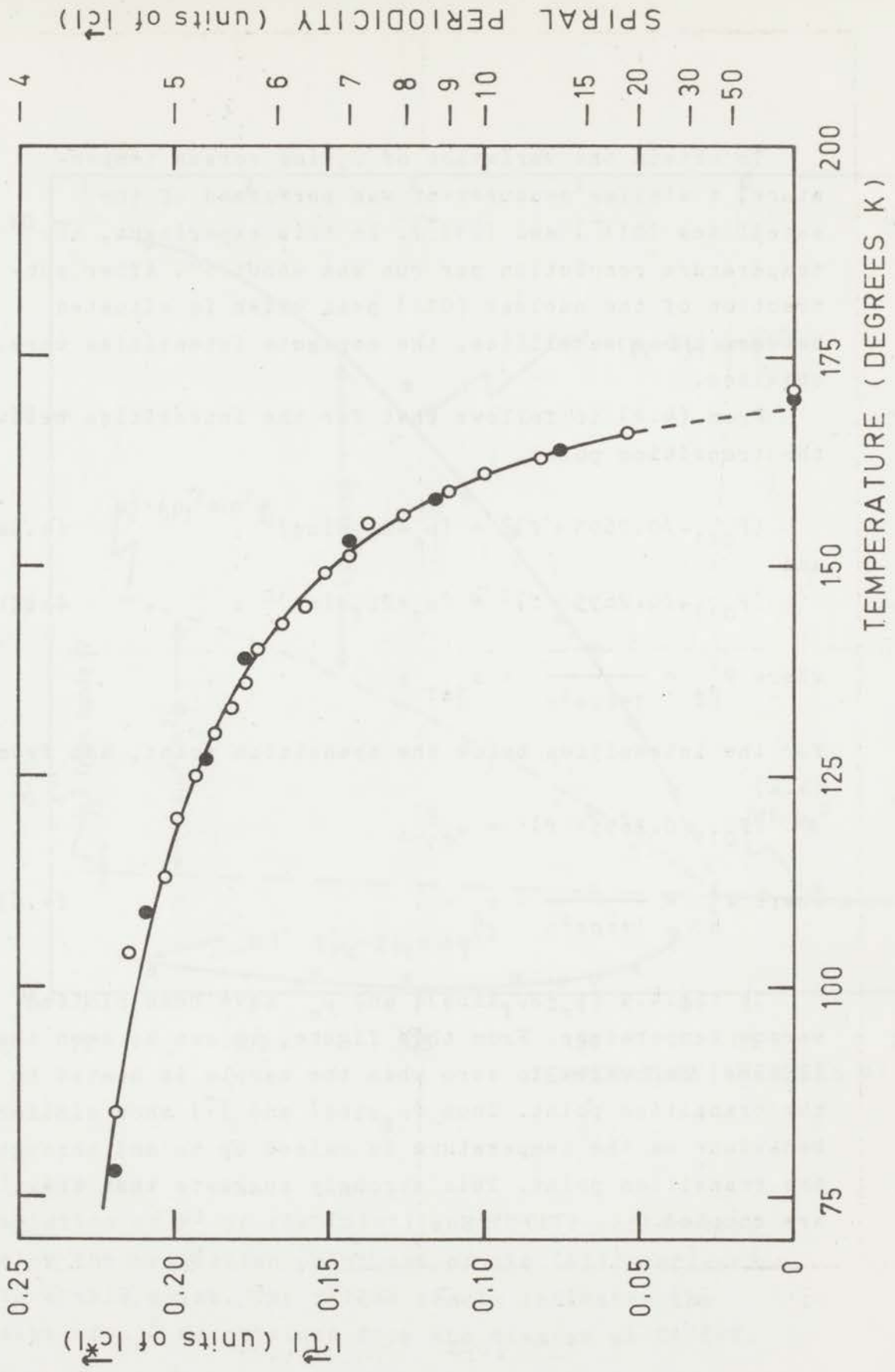

Fig.4.8

Variation of the wave vector $\vec{\tau}$ with temperature in Cr_5S_6. The left-hand ordinate gives the wave vector in units of $|\vec{c}^*|$, the right-hand ordinate the spiral periodicity in units of $|\vec{c}|$. The open and filled circles represent two different runs.

To obtain the variation of $\mu_f \sin\phi$ versus temperature, a similar measurement was performed of the satellites (011^-) and (011^+). In this experiment, the temperature resolution per run was about 6^o. After subtraction of the nuclear (011) peak which is situated between these satellites, the separate intensities were obtained.

From (4.2) it follows that for the intensities below the transition point,

$$(F_{011}-/0.2695 \times f)^2 = (\mu_c - 2\mu_f \sin\phi)^2 \ , \qquad (4.5a)$$

and

$$(F_{011}+/0.2695 \times f)^2 = (\mu_c + 2\mu_f \sin\phi)^2 \ , \qquad (4.5b)$$

where $F^2_{\vec{H}^\pm} = \frac{4}{1+\cos^2\eta} < \sigma_{\vec{H}\pm\vec{\tau}} >$

for the intensities below the transition point, and from (4.4)

$$(F_{011}/0.2695 \times f)^2 = \mu_c{}^2 \ ,$$

where $F^2_{\vec{H}} = \frac{2}{1+\cos^2\eta} < \sigma_{\vec{H}} > \ . \qquad (4.6)$

In fig.4.9 $(\mu_c \pm 2\mu_f \sin\phi)^2$ and $\mu_c{}^2$ have been plotted versus temperature. From this figure, it can be seen that $|\mu_f \sin\phi|$ decreases to zero when the sample is heated to the transition point. Thus $|\mu_f \sin\phi|$ and $|\vec{\tau}|$ show similar behaviour as the temperature is raised up to and through the transition point. This strongly suggests that they are coupled.

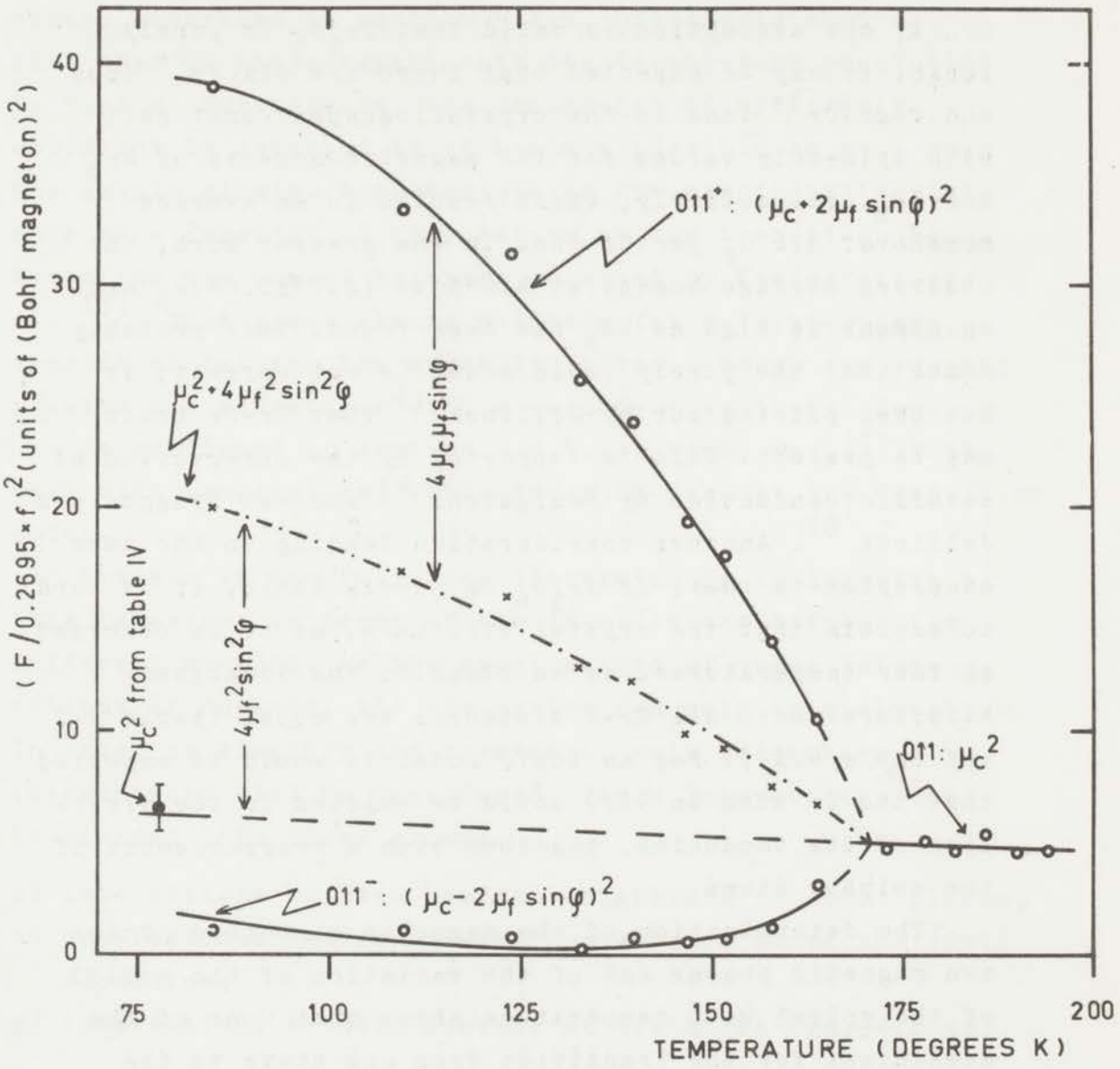

Fig.4.9
Variation of F^2 of the (011^-) and (011^+) reflections below the transition point and of the (011) reflection above this point. The filled circle indicates the value of μ_c^2 as obtained from the diagram at T=78°K.

4.3 Discussion

If the assumption is valid that Cr_5S_6 is purely ionic, it may be expected that there are six Cr^{2+} ions and four Cr^{3+} ions in the crystallographic unit cell with spin-only values for the magnetic moments of $4\mu_B$ and $3\mu_B$, respectively, which results in an average moment of 3.6 μ_B per Cr ion. In the present work, the observed average moment at 4.2°K is $(2.73\pm0.04)\mu_B$ and no moment as high as $4\mu_B$ has been found. This probably means that the purely ionic model is not correct; it has been pointed out by Jellinek [1] that Cr-Cr bonds may be present. This is supported by the observation of metallic conduction by Kamigaichi [4] and van Bruggen and Jellinek [8]. Another consideration leading to the same conclusion is that, if Cr_5S_6 is purely ionic, it is hard to explain that the crystal structure, as it is observed at four temperatures, is so close to the idealized structure where all Cr-S distances are equal (table 4.I and table 4.IV). For an ionic model it would be expected that the Cr atom in 4(f) would be shifted in the direction of the vacancies, together with a rearrangement of the sulphur atoms.

The determination of the magnetic structure of the two magnetic phases and of the variation of the period of the spiral with temperature shows that none of the mechanisms for the transition from one state to the other, proposed so far [1,3,6], is correct. The mechanism following from this investigation is characterized by a gradual change in the period of the spiral (fig.4.8) which accounts very elegantly for the observed jump in the magnetization versus temperature curve.

For the interpretation of the results of the experiments, described in section 4.2.4, one should keep in mind that in these experiments the temperature resolution is finite. Furthermore, the occurrence of hysteresis could not be detected as it was not possible to cool down the sample slowly. A hysteresis in the electrical resistance as a function of temperature at the transition between the two phases has been observed by Kamigaichi et al. [13]. This gives strong evidence for a first-order transition between the magnetic states, though the present results are compatible with a second-order transition.

As mentioned in section 4.2.4, $|\mu_f \sin\phi|$ and $|\vec{\tau}|$ both vary with temperature, while becoming zero at the transition point.

The aim of the following discussion is to illustrate this behaviour in terms of the interactions between the different moments. As the exact nature of these interactions is unknown, the discussion can only be qualitative. In order to simplify the treatment, only Heisenberg interactions will be considered. These interactions can be divided into three groups:

a) interactions between nearest neighbours in (001) planes;
b) interactions between nearest neighbours along the [001] direction;
c) interactions between moments at distances $(\pm\frac{1}{3}, \pm\frac{1}{3}, \frac{1}{4} \pm z)$.

The Cr-S-Cr angles for these three types of interactions in the idealized structure (z=0) are 89°, 72°, and 132° respectively. In the actual structure the angles deviate slightly from these values.

The Heisenberg energies resulting from the three groups of interactions are for half a unit cell:

$$W_a = -6C_{bf}\cos\phi - 3C_{ff}\cos 2\phi + 3C_{ac},$$

$$W_b = +2C_{ab}\cos\alpha - 2C'_{cf}\cos(\alpha+\phi),$$

$$W_c = -6C_{bc}\cos\alpha + 6C_{af}\cos(\alpha+\phi) + 6C'_{af}\cos(\alpha-\phi) - 6C_{cf}\cos(\alpha-\phi).$$

The energy for the whole system is

$$W_{total} = W_a + W_b + W_c. \qquad (4.7)$$

In these equations, $C_{ij} = J_{ij}\mu_i\mu_j$ where J_{ij} is the exchange integral for the interaction between the moments μ_i and μ_j at the crystallographic positions i and j.
C_{af} stands for interactions over a distance $(\frac{1}{3},\frac{1}{3},\frac{1}{4}-z)$,
C'_{af} for interactions over $(\frac{1}{3},\frac{1}{3},\frac{1}{4}+z)$,
C_{cf} for interactions over $(\frac{1}{3},\frac{1}{3},\frac{1}{4}+z)$ and
C'_{cf} for interactions over $(0,0,\frac{1}{2}-z)$.

α is the rotation angle of the spiral between two adjacent Cr layers and ϕ has the same meaning as in table 4.III.
The total energy can then be written as

$$W_{total} = A\cos\alpha + B\cos\phi + C\cos 2\phi + D\cos(\alpha+\phi) + E\cos(\alpha-\phi) + F \qquad (4.8)$$

where $A = 2C_{ab} - 6C_{bc}$,
$B = -6C_{bf}$,
$C = -3C_{ff}$,
$D = 6C_{af} - 2C'_{cf}$,
$E = 6C'_{af} - 6C_{cf}$,
$F = 3C_{ac}$.

From $\frac{\delta W_{total}}{\delta\alpha} = 0$ it is found that, for the relation between the equilibrium values of α and ϕ,

$$\tan\alpha = -\frac{(D-E)\sin\phi}{(D+E)\cos\phi+A}. \qquad (4.9)$$

Thus $|\mu_f \sin\phi|$ goes to zero when α does, which fits the observed behaviour in the helimagnetic state.

The derivatives of W_{total} with respect to α and ϕ both vanish for $\alpha=0^o$ and $\phi=180^o$. These values for α and ϕ, which correspond to the collinear ferrimagnetic structure, indeed minimize the total energy, provided that the following conditions are satisfied:

$$(D-E)^2 - (D+E-A)(D+E+B-4C) < 0, \qquad (4.10a)$$

$$D+E-A > 0. \qquad (4.10b)$$

To simplify the discussion, all individual moments μ_i will be taken equal to the average value μ_{av}. From table 4.IV it can be seen that this is a reasonable assumption. Furthermore, it will be assumed that the exchange integrals J_{ij} are equal for all i,j within each group of interactions (a), (b), and (c). This is a reasonable assumption because within a group the Cr-Cr distances and the Cr-S-Cr angles are practically equal. Then

$$A = -D = (2J_b - 6J_c)\,\mu_{av}^2 ,$$

$$B = 2C = -2F = (-6J_a)\,\mu_{av}^2 ,$$

$$E = 0.$$

Substitution of this in (4.10) yields

$$A < -4C , \qquad (4.11a)$$

$$A < 0 . \qquad (4.11b)$$

If (4.11) is satisfied, the ferrimagnetic phase is stable. It seems reasonable to assume that the interaction in the basalplane is negative, i.e. $J_a<0$ and $C>0$. Then (4.11a) is the more stringent of the conditions (4.11).

Evidently, this condition is satisfied above the transition point. When the temperature is lowered, the axial ratio c/a increases [13,14]. It can be expected that consequently $|J_a|$ becomes relatively more important and the ratio A/C less negative. At a certain point, i.e. the transition point, the condition (4.11a) will no longer be satisfied and W_{total} will no longer be minimized by $\alpha=0^\circ$ and $\phi=180^\circ$. At that temperature the structure becomes helimagnetic. The conditions

$$\frac{\delta W_{total}}{\delta \alpha} = 0 \quad \text{and} \quad \frac{\delta W_{total}}{\delta \phi} = 0$$

must always be satisfied. This leads to

$$\sin\alpha - \sin(\alpha+\phi) = 0, \tag{4.12a}$$

$$A\sin(\alpha+\phi) - 2C(\sin\phi+\sin 2\phi) = 0. \tag{4.12b}$$

From (4.12a) one finds

$$\alpha = 90^\circ - \phi/2 \ . \tag{4.13a}$$

Substituting this in (4.12b) yields

$$\sin\frac{3\phi}{2} = \frac{A}{4C} \ . \tag{4.13b}$$

Once more it is seen that A=-4C corresponds to $\phi=180^\circ$ and $\alpha=0^\circ$. When the temperature is lowered below this transition point, A/4C becomes larger than -1 and ϕ will deviate from 180° with the result that $\alpha>0^\circ$, according to (4.13a).

When A/4C approaches zero, which means $|(3J_c-J_b)/6| \ll |J_a|$, the equilibrium values of ϕ and α approach 120° and 30° respectively. In fact this value of ϕ applies in a simple layer of identical, hexagonally arranged, negatively coupled spins.

Although the above model is very simple, it describes the behaviour of Cr_5S_6 surprisingly well. It also explains the occurrence of the two magnetic phases. The values of α and ϕ at 4.2 and 77°K (table 4.IV) satisfy reasonably well equation (4.13a).

Since the behaviour of the ratio A/4C with temperature in the vicinity of the transition point is not known, it is impossible to deduce whether the model corresponds to a first- or second-order transition.

References:

1) F.Jellinek, Acta Cryst. 10, 620 (1957).
2) H.Haraldsen and A.Neuber, Z.Anorg.Allgem.Chem. 234, 337 (1937).
3) M.Yuzuri, T.Hirone, H.Watanabe, S.Nagasaki, and S.Maeda, J.Phys.Soc.Japan 12, 385 (1957).
4) T.Kamigaichi, J.Sci.Hiroshima Univ.,Ser.A 24, 371 (1960).
5) M.Yuzuri, Y.Kang, and Y.Goto, J.Phys.Soc.Japan 17, Suppl. B1, 253 (1962).
6) K.Dwight, R.W.Germann, N.Menyuk, and A.Wold, J.Appl. Phys. Suppl. 33, 1341 (1962).
7) M.Yuzuri and Y.Nakamura, J.Phys.Soc.Japan 19, 1350 (1964).
8) C.F.van Bruggen and F.Jellinek, Colloque International sur les propriétés thermodynamiques, physiques et structurales des dérivés semi métalliques du Centre National de la Recherche Scientifique, Orsay, 1965, p.31.
9) B.O.Loopstra, Nucl.Instr.Methods 44, 181 (1966).
10) H.M.Rietveld, Acta Cryst. 20, 508 (1966).
11) N.Menyuk, K.Dwight, and A.Wold, J.Appl.Phys. 36, 1088 (1965).
12) R.E.Watson and A.J.Freeman, Acta Cryst. 14, 27 (1961).
13) T.Kamigaichi, T.Okamoto, N.Iwata, and E.Tatsumoto, J.Phys.Soc.Japan 21, 2730 (1966).
14) C.F.van Bruggen and F.Jellinek, private communication.

Chapter V

THE MAGNETIC STRUCTURE OF TRIGONAL Cr_2S_3

5.1 Introduction

In the first section of the previous chapter it has been mentioned that in the Cr-S system two phases exist of the approximate composition Cr_2S_3. Of these two phases, one with composition $Cr_{0.69}S$ has trigonal symmetry, while the other with composition $Cr_{0.67}S$ has rhombohedral symmetry [1].

The crystal structure of both phases can be considered to be of the NiAs type in which from every second metal layer two of each three Cr atoms have been removed. The two phases differ from each other in the stacking sequence of the layers containing the vacancies. In the rhombohedral phase this sequence is abcabc....., leading to a c axis equal to three times that of the NiAs type sub cell; in the trigonal phase the sequence is abab.... with a c axis of twice that of the sub cell. The crystal structure of the trigonal form of Cr_2S_3 is similar to that of Cr_5S_6 (chapter IV) except for the fact that not only the 2(d) site, but also the 2(a) site is unoccupied. The magnetic properties of trigonal Cr_2S_3 are somewhat reminiscent of those of Cr_5S_6, although there are also essential differences which will be discussed in the next section. In this chapter an attempt to correlate the magnetic behaviour of this compound with the spin arrangement will be described.

The crystal structure, as given by Jellinek [1], is

Trigonal, space group $P\bar{3}1c$ (D_{3d}^2),

2 Cr in 2(c) : $(\frac{1}{3},\frac{2}{3},\frac{1}{4};\ \frac{2}{3}\ \frac{1}{3}\ \frac{3}{4})$,

2 Cr in 2(b) : $(0,0,0;\ 0,0,\frac{1}{2})$,

4 Cr in 4(f) : $\pm(\frac{1}{3},\frac{2}{3},z;\ \frac{1}{3},\frac{2}{3},\frac{1}{2}-z)$, with $z=0$,

12 S in 12(i): $\pm(x,y,z;\ \bar{y},x-y,z;\ y-x,\bar{x},z;$

$y,x,\frac{1}{2}+z;\ x-y,\bar{y},\frac{1}{2}+z;\ \bar{x},y-x,\frac{1}{2}+z)$,

with $x=\frac{1}{3}$, $y=0$, $z=\frac{3}{8}$.

It is noted that this is the idealized Cr_5S_6 structure (section 4.1.1) from which the Cr atoms in the 2(a) positions have been removed. Just as in the case of Cr_5S_6 the X-ray powder data indicate that the structure deviates only slightly from the idealized one.

Magnetization measurements on trigonal Cr_2S_3 have been carried out at the University of Groningen and are partially presented in ref. [2].

Magnetization versus temperature curves (fig.5.1) show that trigonal Cr_2S_3 is paramagnetic above approximately 125°K. When the temperature is lowered, the magnetization first increases until the maximum value is reached at about 95°K, and then decreases again gradually. From 15°K to 4.2°K the behaviour of the compound is antiferromagnetic. A sharp drop in the magnetization, as found in Cr_5S_6 (section 4.1.1), has not been observed.

Magnetization versus applied field data at different temperatures are given in fig.5.2 [*] . From these data it is seen that at temperatures below 15°K the magnetization extrapolates to zero at zero field.

---

[*]) Drs.C.F.van Bruggen of the "Laboratorium voor Anorganische Chemie" at Groningen and Mr.J.F.Fast of the "Natuurkundig Laboratorium der N.V.Philips Gloeilampenfabrieken" at Eindhoven are gratefully acknowledged for having made available to the author the data contained in figs.5.1 and 5.2.

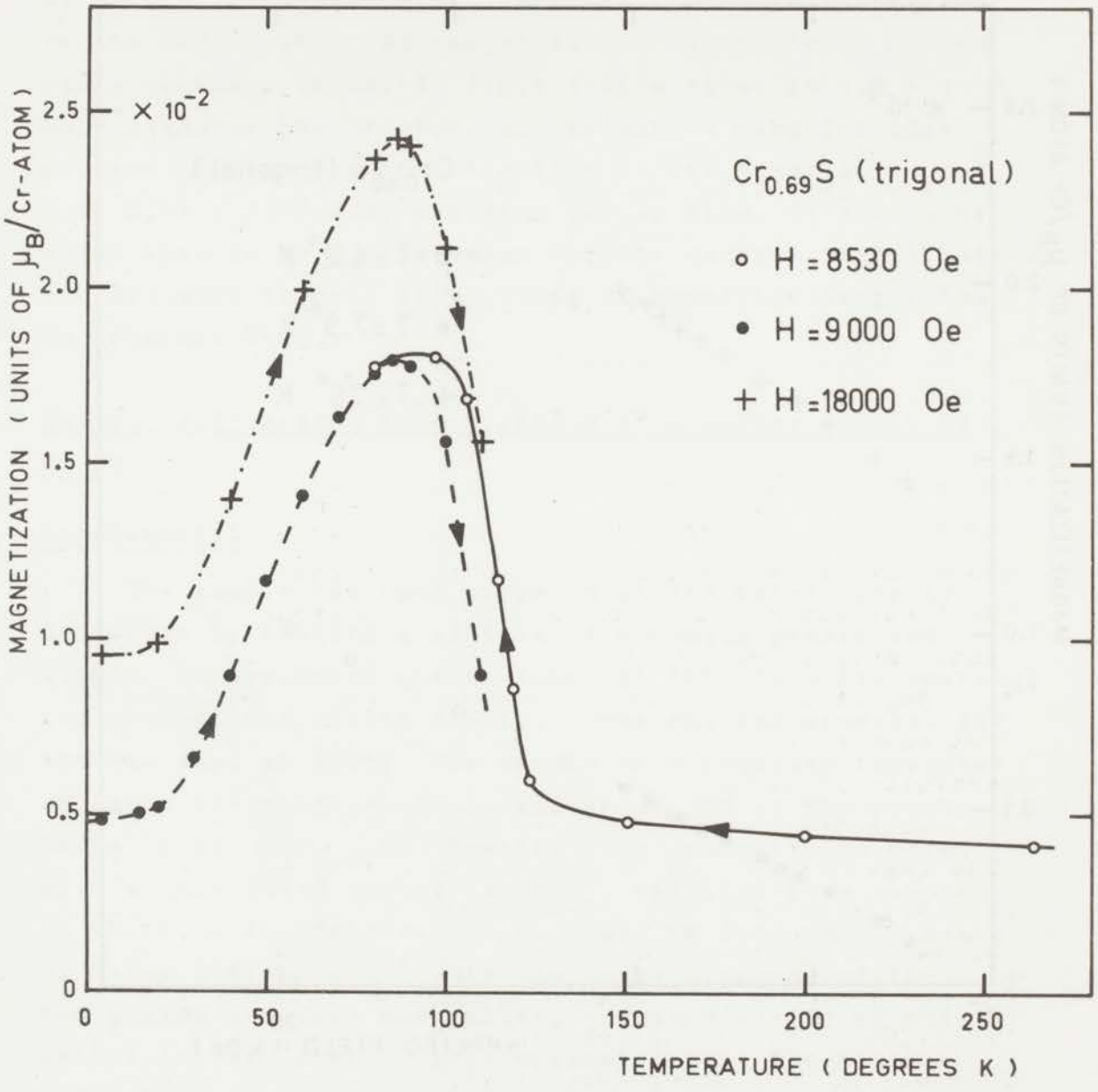

Fig. 5.1
Magnetization versus temperature curves of trigonal Cr_2S_3.

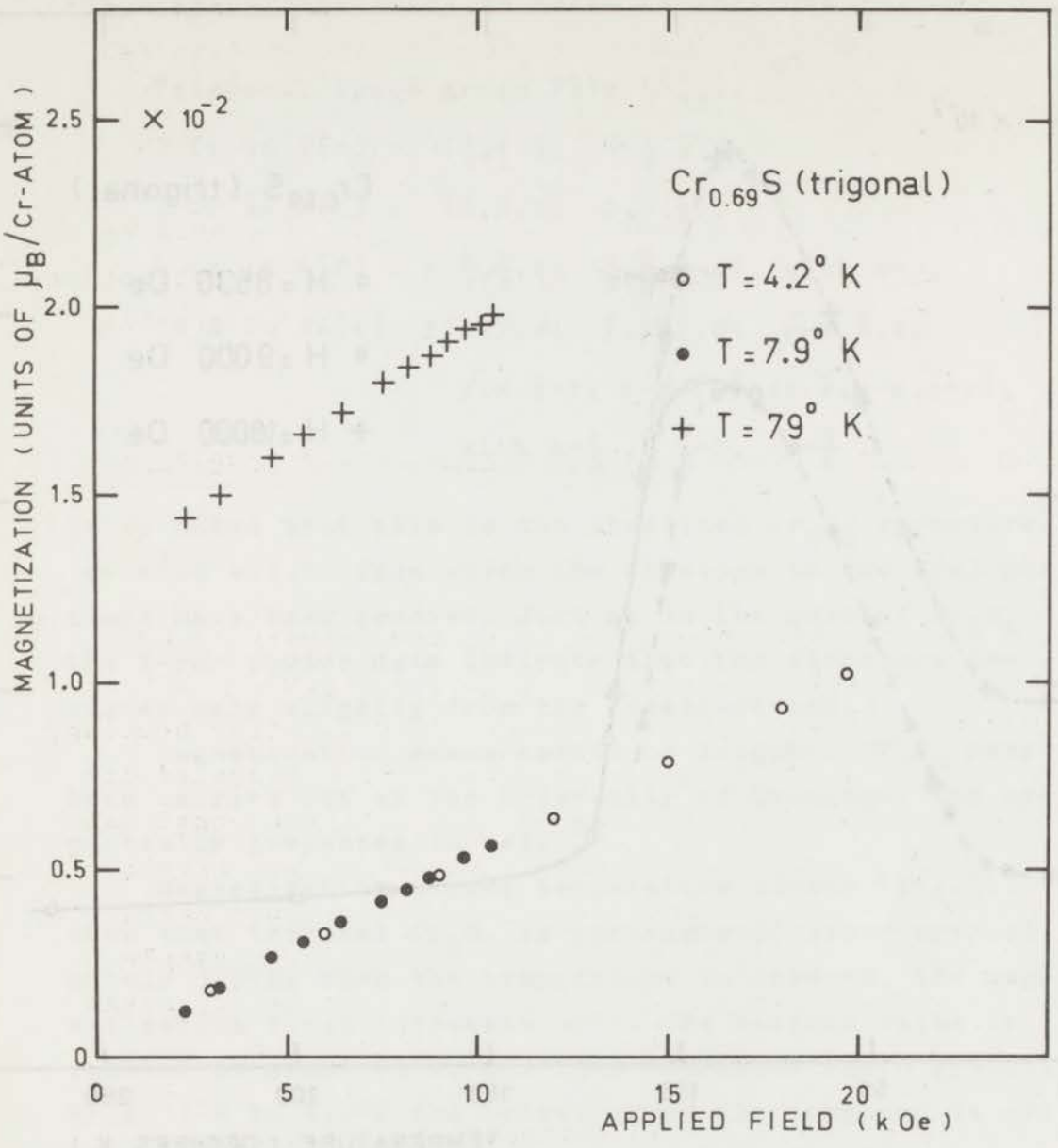

Fig.5.2
Magnetization versus applied field curves of trigonal Cr_2S_3.

At T=79°K, somewhat below the temperature of the maximum in the σ-T curves, the magnetization extrapolated to H=0 has a non-zero value. In fig.5.2 this value is 1.3×10^{-2} Bohr magneton per Cr atom. In the sample used for this neutron diffraction investigation it was somewhat lower, i.e. 0.74×10^{-2} Bohr magneton per Cr atom. It should be noted that in Cr_5S_6 the value for the maximum magnetization, extrapolated to H=0, is an order of magnitude larger than in trigonal Cr_2S_3.

5.2 Neutron diffraction investigation of a powder sample of Cr_2S_3

5.2.1 Experimental

The sample has been prepared at the University of Groningen by heating a mixture of chromium powder and sulphur in evacuated quartz tubes at 1000°C. After heating, the product was cooled slowly, powdered, and annealed for several days at 300°C. The sample thus obtained consisted of about 70% trigonal Cr_2S_3 and about 30% of the rhombohedral phase ($Cr_{0.67}S$). Heating this product once more, with a calculated amount of Cr_3S_4, resulted in a sample in which no rhombohedral Cr_2S_3 could be detected by means of X-ray diffraction *) . As the X-ray diagrams of the two phases are very much alike, the sensitivity of this method is very small. It is estimated that the minimum percentage of the rhombohedral phase that could be detected in the sample is about 5-10% when the two phases constitute a homogeneous mixture. When the rhombohedral phase is concentrated in the inner parts of the grains, this percentage may be higher. The only detectable impurity, however, consisted of small traces of Cr_2O_3.

---

*) The sample has been prepared by Miss A.Bruining and Drs.C.F.van Bruggen of the "Laboratorium voor Anorganische Chemie" at Groningen.

The lengths of the unit-cell edges, as determined by X-ray diffraction (CuKα radiation), were $a=(5.9408\pm0.0009)\text{Å}$ and $c=(11.169\pm0.002)\text{Å}$.

The values for these parameters reported by Jellinek [1] are: (a) in samples of composition $Cr_{0.71}S$ containing some Cr_3S_4: $a=(5.939\pm0.002)\text{Å}$ and $c=(11.192\pm0.003)\text{Å}$; (b) in samples of composition $Cr_{0.68}S$ containing some rhombohedral Cr_2S_3: $a=(5.943\pm0.002)\text{Å}$ and $c=(11.171\pm0.003)\text{Å}$.

Neutron diffraction diagrams were obtained at the Petten High Flux Reactor at temperatures of 4.2, about 80, and 300°K from a sample contained in a cylindrical vanadium holder with a diameter of 20 mm. Due to the extremely low thermal conductivity of trigonal Cr_2S_3 a rather large difference (about 15°) between the temperatures of the lower and upper part of the sample occurred in the experiment at $T\approx80$°K. At T=4.2°K, with the sample immersed in liquid helium, this problem did not exist.

The neutron wavelength of 2.57Å was obtained from the (111) reflection of a copper monochromator. A block of pyrolytic graphite was used as a filter to remove the second-order contamination of the primary beam [3]. Soller slits with a horizontal angular divergence of 30' were placed between the reactor and the monochromator and in front of the BF_3 counter. The neutron diagrams are shown in fig.5.3.

5.2.2 Crystallographic structure in the paramagnetic state

From the neutron data obtained at T=300°K, it was tried to refine the parameters given in section 5.1.1, as these are all idealized values. For this purpose the least-squares program described by Rietveld [4] (cf. section 4.2.2) has been used. At first the parameters were refined in a structural model in which the Cr atoms occur only at the positions given in section 5.1.1 and in which the vacancies are completely ordered.

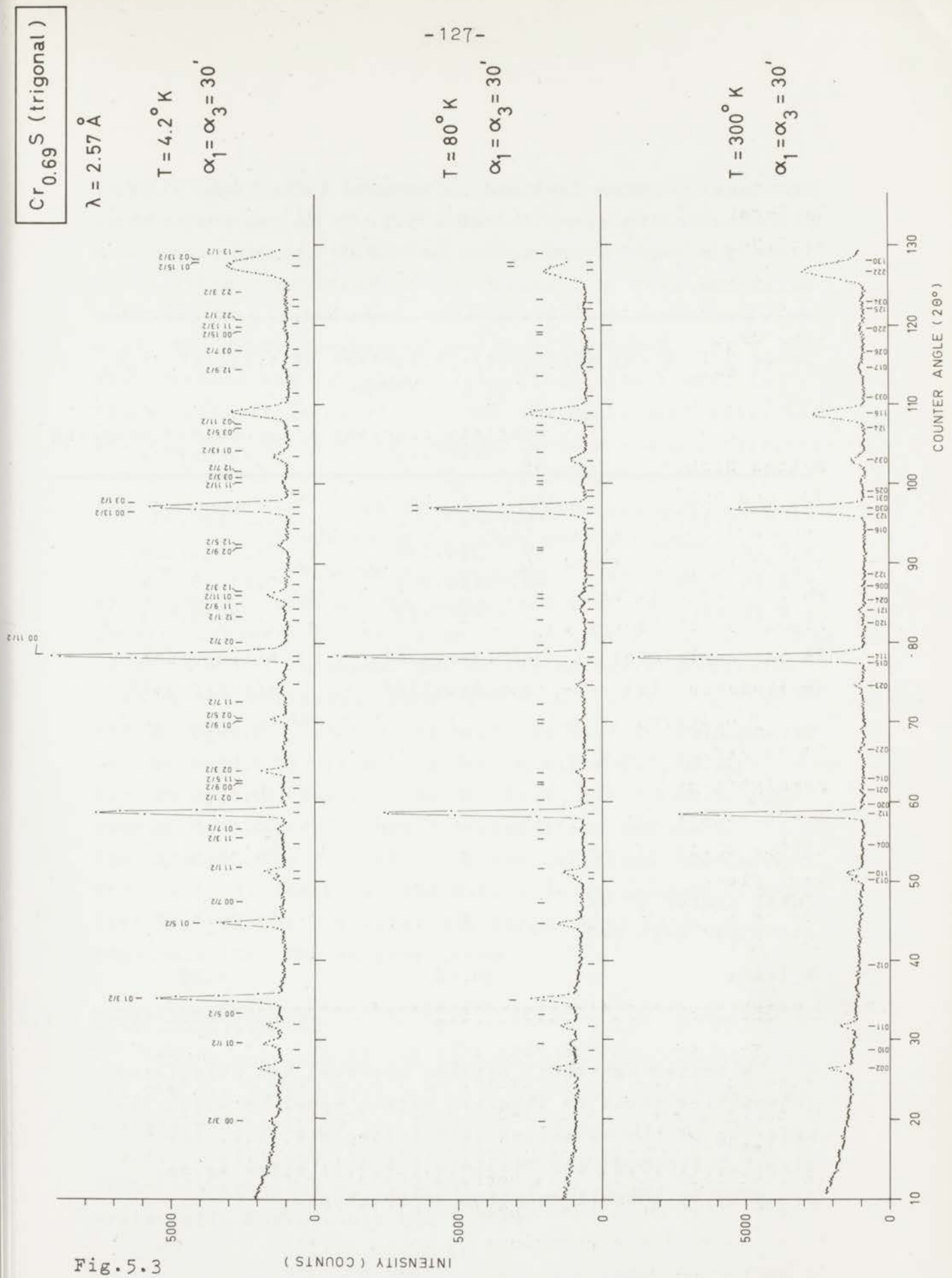

Fig.5.3

Neutron diffraction diagrams of trigonal Cr_2S_3 at three different temperatures. The indices refer to the nuclear unit cell.

The final R index (defined in section 4.2.2) was 10.7%. The results are given in table 5.I. It is seen that the isotropic temperature motion of the Cr atoms is abnormally low.

Table 5.I Final structural parameters of trigonal Cr_2S_3 at T = 300°K

	complete ordering of vacancies	incomplete ordering of vacancies
z[Cr in 4(f)]	-0.002±0.002	-0.005±0.002
x[S in 12(i)]	0.323±0.008	0.310±0.004
y[S in 12(i)]	-0.004±0.005	-0.010±0.004
z[S in 12(i)]	0.374±0.002	0.382±0.003
B isotropic (Cr)	-(0.3±0.4)Å^2	+(1.0±0.6)Å^2
B isotropic (S)	+(0.8±0.5)Å^2	+(1.2±0.3)Å^2
Occ.nr.2(a)	-	0.29±0.08
2(b)	1	1.05±0.10
2(c)	1	0.89±0.06
2(d)	-	0.12±0.06
4(f)	1	0.80±0.06
Total number of Cr atoms per unit cell	8	7.89±0.31
R index	10.7%	6.2%

A better agreement between observed and calculated intensities could be obtained with a model in which the ordering of the vacancies is not complete, i.e. the 2(a)$(0,0,\frac{1}{4};0,0,\frac{3}{4})$ and 2(d)$(\frac{2}{3},\frac{1}{3},\frac{1}{4};\frac{1}{3},\frac{2}{3},\frac{3}{4})$ sites being occupied by a small fraction of Cr atoms.

In this model the occupation number of each site, defined as the fraction of the positions of this site occupied by a Cr atom, and the postional parameters of the 4(f) and 12(i) sites were determined by means of a full-matrix least-squares refinement. This led to a final R index of 6.2%. The final parameters are shown in table 5.I. The observed and calculated intensities are listed in table 5.II. It is noted that for the disordered model the individual isotropic temperature factors are approximately equal to those found in Cr_5S_6. The occupation numbers of the 2(a) and 2(d) sites deviate significantly from zero while the total number of Cr atoms per unit cell (7.89 ± 0.31) corresponds to the composition Cr_xS with $x=0.66\pm0.03$. It should be emphasized that this value depends directly on the ratio of the scattering amplitudes of sulphur and chromium. The values of these amplitudes used in the refinement were 0.28×10^{-12} cm for sulphur [5] and 0.351×10^{-12} cm for chromium (as used for Cr_5S_6). Comparing the two results given in table 5.I, it has been concluded that in trigonal Cr_2S_3 (at least in our sample) the vacancies are not completely ordered). Furthermore, the deviations of the positional parameters from those in the idealized NiAs type structures with strictly ordered vacancies are larger than in Cr_5S_6, especially for the sulphur atoms.

5.2.3 Magnetic structure

The appearance of the neutron diagrams, obtained at T=4.2°K and T≈80°K (fig.5.3), is the same, apart from an overall reduction of the magnetic intensities at the higher temperature. From this it is concluded that the magnetic structure of trigonal Cr_2S_3 does not change essentially between 4.2 and ≈ 80°K.

Table 5.II Calculated and observed intensities of trigonal Cr_2S_3 in the paramagnetic state ($T = 300^{\circ}K$).

h k l	j	I_{calc}	$\Sigma_r I_{calc}$	$\Sigma_r I_{obs}$ [a]
0 0 2	2	3098	3098	2780 (180)
0 1 0	6	327	327	410 (170)
0 1 1	12	2164	2164	2130 (180)
0 1 2	12	682	682	0 (160)
0 1 3	12	843	843	966 (120)
1 1 0	6	2255	2255	2016 (130)
0 0 4	2	140	140	137 (140)
1 1 2	6	18441		
1 1 $\bar{2}$	6	5643	24083	23903 (210)
0 2 0	6	213	213	193 (100)
0 2 1	12	203	203	255 (135)
0 1 4	12	98	98	0 (125)
0 2 2	12	194	194	657 (150)
0 2 3	12	1067	1067	1098 (140)
0 1 5	12	131		
1 1 4	6	21187		
1 1 $\bar{4}$	6	13525	34842	35635 (260)
1 2 0	12	26	26	110 (100)
1 2 1	12	106		
1 2 $\bar{1}$	12	628	734	579 (120)
0 2 4	12	308	308	0 (120)
0 0 6	2	2	2	0 (120)
1 2 2	12	1242		
1 2 $\bar{2}$	12	107	1349	0 (145)
0 1 6	12	114	114	0 (140)
1 2 3	12	246		
1 2 $\bar{3}$	12	732		
0 3 0	6	24808	25786	25068 (230)
0 3 1	12	0		

Table 5.II (continued)

h k l	j	I_{calc}	$\Sigma_r I_{calc}$	$\Sigma_r I_{obs}$ [a]
0 2 5	12	278	278	554 (145)
0 3 2	12	2052	2052	2383 (175)
1 2 4	12	98		
1 2 $\bar{4}$	12	7	105	27 (115)
1 1 6	6	1210		
1 1 $\bar{6}$	6	10959	12170	12476 (195)
0 3 3	12	0	0	0 (130)
0 1 7	12	772	772	1161 (160)
0 2 6	12	262	262	182 (130)
2 2 0	6	1021	1021	764 (160)
1 2 5	12	378		
1 2 $\bar{5}$	12	18		
0 3 4	12	121	517	322 (160)

a) numbers in parentheses are estimated standard deviations.

At both temperatures magnetic scattering only occurs in directions associated with reciprocal lattice points located on the c^* axis midway between the nuclear reciprocal lattice points. This means that, within the limits set by the accuracy of the observation, at both temperatures there is no ferromagnetic component in the spin structure. The period in the c direction is twice that of the nuclear structure and each spin has an antiparallel partner at a vector distance $\vec{c}$. As the indices in fig.5.3 refer to the crystallographic unit cell, the l indices of the magnetic peaks are of the form (2n+1)/2.

The magnetic part of the neutron diagram of trigonal Cr_2S_3 at T=4.2°K (fig.5.3) shows a strong resemblance with the magnetic part of the diagram of Cr_5S_6 at T=4.2°K (fig.4.3) when each magnetic reflection (h k (2n+1)/2) of trigonal Cr_2S_3 is compared with the sum of the reflections (hkn^+) and ($hk(n+1)^-$) of Cr_5S_6. From this observation it is deduced that the spin structure of trigonal Cr_2S_3 should be closely related to that of Cr_5S_6 in the antiferromagnetic state, i.e. it can be described as a screw type spiral structure with a periodicity of exactly twice the crystallographic c axis.

The adopted model for the spin structure is given in table 5.III. In this table the phase angles of the different moments are given as well as the angles between these moments and the moment of the Cr atom at (0,0,0). It should be noted that, with this spiral period, this structure is the only one in which equivalent distance vectors correspond to equal angles between the spins.

The expression for the scattering cross section, averaged over equivalent reflections, for this type of magnetic structure is (section 2.3.2)

$$\langle \sigma_{\vec{H}} \rangle = \frac{1+\cos^2\eta}{2} \left| 0.2695 \sum_{\nu} \hat{K}_\nu \mu_\nu f_\nu(\vec{H}) \exp 2\pi i \, \vec{H}\cdot\vec{r}_\nu \right|^2 \qquad (5.1)$$

$$\text{for } \vec{H} = h\vec{a}^* + k\vec{b}^* + (2n+1)\,\vec{c}^*/2. \qquad (5.2)$$

$\hat{K}_\nu$ is a unit vector in the direction of the moment of the ν-th atom, $f_\nu(\vec{H})$ is the form factor of the magnetic atom ν, and μ_ν is its moment in Bohr magnetons. The angle between the scattering vector and the c^* axis is indicated by η. The position vectors $\vec{r}_\nu$ refer to the crystallographic unit cell and the sum is taken over all atoms in this cell. From the neutron powder data only relative angles between the moments in the basal plane can be deduced.

Table 5.III Schematic representation of magnitude and relative phase angle of magnetic moments in the magnetic phase of trigonal Cr_2S_3. The values in the last column refer to the idealized structure (z=0). The structural parameters refer to the nuclear cell.

Position	x	y	z	Moment	Phase angle	Angle with moment at (0,0,0)
2(b)	0	0	0	μ_b	0°	0°
2(b)	0	0	$\frac{1}{2}$	μ_b	0°	90°
4(f)	$\frac{1}{3}$	$\frac{2}{3}$	z	μ_f	$+\phi$	$-\phi$
2(c)	$\frac{1}{3}$	$\frac{2}{3}$	$\frac{1}{4}$	μ_c	0°	45°
4(f)	$\frac{1}{3}$	$\frac{2}{3}$	$\frac{1}{2}-z$	μ_f	$-\phi$	$90°+\phi$
4(f)	$\frac{2}{3}$	$\frac{1}{3}$	$\frac{1}{2}+z$	μ_f	$+\phi$	$90°-\phi$
2(c)	$\frac{2}{3}$	$\frac{1}{3}$	$\frac{3}{4}$	μ_c	0°	135°
4(f)	$\frac{2}{3}$	$\frac{1}{3}$	$\bar{z}$	μ_f	$-\phi$	$+\phi$

The magnetic parameters to be determined are the moments on the different sites and the phase angle ϕ. In addition, the position parameters of the Cr atom in 4(f) and of the sulphur atoms should be refined. For the refinement of the form factor the same analytical expression was used as in the case of Cr_5S_6 (section 4.2.3.1). The refinement was carried out by a full-matrix least-squares program minimizing the quantity mentioned in section 4.2.2. The occupation numbers of the different sites were kept fixed at the values derived from the data at T=300°K (section 5.2.2).

The parameters resulting from the refinement are given in table 5.IV. It should be noted that it was not possible to detect a magnetic moment on the 2(a) and 2(d) sites. The moments in table 5.IV are the moments per site. To obtain the moment per Cr atom, the values in the table should be divided by the occupation number of the site.

Inspection of table 5.IV shows that at both temperatures the phase angle is, within its standard deviation, equal to 135°. When this angle is taken to be equal to 135°, the moment on a 2(c) position is antiparallel to the moments on the neighbouring 4(f) positions situated at a distance of $\pm \vec{c}/4$. In the columns II of table 5.IV the final parameters are shown. It is seen that the R index increases only slightly compared with the refinement in which there were no restrictions on the value of ϕ, while the standard deviations of the moments of the different sites become much smaller. The average moments, which were already much better defined than the moments per site due to the rather large correlation factors appearing in the refinement, are not affected at all. It is concluded that a deviation of the phase angle ϕ from 135° cannot be deduced from the experimental data. In table 5.V the observed and calculated intensities are listed. The spin structure is shown in fig.5.4.

The standard deviations of the final parameters in table 5.IV have been calculated on the assumption that the only errors occurring in the observed intensities are those due to counting statistics. As has already been mentioned in section 5.2.1, in the experiment at $T \approx 80°K$ a large temperature gradient existed over the sample which causes the actual uncertainty of the final parameters at $T \approx 80°K$ to differ from the listed standard deviations by an unknown systematic error.

Table 5.IV Final structural and magnetic parameters of trigonal Cr_2S_3 in the magnetic state. In the columns I the results are given from a refinement in which there are no restrictions on the phase angle ϕ. In column II the data from a refinement, in which ϕ is kept fixed at 135°, are given.

	T=4.2°K		T≈80°K	
	I	II	I	II
a	(5.924±0.002)Å		(5.933±0.002)Å	
c	(11.157±0.005)Å		(11.158±0.003)Å	
c_{magn}	(22.314±0.009)Å		(22.316±0.007)Å	
z[Cr in 4(f)]	-0.003±0.001	-0.003±0.001	-0.003±0.001	-0.003±0.001
x[S in 12(i)]	0.318±0.005	0.318±0.005	0.329±0.035	0.329±0.035
y[S in 12(i)]	-0.008±0.005	-0.008±0.005	-0.010±0.004	-0.010±0.004
z[S in 12(i)]	0.382±0.003	0.382±0.003	0.382±0.002	0.382±0.002
μ_b	$(2.0\pm1.9)\mu_B$	$(2.6\pm0.3)\mu_B$	$(1.8\pm0.5)\mu_B$	$(1.7\pm0.4)\mu_B$
μ_c	$(2.1\pm0.4)\mu_B$	$(2.4\pm0.3)\mu_B$	$(2.2\pm0.7)\mu_B$	$(2.3\pm0.7)\mu_B$
μ_f	$(2.1\pm1.1)\mu_B$	$(1.5\pm0.2)\mu_B$	$(0.8\pm0.3)\mu_B$	$(0.8\pm0.3)\mu_B$
$\mu_{average}$	$(2.1\pm0.2)\mu_B$	$(2.0\pm0.1)\mu_B$	$(1.4\pm0.3)\mu_B$	$(1.4\pm0.2)\mu_B$
ϕ	(113±39)°	135°	(132±14)°	135°
form factor constants:				
a	0.22±0.16	0.17±0.23	0.28±0.06	0.28±0.07
b	$(4.9\pm2.7)Å^2$	$(4.3\pm2.6)Å^2$	$(9.5\pm3.6)Å^2$	$(9.1\pm5.0)Å^2$
$B_{overall}$	$0\ Å^2$	$0\ Å^2$	$(1.2\pm0.3)Å^2$	$(1.2\pm0.3)Å^2$
R index	9.9%	10.5%	9.2%	9.4%

The listed magnetic moments are the moments per site.

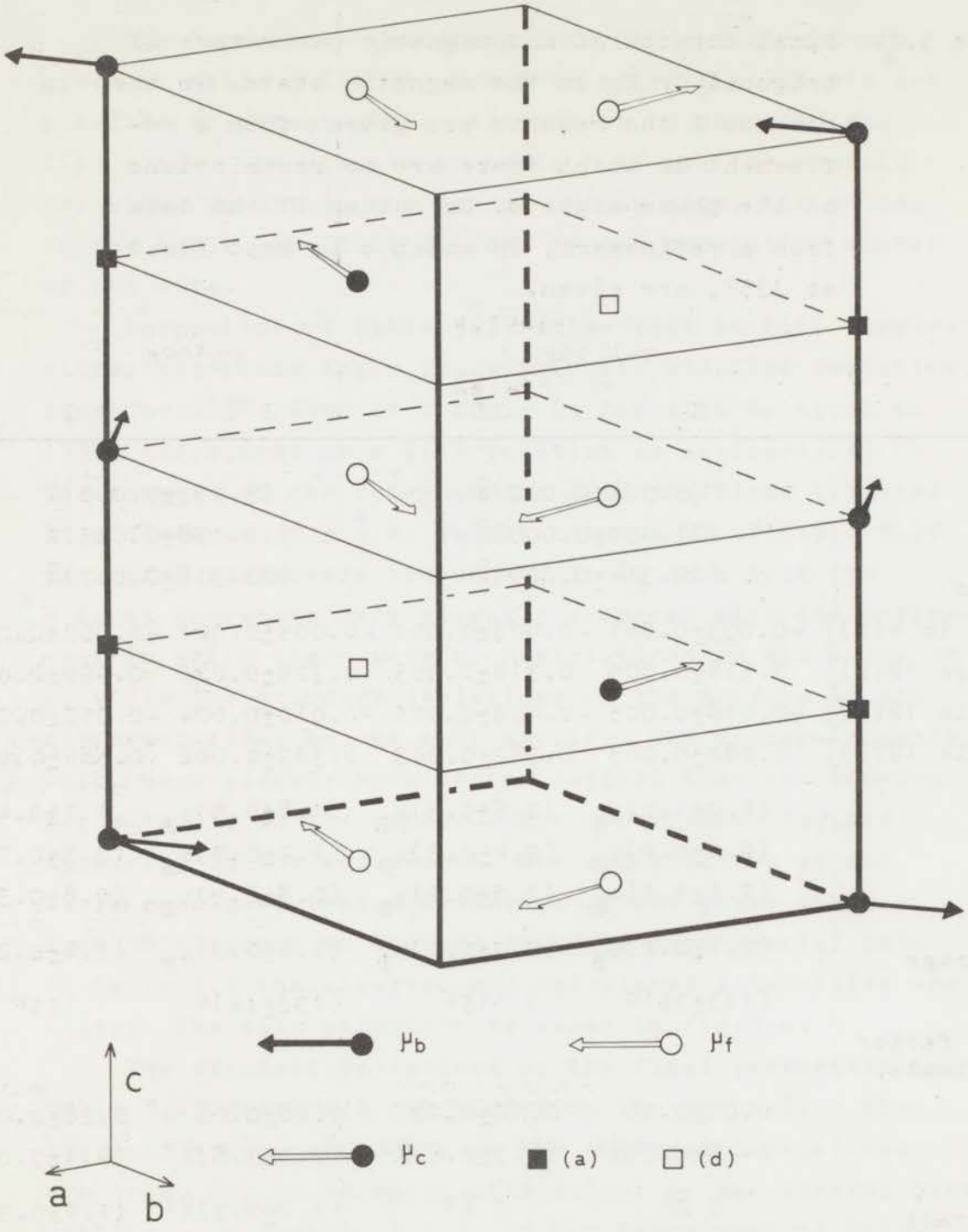

Fig.5.4
Antiferromagnetic spin arrangement in trigonal Cr_2S_3.
Only one crystallographic unit cell is shown.

Table 5.V Calculated and observed intensities of trigonal Cr_2S_3 in the antiferromagnetic state

		T=4.2°K			T≳80°K		
		I_{calc}	$\Sigma_r I_{calc}$	$\Sigma_r I_{obs}$ a)	I_{calc}	$\Sigma_r I_{calc}$	$\Sigma_r I_{obs}$ a)
0 0 3/2	2	1741	1741	783 (250)	1342	1342	0 (250)
0 0 2	2	2863	2863	3199 (190)	3511	3511	3577 (170)
0 1 0	6	127	127	182 (130)	2	2	538 (110)
0 1 1/2	12	3028	3028	2374 (170)	1112	1112	934 (120)
0 1 1	12	1843	1843	1887 (160)	2238	2238	2658 (110)
0 0 5/2	2	382	382	459 (130)	266	266	666 (110)
0 1 3/2	12	16686	16686	17446 (220)	7532	7532	7659 (170)
0 1 2	12	604	604	0 (160)	645	645	0 (130)
0 1 5/2	12	9608	9608	9068 (200)	3798	3798	3808 (160)
0 0 7/2	2	319	319	353 (160)	256	256	226 (110)
0 1 3	12	871	871	1440 (140)	979	979	965 (110)
1 1 0	6	2023			2241		
1 1 1/2	12	915	2938	2175 (150)	646	2887	2542 (130)
0 0 4	2	144	144	165 (100)	156	156	227 (100)
1 1 3/2	12	426	426	344 (100)	203	203	90 (80)
0 1 7/2	12	939	939	925 (140)	207	207	365 (100)
1 1 $\bar{2}$	6	5712			6441		
1 1 2	6	18033	23745	24148 (220)	19767	26208	27296 (210)
0 2 0	6	81			0		
0 2 1/2	12	406	488	344 (130)	100	100	158 (100)
0 2 1	12	253			231		
0 0 9/2	2	206	459	517 (130)	122	353	117 (100)
1 1 5/2	12	248			120		
0 1 4	12	31	279	226 (90)	3	123	0 (80)
0 2 3/2	12	2505	2505	2696 (140)	805	805	814 (100)
0 2 2	12	205	205	364 (150)	258	258	0 (100)
0 1 9/2	12	409			113		
0 2 5/2	12	1878	2286	1798 (150)	596	709	553 (120)
1 1 7/2	12	370	370	1023 (150)	248	248	1517 (120)
0 2 3	12	953	953	1025 (130)	1139	1139	1180 (110)

Table 5.V (continued)

		T=4.2°K			T≈80°K		
		I_{calc}	$\Sigma_r I_{calc}$	$\Sigma_r I_{obs}$ a)	I_{calc}	$\Sigma_r I_{calc}$	$\Sigma_r I_{obs}$ a)
0 1 5	12	131			92		
1 1 $\bar{4}$	6	13614			13727		
1 1 4	6	21879			23125		
0 0 11/2	2	51	35675	38234 (250)	21	36965	35341 (220)
0 2 7/2	12	247	247	517 (120)	52	52	146 (90)
1 2 0	12	6			2		
1 2 1/2	24	283	289	415 (130)	69	71	190 (100)
1 2 $\bar{1}$	12	550			601		
1 2 1	12	129	679	591 (110)	67		
1 1 9/2	12	356	356	0 (200)	216	884	847 (100)
0 2 4	12	145			2		
0 1 11/2	12	1729			566		
1 2 3/2	24	1796	3671	4054 (170)	598	1166	1029 (110)
0 0 6	2	0	0	0 (200)	1	1	0 (100)
1 2 $\bar{2}$	12	3			183		
1 2 2	12	761	764	368 (110)	169	352	0 (100)
0 2 9/2	12	142			44		
1 2 5/2	24	1453	1595	1678 (160)	515	558	394 (110)
0 1 6	12	139	139	158 (130)	180	180	0 (110)
1 2 $\bar{3}$	12	746			921		
1 2 3	12	321			329		
0 0 13/2	2	10			6		
0 3 0	6	27582			27329		
0 3 1/2	12	121	28780	26255 (230)	88	28674	29061 (220)
0 3 1	12	0			0		
0 2 5	12	240	240	199 (110)	207	207	155 (80)
1 1 11/2	12	122			60		
0 3 3/2	12	60	182	1114 (140)	32		
1 2 7/2	24	217	217	171 (110)	55	147	823 (125)
0 3 2	12	2297			2309		

Table 5.V (continued)

		T=4.2°K			T≈80°K		
		I_{calc}	$\Sigma_r I_{calc}$	$\Sigma_r I_{obs}$ a)	I_{calc}	$\Sigma_r I_{calc}$	$\Sigma_r I_{obs}$ a)
0 1 13/2	12	774	3070	2990 (170)	312	2621	3167 (140)
0 3 5/2	12	41			25		
1 2 $\bar{4}$	12	3			1		
1 2 4	12	45			0		
0 2 11/2	12	791	879	552 (120)	322	348	316 (100)
1 1 $\bar{6}$	6	12596			11973		
1 1 6	6	1422	14018	13168 (210)	1261	13233	13867 (170)
0 3 3	12	0	0	0 (130)	0	0	0 (90)
1 2 9/2	24	150	150	0 (200)	59	59	0 (80)
0 1 7	12	857	857	1098 (140)	951	951	748 (90)
0 3 7/2	12	80			78		
0 2 6	12	251	332	336 (130)	162	240	178 (110)
0 0 15/2	2	18			19		
1 1 13/2	12	34			27		
2 2 0	6	975			843		
2 2 1/2	12	77	1104	1097 (160)	71	961	861 (130)
1 2 $\bar{5}$	12	33			7		
1 2 5	12	361			383		
0 3 4	12	335			350		
2 2 3/2	12	40	769	1045 (170)	27	766	439 (130)

a) Numbers in parentheses are estimated standard deviations.

5.3 Discussion

The final R indices (table 5.IV), defined in section 4.2.2, are rather large compared with, for example, those obtained in the determination of the structures of Cr_5S_6 (chapter IV). This may be explained by assuming that the conversion of the 30% of rhombohedral Cr_2S_3, initially present in the sample (section 5.2.1), was incomplete, resulting in a rather impure sample. As has been pointed out previously, the sensitivity of X-ray diffraction methods to the presence of the rhombohedral form is rather small.

However, the conclusion that the spin structures at T=4.2°K and at T≳80°K are essentially the same remains valid. Thus it is concluded that the observed maximum in the magnetization versus temperature curve (fig.5.1) cannot be attributed to a major change in the spin arrangement as is the case in Cr_5S_6. Here it should be emphasized that, if the maximum in the magnetization is caused by the occurrence of a ferromagnetic component of about 0.01 μ_B/Cr atom in the spin arrangement, this component is far too small to be detected by powder neutron diffraction.

Finally, when Cr_2S_3 is completely ionic ($Cr_2^{3+}S_3^{2-}$), a Cr moment of $3\mu_B$ could be expected. The average moment, found in this work, is $(2.0\pm0.1)\mu_B$. This is similar to what has been found in chapter IV in Cr_5S_6. In the case of Cr_2S_3, however, the reduction cannot be attributed to metallic bonding since trigonal Cr_2S_3 shows no metallic conduction. Comparable reductions have been observed in Cr_2NiS_4 (30%) [6] and in Cr_3S_4 (25%) [7], where they were ascribed to covalency effects.

References

1) F.Jellinek, Acta Cryst. 10, 620 (1957).
2) C.F.van Bruggen and F.Jellinek, Colloque International sur les propriétés thermodynamiques, physiques et structurales des derivés semi-metalliques du Centre National de la Recherche Scientifique, Orsay, 1965, p.31.
3) B.O.Loopstra, Nucl.Instr. and Meth. 44, 181 (1966).
4) H.M.Rietveld, Acta Cryst. 20, 508 (1966).
5) N.Menyuk, K.Dwight, and A.Wold, J.Appl.Phys. 36, 1088 (1965).
6) B.Andron and E.F.Bertaut, J.Physique 27, 619 (1966).
7) B.Andron and E.F.Bertaut, J.Physique 27, 626 (1966).

SUMMARY

This thesis describes the determination, by means of neutron diffraction, of the magnetic structures of CoO, Cr_5S_6, and the trigonal form of Cr_2S_3.

The major part of the work has been carried out with powder samples.

In chapter I, some criteria have been formulated by means of which the different components of a powder diffractometer can be selected to optimize the luminosity while keeping the resolving power at the same level.

In chapter II, a connection has been deduced between the directions in which neutrons are scattered and the intensity of this scattering, and the amplitude and the propagation vector of each constituent Fourier component of a spin structure. First the most general case of a spin structure, with one or more Fourier components with different propagation vectors, has been treated. The results have then been applied to a number of special types of structure.

Chapter III describes an investigation of the spin arrangement in CoO. This arrangement has already been the subject of several earlier investigations. However, a reasonable doubt still existed about the correctness of the result, partly because this result had been obtained using a diffractometer with a rather low resolving power. With the higher resolving power of the diffractometer at the High Flux Reactor at Petten, however, more additional information could be obtained.

The powder diagram could be interpreted on the basis of two models for the spin structure

a) a collinear model with an angle of 27.4° between the spin axis and the tetragonal c axis. This model is equivalent to the earlier proposed model apart from the stated deviation angle of 11.5°.

b) a multi-spin-axis model in which the spin axes of the four antiferromagnetic submotives are not parallel. All spin axes, however, do make an angle of 27.4° with the c axis.

Single-crystal data could also be interpreted on the basis of these two models. For the collinear model it had to be assumed that in each crystallographic twin the four possible antiferromagnetic domains occurred with equal volumes.

During, and after the completion of, the diffraction work, several other papers on the magnetic structure of CoO were published. In particular, the torque measurements on thin CoO films yielded strong evidence for the collinear arrangement.

In chapter IV, the determination of the magnetic structures of Cr_5S_6 has been described. This compound is ferrimagnetic between 168°K and 305°K; below 168°K its behaviour is antiferromagnetic. The transition at 168°K is very abrupt. In the low temperature phase the magnetic moments are ordered in a spiral resulting in a zero net moment.

The period of the spiral is a function of temperature. The higher the temperature, the more the spiral unwinds until at 168°K the period becomes infinite and the transition to the ferrimagnetic state occurs.

The crystal structure of trigonal Cr_2S_3 is reminiscent of that of Cr_5S_6. Although the magnetization curve also showed a maximum (at 95°K), two differences with Cr_5S_6 exist: (a) the maximum value of the magnetization is about one order of magnitude smaller and (b) no discontinuity in the magnetization has been observed.

The investigation described in chapter V showed that at 4.2°K, as well as at $\approx$80°K, the spin arrangement can be described as a spiral with a period equal to twice the crystallographic c axis. The occurrence of a maximum in the magnetization curve, however, could not be explained.

SAMENVATTING

Dit proefschrift beschrijft de bepaling met behulp van neutronendiffraktie van het ordeningsschema van de magnetische momenten in CoO, Cr_5S_6 en de trigonale vorm van Cr_2S_3.

Het grootste deel van het werk is uitgevoerd met poedervormige preparaten.

In hoofdstuk I worden enige kriteria geformuleerd met behulp waarvan de verschillende komponenten in een poederdiffraktometer zo gekozen kunnen worden, dat de intensiteit optimaal wordt bij gelijkblijvend oplossend vermogen.

In hoofdstuk II wordt aangegeven hoe de richtingen waarin de neutronen verstrooid worden en de intensiteit van de strooiïng samenhangen met de voortplantingsvektor en de grootte van iedere Fourier komponent van een (periodieke) magnetische struktuur. Eerst wordt het meest algemene geval van een spinstruktuur met één of meer Fourier komponenten met verschillende voortplantingsvektoren behandeld. De resultaten worden uitgewerkt voor enkele met name genoemde struktuurtypen.

Hoofdstuk III omvat een onderzoek naar de magnetische struktuur van CoO. Deze struktuur was reeds het onderwerp geweest van vroegere onderzoekingen. Er bestond echter reden tot twijfel aan de juistheid van het resultaat, mede doordat dit resultaat verkregen was met een poederdiffraktometer met laag oplossend vermogen. Het oplossend vermogen van de diffraktometer in Petten was hoog genoeg om nieuwe informatie te kunnen krijgen.

Het poederdiagram kan door twee modellen voor de magnetische struktuur verklaard worden

a) een kollineair model met een hoek tussen de spinas en de tetragonale c as, gelijk aan 27,4°. Dit model is gelijk aan het voorgestelde model, afgezien van de deviatiehoek die gegeven was als 11,5°.

b) Een multispinas model waarin de spinassen van de vier antiferromagnetische submotieven niet parallel zijn. Wel maken alle spinassen een hoek van 27,4° met de c as.

Metingen, uitgevoerd aan één-kristallen kunnen ook met beide modellen verklaard worden. Voor het kollineaire model moet dan aangenomen worden, dat de vier mogelijke antiferromagnetische domeinen voorkomen met exact gelijk volume. Tijdens en na het beëindigen van het diffraktiewerk zijn enige andere studies van CoO gepubliceerd. Deze worden in de tekst besproken. Torsiemetingen aan dunne CoO films geven sterke aanwijzingen dat de kollineaire struktuur de juiste is.

In hoofdstuk IV wordt de bepaling van de magnetische strukturen van Cr_5S_6 beschreven. Deze stof is ferrimagnetisch tussen 168° en 305°K, beneden 168°K gedraagt hij zich antiferromagnetisch. De overgang bij 168°K is zeer scherp. Uit het neutronendiffraktie onderzoek is gebleken, dat in de lage temperatuurfase de magnetische momenten volgens een spiraal geordend zijn, waardoor het netto moment nul is. De spoed van de spiraal is afhankelijk van de temperatuur; als deze hoger wordt, ontwindt de spiraal zich. Bij 168°K is de spoed oneindig geworden en de magnetische struktuur gaat over in de ferrimagnetische, kollineaire fase.

De kristalstruktuur van trigonaal Cr_2S_3 is sterk verwant aan die van Cr_5S_6. Hoewel de magnetizatiekurve ook een maximum (bij 95°K) vertoont, zijn er twee verschillen met Cr_5S_6. Ten eerste: de maximale magnetizatie is een orde van grootte kleiner, ten tweede: er is geen diskontinuiteit in de magnetizatie. Het onderzoek, beschreven in hoofdstuk V, heeft aangetoond dat zowel bij 4,2°K als bij $\approx$ 80°K de spinstruktuur beschreven kan worden als een spiraal met een spoed, gelijk aan tweemaal de kristallografische c as. Het is niet duidelijk, waaraan het maximum in de magnetizatiekurve moet worden toegeschreven.

STELLINGEN

1. Saito, Nakahigashi en Shimomura hebben een rhomboedrische deformatie van CoO in de antiferromagnetische toestand waargenomen. Hun konklusie, dat deze deformatie beter in overeenstemming is met een hoek van 10^{o} tussen de spin-as en de [001] richting dan met een hoek van $27,4^{o}$, is niet gerechtvaardigd.

   S.Saito, K.Nakahigashi en Y.Shimomura,
   J.Phys.Soc.Japan 21, 850 (1966).

   Dit proefschrift, hoofdstuk III.

2. De konklusies van D.C.Khan over de spindichtheidsverdeling in CoO berusten op een foutieve interpretatie van zijn meetgegevens.

   D.C.Khan, Ph.D.Thesis,
   The Ohio State University, 1965.

3. Werner, Arrott, King en Kendrick suggereren ten onrechte, dat "gaten" in de mozaïekspreiding verantwoordelijk zijn voor het verschil tussen gemeten en berekende intensiteit van monochromatorkristallen.

   S.A.Werner, A.Arrott, J.S.King en H.Kendrick,
   J.Appl.Phys. 37, 2343 (1966).

4. De röntgenpoederdiffraktiegegevens, gepubliceerd door Eibschütz, Hermon en Shtrikman, wettigen niet hun konklusie dat MNb_2S_4 (M=Mn,Fe,Co) isomorf is met het mineraal berthieriet ($FeSb_2S_4$).

   M.Eibschütz, E.Hermon en S.Shtrikman,
   Acta Cryst. 22, 944 (1967).

5. Teneinde de koppelingscoëfficiënten in de dynamische matrix voor Fe_3Al te berekenen, worden door Borgonovi, Logiudice en Tocchetti matrices van krachtconstanten geformuleerd. In deze formulering is de symmetrie van het kristalrooster op niet geheel juiste wijze in rekening gebracht.

   G.Borgonovi, G.Logiudice en D.Tocchetti,
   J.Phys.Chem.Solids 28, 476 (1967).

6. De door van Dam aangetoonde verschillen in de samenstelling van α-crystalline van rund en kalf, maakt de vergelijking van deze samenstellingen met die van het paard en het varken, van niet meer dan empirische betekenis.

   A.F.van Dam
   Proefschrift Universiteit van Nijmegen, 1967,
   hoofdstuk IV.

7. Er is reden aan te nemen, dat recente metingen van de thermodynamische potentiaal van uraniummononitride te hoge uitkomsten hebben gegeven.

W.M.Olsen en R.N.R.Mulford,
J.Phys.Chem. 67, 952 (1963).

J.Bugl en A.A.Bauer,
J.Amer.Ceram.Soc. 47, 425 (1964).

P.A.Vozella en M.A.DeCrescente,
PWAC - 479 (1965).

T.Sano, M.Katsura en H.Kai,
Symp. on Thermodynamics of Nuclear Materials,
Wenen (1967), SM 98/20.

8. In snel-thermisch gekoppelde kernreaktorsystemen wordt als regel een filter van natuurlijk uranium toegepast tussen de snelle en de thermische zone. Deze keuze voor het filter is niet in alle gevallen de juiste.

9. Uit de vergelijking van poederdiffraktieresultaten, verkregen met neutronen- en röntgenstralen, blijkt dat bij röntgendiffraktie de systematische fouten belangrijker zijn dan de statistische.

10. Het is betreurenswaardig dat de overheid in Nederland geen initiatieven ontwikkelt om de bevolkingstoename tegen te gaan.

Tweede nota over de ruimtelijke ordening in
Nederland, 1966.

11. Stellingen bij academische proefschriften zijn veelal meer representatief voor de kennissenkring van de promovendus dan voor zijn kennis.

B. van Laar

3 april 1968.